

**UNIVERSIDADE FEDERAL DE SANTA CATARINA
PROGRAMA DE PÓS-GRADUAÇÃO EM
ENGENHARIA MECÂNICA**

Juan Sebastián Zuleta Marín

**ANÁLISE DE UMA PLANTA DE COGERAÇÃO A
GÁS NATURAL ASSISTIDA POR ENERGIA SOLAR**

**ANALYSIS OF A SOLAR-ASSISTED NATURAL
GAS COGENERATION PLANT**

Florianópolis
2018

Juan Sebastián Zuleta Marín

**ANÁLISE DE UMA PLANTA DE COGERAÇÃO A
GÁS NATURAL ASSISTIDA POR ENERGIA SOLAR**

Dissertação submetida ao Programa de Pós-Graduação em Engenharia Mecânica da Universidade Federal de Santa Catarina para a obtenção do título de Mestre em Engenharia Mecânica.

Orientador: Prof. Edson Bazzo, Dr. Eng.

Coorientador: Prof. Eduardo Konrad Burin, Dr. Eng.

Florianópolis
2018

Ficha de identificação da obra elaborada pelo autor,
através do Programa de Geração Automática da Biblioteca Universitária da UFSC.

Zuleta Marin, Juan Sebastian

Análise termodinâmica de uma planta de cogeração
assistida por energia solar / Juan Sebastian

Zuleta Marin ; orientador, Edson Bazzo Bazzo,
coorientador, Eduardo Konrad Burin Burin, 2018.

144 p.

Dissertação (mestrado) - Universidade Federal de
Santa Catarina, Centro Tecnológico, Programa de Pós
Graduação em Engenharia Mecânica, Florianópolis, 2018.

Inclui referências.

1. Engenharia Mecânica. 2. Engenharia mecânica .
3. Energia Solar. 4. Cogeração . 5. Híbridação . I.
Bazzo, Edson Bazzo. II. Burin, Eduardo Konrad
Burin. III. Universidade Federal de Santa Catarina.
Programa de Pós-Graduação em Engenharia Mecânica. IV.
Título.

Juan Sebastián Zuleta Marín

**ANÁLISE DE UMA PLANTA DE COGERAÇÃO A
GÁS NATURAL ASSISTIDA POR ENERGIA
SOLAR**

Esta Dissertação foi julgada adequada para obtenção do Título de “Mestre em Engenharia Mecânica”, e aprovada em sua forma final pelo Programa de Pós-Graduação em Engenharia Mecânica.

Florianópolis, 4 de junho de 2018.

Prof. Jonny Carlos da Silva, Dr. Eng.
Coordenador do programa de Pós-Graduação em Engenharia
Mecânica - POSMEC/UFSC

Prof. Edson Bazzo, Dr. Eng.
Orientador
Universidade Federal de Santa Catarina

Prof. Eduardo Konrad Burin, Dr. Eng.
Coorientador
Universidade Federal do Paraná

Banca Examinadora:

Prof. Edson Bazzo, Dr. Eng. – Presidente
Universidade Federal de Santa Catarina

Prof. José Alexandre Matelli, Dr. Eng.
Universidade Estadual Paulista (UNESP)

Prof. Vicente de Paulo Nicolau, Dr. Eng.
Universidade Federal de Santa Catarina

Prof. Júlio César Passos, Dr. Eng.
Universidade Federal de Santa Catarina

To my mother, my brother and my entire family.
Especially to my always beloved and never forgotten father Victor
Manuel Zuleta Araujo.

ACKNOWLEDGMENTS

Firstly, very specially I would like to acknowledge the Prof. Edson Bazzo for his invaluable advices and patience, for always being available to reply a question and be opened for discussion. Also, I am grateful to the Prof. Eduardo Burin for his friendship, trust and patience during the realization of this work.

I would like to acknowledge the PETROBRAS for the opportunity to participate in the project developed related to cogeneration systems.

I would like to thank my mother, my brother and my father for their support, patience, dedication and love during each stage of my life, without them this work would not have been possible to carry out.

I am greatly grateful to my family for their support and their teachings that made me who I am today.

I would like to thank my colleagues at Labcet, especially, Thiago, Jonatas Vicente, Nury, Teresa, Marcos, Raul, Abilio and Julian for their friendship and support. I thank my Colombian friends Alejandro, Alex, Jaime, Renzo, Juan Carlos, Diego Gutierrez, Diego Tabares, Jaime Lozano and Andrea. Likewise, I thank the worldwide people that I have had the opportunity to meet during my life in Brazil.

I am deeply grateful to Brazil and the Federal University of Santa Catarina for the opportunity. In the same way, I am grateful to Florianopolis for the opportunity that I had to see and know its wonderful landscapes.

I would like to thank the jury members, Prof. Vicente de Paulo Nicolau, Prof. José Alexandre Matelli and Prof. Júlio César Passos for agreeing to evaluate this work and for their suggestions to improve this manuscript.

Finally, I would like thank all the people whom in one way or another contributed to this work.

*"Escolha uma ideia
Faça dessa ideia a sua vida
Pense nela, sonhe com ela, viva pensando nela.
Deixe cérebro, músculos, nervos, todas as partes do seu corpo
serem preenchidas com essa ideia.
Esse é o caminho para o sucesso "*
Swami Vivekananda (1863-1902)

RESUMO

Nos últimos anos, a energia solar tem sido considerada como importante alternativa para reduzir o impacto negativo dos gases de efeito estufa no aquecimento global da terra. Neste contexto, com a possibilidade de integração da energia solar com o uso de gás natural, dois cenários de cogeração foram considerados para análise no sentido de atender às demandas elétricas e térmicas de uma indústria de médio porte no setor têxtil de Santa Catarina. O primeiro cenário consistiu de uma planta de cogeração a gás natural com motor de combustão interna para a produção de eletricidade, vapor saturado e água gelada para fins de climatização. Os gases de exaustão são conduzidos para uma caldeira de recuperação para pré-aquecer a água de alimentação e produzir vapor saturado. O calor remanescente associado aos gases de exaustão e a água de resfriamento do motor são considerados para aquecer água requerida por um chiller de absorção para a produção de água gelada. O segundo cenário consistiu na mesma planta de cogeração, agora integrada a um campo solar baseado na tecnologia Fresnel para a produção direta de vapor saturado (DSG), de modo a reduzir o consumo de combustível e as emissões de CO₂. Ambos cenários são comparados com um caso base, típico para a indústria têxtil em Santa Catarina, onde eletricidade é importada da rede pública, vapor saturado é produzido por caldeiras convencionais e água gelada é fornecida por chillers elétricos. O campo solar foi analisado durante um ano meteorológico típico para a cidade de Florianópolis. A planta de cogeração foi analisada de acordo com a primeira lei da termodinâmica, tendo como dados de entrada as características técnicas disponibilizadas em catálogos técnicos fornecidos pelos fabricantes do motor e chiller de absorção. No caso da caldeira de recuperação, foram consideradas pressões típicas do setor têxtil, levando em conta valores de pinch point e de approach point recomendados na literatura técnica. O Valor Presente Líquido (VPL), a Taxa Interna de Retorno (TIR) e o Payback (PB) foram considerados no estudo de pré-viabilidade econômica dos cenários propostos. Uma análise de sensibilidade foi também realizada, considerando diferentes valores de área do campo solar, incidência

de radiação, custos dos coletores Fresnel, preço de gás natural e tarifas de eletricidade. Como esperado, foi identificado um grande potencial de redução do consumo de combustível e das emissões de CO₂ nos sistemas híbridos, mas ainda com uma elevação significativa nos valores de investimento, devido principalmente aos altos custos dos coletores Fresnel e baixo preço do gás natural.

Palavras Chave: Indústria têxtil, Cogeração, Sistemas híbridos, CSP.

RESUMO EXPANDIDO

INTRODUÇÃO

Uma planta de cogeração a gás natural assistida por energia solar é proposta como uma alternativa para atender as demandas térmicas e elétricas de uma empresa de médio porte no setor têxtil em Santa Catarina. De acordo com o Balanço energético de Santa Catarina o setor têxtil é responsável por 5 % do consumo energético industrial no estado. Adicionalmente, o gás natural é um dos principais combustíveis utilizados nas indústrias para a geração de vapor saturado. Não obstante, a queima de combustíveis fósseis está causando uma série de problemas ambientais devido às emissões de gases de efeito estufa. Neste contexto, dois diferentes cenários são propostos para este setor industrial. O primeiro cenário consistiu de uma planta de cogeração a gás natural utilizando um motor de combustão interna para a produção de eletricidade e assim mesmo atender as demandas térmicas. Deste modo, os gases de exaustão são aproveitados por uma caldeira de recuperação para a produção de vapor saturado. Igualmente, o calor remanescente associado aos gases de exaustão e a água de resfriamento do motor são utilizados para aquecer a água de alimentação requerida por um chiller de absorção para a produção de água gelada para fins de climatização. O segundo cenário consistiu na mesma planta de cogeração, agora integrada a um campo solar de coletores Fresnel para a produção direta de vapor saturado (DSG), de modo a reduzir o consumo de combustível e as emissões de CO₂.

OBJETIVOS

O objetivo principal deste trabalho consistiu na análise econômica e técnica de uma planta de cogeração a gás natural e uma planta híbrida propostas como uma alternativa para uma planta de médio porte no setor têxtil em Santa Catarina com capacidade de atender as demandas de vapor saturado, água gelada e eletricidade.

1. Resgatar trabalhos prévios relacionados ao estudo de plantas

de cogeração e plantas híbridas.

2. Analisar termodinamicamente e economicamente o cenário base, a planta de cogeração proposta e a planta híbrida proposta.
3. Realizar uma análise de sensibilidade dos parâmetros econômicos e de projeto que influenciam na viabilidade técnica e econômica das plantas propostas.
4. Comparar os resultados obtidos do ponto de vista técnico e econômico.

MATERIAIS E MÉTODOS

Ambos cenários são comparados com um caso típico de uma planta de médio porte no setor têxtil em Santa Catarina, onde a eletricidade é importada da rede pública, vapor saturado é produzido por caldeiras convencionais e água gelada é fornecida por chillers elétricos. O campo solar foi analisado durante um ano meteorológico típico para a cidade de Florianópolis como uma aproximação do recurso solar em Santa Catarina. A planta de cogeração foi analisada de acordo com a primeira lei da termodinâmica, tendo como dados de entrada as características técnicas disponibilizadas em catálogos técnicos fornecidos pelos fabricantes do motor e chiller de absorção. No caso da caldeira de recuperação, foram consideradas pressões típicas do setor têxtil, levando em conta valores de pinch point e de approach point recomendados na literatura técnica. A simulação anual é realizada na ferramenta computacional EES (Engineering Equation Solver). O Valor Presente Líquido (VPL), a Taxa Interna de Retorno (TIR) e o Payback (PB) foram considerados no estudo de pré-viabilidade econômica dos cenários propostos. Do mesmo modo, uma análise de sensibilidade foi também realizada, considerando diferentes valores de área do campo solar, incidência de radiação, custos dos coletores Fresnel, preço de gás natural e tarifas de eletricidade. Como esperado, foi identificado um grande potencial de redução do consumo de combustível e das emissões de CO₂ nos sistemas híbridos, mas ainda com uma elevação significativa nos valores de investimento, devido principalmente aos altos custos dos coletores Fresnel e baixo preço do gás natural.

RESULTADOS E DISCUSSÃO

Conforme mencionado anteriormente, neste trabalho foram analisadas do ponto de vista termodinâmico e econômico duas plantas propostas para uma planta de médio porte típica do setor têxtil em Santa Catarina.

O primeiro cenário analisado consistiu no caso típico de uma planta do setor têxtil, caracterizado pela importação da demanda elétrica (3000 kW) da rede pública. A demanda de vapor (12 t/h) é produzida por uma caldeira de queima de gás natural convencional. Finalmente, a demanda de água gelada (300 TR) utilizada para condicionamento de ar é atendida por um chiller elétrico com uma demanda correspondente a 412 kW considerando um $COP_e=3.0$. Portanto, a demanda elétrica total deste cenário é 3412 kW.

O segundo cenário analisado consistiu numa planta de cogeração utilizando dois motores de combustão interna a gás natural com potência nominal de 4000 kW para atender a demanda elétrica. O excedente de eletricidade é exportado para a rede pública. Do mesmo modo, o déficit de eletricidade devido a paradas para manutenção do sistema de cogeração considerando um fator de disponibilidade da planta de 95 % é importado da rede pública. Os gases de exaustão do motor são aproveitados por uma caldeira de recuperação para produzir vapor saturado. Na simulação desta planta proposta foram levados em conta aspectos técnicos relacionados com pressão típica (8 bar efetivo). Valores de pinch point (15 °C) e approach point (15 °C) também foram considerados. A produção de vapor pela caldeira de recuperação (2,2 t/h) é complementada pela caldeira de queima de gás natural convencional existente (9,8 t/h), atendendo assim a demanda total de vapor de 12 t/h. Um chiller de absorção é usado com capacidade para atender 128,5 TR de água gelada, sendo complementada pelo chiller elétrico existente (172,5 TR), atendendo assim a demanda total de 300 TR. Deste modo o consumo elétrico do chiller cai para 283,1 kW, cerca de 31 % menor quando comparado com o caso base. Nessa condição, o excedente de eletricidade corresponde a valores da ordem de 690 kW.

Finalmente, o terceiro cenário consistiu na integração de um campo de coletores Fresnel na planta de cogeração (segundo cenário). O campo solar é projetado para produzir 4 t/h de vapor saturado na condição de projeto. O campo solar é simulado durante o ano típico meteorológico (TMY) para a cidade de Florianópolis. Deste modo,

a integração do campo solar permite uma economia de combustível, portanto, uma redução das emissões de CO₂.

Os resultados econômicos mostraram uma grande influência do custo do gás natural na viabilidade econômica da planta de cogeração. Foi encontrado na condição de projeto (considerando um preço do gás natural de 1,5 R\$/m³ e tarifa elétrica verde) um valor para Valor Presente Líquido (VPL) de R\$ 17.638.156, prazo de retorno (Payback) de 81,2 meses e uma Taxa Interna de Retorno (TIR) da ordem de 20,56 %. Neste sentido, os VPL e TIR diminuem cerca de 12 % e de 8 %, respectivamente, para acréscimos do preço do gás natural da ordem de 0,1 R\$/m³. Por outro lado, o prazo de retorno aumenta aproximadamente 19 % com um aumento de 0,1 R\$/m³ no preço do gás natural. Igualmente, os resultados mostraram que as opções de tarifa verde ou tarifa elétrica azul apresentam pouca influência na viabilidade econômica da planta de cogeração.

Por outro lado, os resultados são desfavoráveis para o caso híbrido quando comparado com o caso de cogeração do ponto de vista econômico devido principalmente aos altos custos de investimento dos coletores solares, baixo nível de incidência solar (1423 kW/m²-ano) em Florianópolis, além de um cenário de baixos preços de gás natural para fins de cogeração. Neste sentido, foi encontrado na condição de projeto (considerando um preço de gás natural de 1.5 R\$/m³ e tarifa elétrica verde) que a TIR e o VPL diminuem cerca de 16 % e 12 %, respectivamente e o retorno aumenta 26 % quando o sistema de coletores Fresnel é integrado na planta de cogeração. Adicionalmente, foi encontrado que acréscimos no preço do gás natural favorecem o uso do sistema híbrido tendo em vista a economia de combustível devido ao uso da energia solar. Porém, o aumento do custo do gás natural não é suficiente para viabilizar o sistema híbrido do ponto de vista econômico considerando os atuais custos dos coletores Fresnel.

Neste contexto, outros casos de maior incidência solar foram avaliados, considerando como exemplo a cidade de Port Land na Austrália (2738 kW/m²-ano) e a cidade do Bom Jesus da Lapa na região nordeste do Brasil (2198 kW/m²-ano). Os resultados mostraram maior viabilidade econômica quando comparados com o caso de Florianópolis. Porém, o caso de cogeração ainda apresenta a maior viabilidade econômica. Neste sentido, os atuais custos dos coletores Fresnel devem reduzir de modo a competir com o atual cenário de custos do gás natural. Atualmente, no

estado de Santa Catarina a incidência solar é de aproximadamente 1500 kWh/m²-ano. Portanto, o investimento em coletores Fresnel devem se limitar na faixa de 100 - 140 €/m². O anterior significa uma diminuição de cerca de 55 % o custo atual do coletor Fresnel no Brasil (265 €/m²).

Apesar das limitações econômicas, foi identificado um grande potencial dos sistemas híbridos do ponto de vista ambiental devido à redução das emissões de CO₂. Neste sentido, é importante que os governos locais incentivem o uso da energia solar através de políticas governamentais que permitam a redução dos atuais custos.

Finalmente, foi estabelecido que os sistemas híbridos têm um grande potencial de se integrar aos sistemas de cogeração do ponto de vista técnico. Neste sentido, se espera que sistemas híbridos apresentem grande desenvolvimento nos próximos anos, tendo em vista o potencial de redução de custos da tecnologia CSP, bem como sua contribuição como fonte energética de baixo carbono.

Palavras Chave: Setor têxtil, Cogeração, Sistemas híbridos CSP, Coletores Fresnel.

ABSTRACT

A solar-aided natural gas cogeneration plant is proposed as a promising alternative for supplying the thermal and electrical energy demands of a typical textile plant in Santa Catarina. The textile sector is responsible by about 5 % of the total energy consumption in the state. As it is known, natural gas is widely used by these facilities for producing saturated steam. However, the burning of traditional fossil fuels is causing negative impacts from an environmental point of view, such as global warming, air pollution, among others. As an important alternative to reduce these negative impacts, solar energy has been considered in the recent years. In this context, the main objective of this work consisted on the technical and economic evaluation of two different scenarios proposed for supplying the thermal and electrical energy demands of a medium-sized textile plant. The first alternative consisted on the operation of a natural gas engine and a Heat Recovery Steam Generator (HRSG) to produce electricity and saturated steam, respectively. The engine exhaust gas remaining heat and the water's engine radiator are used for an absorption chiller for producing chilled water for air conditioning purposes. Under the second proposed concept, a linear Fresnel solar field is integrated into the cogeneration plant in order to provide fuel economy during the sunny hours in which the conventional natural gas steam generator operates at part load. Thereby, this hybrid concept is able to reduce natural gas consumption and CO₂ emissions. The proposed concepts were compared to a base case plant scenario in which electricity is imported from the grid, saturated steam is produced by a natural gas steam generator and chilled water is provided by electric chillers. Simulations were performed by using Engineering Equation Solver (EES) simulation tool by implementing mass and energy conversation equations, by using performance cost and data provided by equipment manufacturers and by considering the Typical Meteorological Year (TMY) data for the city of Florianopolis as an approximation of the solar data in Santa Catarina. The economic analysis of proposed concepts was performed by calculating the Net Present

Value (NPV), the Internal Rate of Return (IRR) and the Payback Period (PB) of investments. Finally, a sensitive analyses were performed to evaluate the influence of parameters such as Direct Normal Irradiation (DNI), Fresnel collectors cost, solar field size, natural gas cost and electricity tariffs on the economic and technical feasibility of the proposed plants. As expected, it was identified a great potential of the hybrid system for reducing the fuel consumption and CO₂ emissions. However, the high investments associated to the Fresnel collectors coupled to low prices of natural gas have turned it economically unfeasible. Nonetheless, it is expected that the hybrid systems have an important role in the near future, once Concentrated Solar Power (CSP) technology costs are expected to decrease, due to its substantially contribution to the global energy transition to a low carbon future.

Keywords: Textile sector, Cogeneration, Hybrid systems, CSP.

LIST OF FIGURES

| | |
|--|----|
| Figure 1 – Comparison between CHP and conventional production | 41 |
| Figure 2 – Qualified cogeneration plants operating in Brazil | 44 |
| Figure 3 – Brazilian electricity supply by source | 45 |
| Figure 4 – Brazilian energy supply by source | 45 |
| Figure 5 – Basic scheme of interaction between cogeneration plant and multiple suppliers. | 47 |
| Figure 6 – Scheme of a engine cogeneration plant | 48 |
| Figure 7 – DNI around the world | 50 |
| Figure 8 – Parabolic trough solar collector unit and cross section of collector tube | 51 |
| Figure 9 – Fresnel collector representation | 51 |
| Figure 10 – Cosine optical losses (left), blocking (center) and shading (right) | 52 |
| Figure 11 – Solar Tower plant | 53 |
| Figure 12 – Parabolic dish | 54 |
| Figure 13 – CSP projects around de world | 55 |
| Figure 14 – Average daily DNI in Brazil | 59 |
| Figure 15 – States participation in the Brazilian textile sector | 60 |
| Figure 16 – Energy sources participation in the textile industry in Santa Catarina | 62 |
| Figure 17 – Energy consumption in the Brazilian textile industry during the year 2009 | 63 |
| Figure 18 – Base case scenario layout | 66 |
| Figure 19 – Proposed cogeneration plant layout | 68 |
| Figure 20 – Proposed solar-aided cogeneration plant layout . | 70 |
| Figure 21 – Scheme of HRSG | 76 |
| Figure 22 – Temperature profile at the HRSG. | 77 |
| Figure 23 – Energy balance at the absorption chiller | 79 |
| Figure 24 – Cooling tower scheme | 80 |
| Figure 25 – Scheme of Fresnel collector | 83 |
| Figure 26 – Linear Fresnel collector receiver protected with a glass plate b) glass tube) | 84 |
| Figure 27 – Definition of angles in Fresnel collector | 85 |

| | |
|---|-----|
| Figure 28 – The equation of time E in minutes, as function of time of year | 87 |
| Figure 29 – Correction factor | 88 |
| Figure 30 – Base case scenario monthly electrical consumption | 94 |
| Figure 31 – Base case scenario monthly electrical expense account | 96 |
| Figure 32 – Monthly electrical production and electrical consumption | 101 |
| Figure 33 – Monthly earnings due to the electricity sale . . . | 105 |
| Figure 34 – Payback period as a function of natural gas cost for green and blue electricity tariffs | 107 |
| Figure 35 – NPV as a function of natural gas cost for green and blue electricity tariffs | 107 |
| Figure 36 – IRR as a function of natural gas cost for green and blue electricity tariffs | 108 |
| Figure 37 – Solar field performance during the summer solstice | 110 |
| Figure 38 – Solar field performance during the winter solstice | 111 |
| Figure 39 – Economized natural gas during a year | 112 |
| Figure 40 – Optical efficiency during a year | 112 |
| Figure 41 – IRR as a function of natural gas cost for the conventional and the solar-aided proposed cogeneration plants | 117 |
| Figure 42 – NPV as a function of natural gas cost for the conventional and the solar-aided proposed cogeneration plants | 117 |
| Figure 43 – Payback period as a function of natural gas cost for the conventional and the solar-aided proposed cogeneration plants | 118 |
| Figure 44 – Solar fraction throughout the year for different SM values | 119 |
| Figure 45 – Solar fraction as a function of SM for different DNI incidence levels | 120 |
| Figure 46 – Reduction of CO ₂ emissions as a function of SM for different DNI incidence levels | 121 |
| Figure 47 – IRR as a function of Fresnel collector cost for different DNI incidence levels considering a natural gas cost of 1.5 R\$/m ³ | 122 |
| Figure 48 – Fresnel collector cost as a function of natural gas cost for different DNI incidence levels | 124 |
| Figure 49 – Steam Generator operation efficiency as a function of load | 141 |

LIST OF TABLES

| | |
|---|-----|
| Table 1 – Values of X and F_c , Resolution 021/2006 ANEEL | 43 |
| Table 2 – Typical CHP loads. | 47 |
| Table 3 – Average LCOE of existing plants in the world . . . | 56 |
| Table 4 – Hybrid CSP projects around the world. | 58 |
| Table 5 – Energy sources participation in the Brazilian textile sector | 61 |
| Table 6 – Characteristics of each module | 84 |
| Table 7 – Thermal demands and electrical demands | 91 |
| Table 8 – Plant site and TMY data | 92 |
| Table 9 – Assumptions adopted for economic analysis . . . | 92 |
| Table 10 – Thermodynamic results at design point for the base case scenario | 93 |
| Table 11 – Base case scenario annual performance | 95 |
| Table 12 – Base case scenario annual expense account | 97 |
| Table 13 – Assumptions adopted for cogeneration plant simulation | 98 |
| Table 14 – Thermodynamic results at design point | 99 |
| Table 15 – Qualified cogeneration plant | 100 |
| Table 16 – Cogeneration plant scenario annual performance . | 100 |
| Table 17 – Assumptions adopted for economic analysis . . . | 102 |
| Table 18 – Cogeneration plant cost | 103 |
| Table 19 – Cogeneration plant scenario annual expense account | 104 |
| Table 20 – Economic parameters for cogeneration plant scenario | 106 |
| Table 21 – Adopted parameters for solar field simulation . . . | 109 |
| Table 22 – Results at the design point | 110 |
| Table 23 – Solar field annual performance | 113 |
| Table 24 – Adopted assumptions for economic analysis | 113 |
| Table 25 – Solar assisted cogeneration plant cost | 114 |
| Table 26 – Solar assisted cogeneration plant annual expense account | 115 |
| Table 27 – Economic parameters for solar-aided cogeneration plant | 116 |
| Table 28 – Enthalpy of reactants at 298 K | 140 |
| Table 29 – Enthalpy of products at 298 K | 140 |

Table 30 – Water thermodynamic properties 143
Table 31 – Exhaust gas thermodynamic properties 144

LIST OF SYMBOLS AND ABBREVIATIONS

Roman

| | |
|-----------|---|
| \dot{m} | Mass flow rate, [kg/s] |
| \dot{Q} | Heat transfer rate, [W] |
| \dot{V} | Volume flow rate, [m ³ /h] |
| A | Area, [m ²] |
| AP | Approach Point, [°C] |
| C_p | Specific heat at constant pressure, [kJ/kg-K] |
| COP | Coefficient of Performance |
| DNI | Direct Normal Irradiation, [kWh/m ² -year] |
| ENG | Economized Natural Gas, [m ³ /h] |
| EPC | Engineering, Procurement, and Construction costs, [USD] |
| ET | Equation of time, [min] |
| G_{bn} | Direct Normal Irradiance, [kW/m ²] |
| h | Enthalpy, [kJ/kg] |
| IRR | Interest Rate of Return, [%] |
| k | Specific heat |
| LCOE | Levelized Cost of Electricity, [USD/kWh] |
| lt | Life time, [years] |
| n | Day of the year, [day] |
| NPV | Net Present Value, [USD] |

| | |
|-----|---------------------------------------|
| O&M | Operation and maintenance cost, [USD] |
| OPH | Off-peak hours, [Hours] |
| p | Pressure, [kPa] |
| PB | Payback period, [Months] |
| PH | Peak hours, [Hours] |
| PP | Pinch Point, [°C] |
| r | Interest rate, [%] |
| T | Temperature, [°C] |

Greek

| | |
|----------------|------------------------------|
| η | Efficiency |
| θ_z | Zenith angle, [deg] |
| α_s | Solar altitude angle, [deg] |
| δ | Declination, [deg] |
| Γ | Surface azimuth angle, [deg] |
| Γ_s | Solar azimuth angle, [deg] |
| ω | Hour angle, [deg] |
| ω_{air} | Air humidity ratio, [kg/kg] |
| ω_s | Solar hour angle, [deg] |
| ϕ | Latitude, [deg] |

Subscript

| | |
|-----|--------------------|
| a | Annual |
| cog | Cogeneration plant |
| ct | Cooling tower |
| cw | Chilled water |
| DP | Desing Point |
| e | Electrical |

| | |
|-----|--------------------|
| f | Fuel |
| fw | Feed water |
| ht | How water |
| hyb | Hybrid |
| in | Inlet |
| L | Refrigeration load |
| m | Period |
| mk | Make-up water |
| opt | Optical |
| out | Outlet |
| t | Thermal |

Abbreviation

ANEEL Agência Nacional de Energia Elétrica

BEB Brazilian Energy Balance

BESC Balanço energético de Santa Catarina

BEU Balanço de Energia Útil

CHP Cogeneration Heat Power

CSP Concentrated Solar Power

CT Central Tower

DSG Direct Steam Generation

EES Engineering Equation Solver

HRSG Heat Recovery Steam Generator

HTF Heat Transfer Fluid

ICMS Imposto sobre Operações relativas à Circulação de Mercadorias e Prestação de Serviços

IEA International Energy Agency

INMET Instituto Nacional de Meteorologia
IRENA International Renewable Energy Agency
LABCET Laboratory of Combustion and Thermal System
Engineering
LF Linear Fresnel
NGSG Natural Gas Steam Generator
NREL National Renewable Energy Laboratory
PT Parabolic Trough
SAM System Advisor Model
SM Solar Multiple
SWERA Solar and Wind Energy Resource Assessment
TES Thermal Energy Storage
TMY Typical Meteorological Year
UFSC Federal University of Santa Catarina

CONTENTS

| | Page |
|--|-----------|
| 1 INTRODUCTION | 37 |
| 1.1 OBJECTIVES | 39 |
| 1.2 STRUCTURE OF DOCUMENT | 39 |
| 2 BACKGROUND | 41 |
| 2.1 COMBINED HEAT AND POWER (CHP) | 41 |
| 2.1.1 Definition and importance of the cogeneration | 41 |
| 2.1.2 Natural gas | 44 |
| 2.1.3 CHP plant design | 46 |
| 2.2 CONCENTRATED SOLAR POWER (CSP) | 49 |
| 2.2.1 CSP technologies | 50 |
| 2.2.2 CSP in the world | 54 |
| 2.2.3 CSP cost | 55 |
| 2.2.4 Concentrated solar power hybridization | 57 |
| 2.3 THE BRAZILIAN SOLAR POTENTIAL | 59 |
| 2.4 THE BRAZILIAN TEXTILE SECTOR | 60 |
| 3 PROPOSED SCENARIOS | 65 |
| 3.1 INTRODUCTION | 65 |
| 3.2 BASE CASE SCENARIO | 65 |
| 3.3 COGENERATION PLANT SCENARIO | 67 |
| 3.4 SOLAR-AIDED COGENERATION PLANT SCENARIO | 69 |
| 3.5 THERMODYNAMIC ANALYSIS | 71 |
| 3.6 ECONOMIC ANALYSIS | 72 |
| 3.6.1 Net present value | 72 |
| 3.6.2 Internal rate of return | 73 |
| 3.6.3 Payback period | 73 |
| 4 COGENERATION PLANT MODELING | 75 |
| 4.1 INTRODUCTION | 75 |
| 4.2 NATURAL GAS ENGINE | 75 |
| 4.3 HEAT RECOVERY STEAM GENERATOR | 76 |

| | | |
|----------|--|------------|
| 4.4 | ABSORPTION CHILLER | 78 |
| 4.5 | COOLING TOWER | 80 |
| 4.6 | STEAM GENERATOR | 81 |
| 5 | LINEAR FRESNEL SOLAR FIELD MODELING | 83 |
| 5.1 | INTRODUCTION | 83 |
| 5.2 | MAIN COMPONENTS | 83 |
| 5.3 | OPTICAL AND THERMAL PERFORMANCE MODEL | 85 |
| 5.3.1 | Sun position and geometrical parameters . . | 85 |
| 5.3.2 | Optical efficiency | 87 |
| 5.3.3 | Heat losses | 88 |
| 5.4 | NET HEAT RATE AND SATURATED STEAM PRODUCED | 89 |
| 5.5 | SOLAR FIELD DESIGN | 90 |
| 5.5.1 | Desing point | 90 |
| 5.5.2 | Solar multiple | 90 |
| 6 | SCENARIOS COMPARISON | 91 |
| 6.1 | INTRODUCTION | 91 |
| 6.2 | GENERAL ASSUMPTIONS | 91 |
| 6.3 | BASE CASE SCENARIO | 93 |
| 6.3.1 | Thermodynamic analysis | 93 |
| 6.3.2 | Economic analysis | 96 |
| 6.4 | COGENERATION PLANT SCENARIO | 97 |
| 6.4.1 | Thermodynamic analysis | 97 |
| 6.4.2 | Economic analysis | 102 |
| 6.4.3 | Sensitive analysis | 106 |
| 6.5 | SOLAR-AIDED COGENERATION PLANT SCENARIO | 108 |
| 6.5.1 | Thermodynamic analysis | 108 |
| 6.5.2 | Economic analysis | 113 |
| 6.5.3 | Sensitive analysis | 116 |
| 7 | CONCLUDING REMARKS | 125 |
| | BIBLIOGRAPHY | 129 |
| | Appendix A - LHV Calculation | 139 |
| | Appendix B - Steam generator operation efficiency . | 141 |

Appendix C - Cogeneration plant simulation 143

Chapter 1

INTRODUCTION

The Combined Heat and Power (CHP) systems provide the simultaneous production of electricity and heat taking advantage from an unique fuel. The CHP systems are used for different types of applications (e.g., hospitals, malls, industries, hotels, among others). The CHP systems are characterized by the combination of different devices such as engines, steam generators, absorption chillers, turbines, heat exchangers, among others. These systems are benefited with global efficiencies by about 80 %. In addition, cogeneration systems can provide economic advantages compared to separate processes used for supplying thermal and electrical energy demands. In the same way, these systems have advantages related to fuel economy (Abusoglu & Kanoglu, 2009).

As it is known, the electrical and thermal demands are increasing in the world. Therefore, the use of fossils fuels is important for attending this growth. However, burning traditional fossil fuels is causing environmental problems, such as climate change, global warming, air pollution, acid rain, among others. In this context, the solar energy represents an important alternative to mitigate this global problem (Sampaio & González, 2017). However, one disadvantage of the solar systems is related to the daily fluctuations of the solar irradiation influencing on the thermal and electrical generation. In order to mitigate this negative effect, fossil fuels can be an important support for solar systems, taking advantage from the solar resources and availability of fossil fuels. Thereby, the solar energy can help to overcome partially the drawbacks associated to climate change. In this respect, it is important to analyze the potential of the alternative sources in Brazil, including the option of solar energy. Despite the positive impacts of the solar systems as defined above, the high investment cost of these systems is the main disadvantage. Therefore, the efforts are concentrated on accelerated the cost reductions and efficiency improvements of these systems (Erdinc & Uzunoglu, 2012). According to IRENA (2017) the current cost is expected to be reduced, due to its contribution to the global

energy transition to a low carbon future and the increase of the installed capacity.

During the recent years, the main sources used in the textile industry in Santa Catarina have been electricity and biomass with an equivalent share by 41 % and 36 %, respectively. Particularly, natural gas has been an important role with a participation by 23 % (BESC, 2013). According to Santana & Bajay (2010), there is a potential to improve energy efficiency at various stages of the textile chain in Brazil. It was calculated a potential energy conservation for the Brazilian textile sector by 22 % of the total energy used in the sector. In this regard, it was identified an opportunity related to energy efficiency. Therefore, cogeneration plants can be a great option to the textile sector taking advantage of the availability of the fossil fuels. In the same way, the solar systems can be a great alternative, in order to mitigate the negative effects caused by CO₂ emissions.

In Laboratory of Combustion and Thermal System Engineering (LABCET) in the Federal University of Santa Catarina (UFSC) preliminary works have been developed focused on the design and optimization of the solar hybrid systems. Burin *et al.* (2016) evaluated the integration of a parabolic trough solar field with a typical sugarcane bagasse cogeneration plant located in Campo Grande, in the state of Mato Grosso do Sul (Brazil). The plant was analyzed under thermodynamic and economics aspects. As an important result, it was identified that the solar energy can be integrated into bagasse power plant in the sugarcane sector. However, the current parabolic trough concentrators costs have limited its implementation in terms of economic feasibility.

Galante (2015) analyzed a biomass power plant assisted by solar energy. The system was analyzed for each hour based on a TMY for the city of Santa Maria in the state of Rio Grande do Sul (Brazil). As an important result, it was identified that the hybrid power systems represent a transition between an economy based on fossil fuels to an economy supported by renewables energy sources. However, it is unlikely that fossil fuels lose its prominence in the next years.

Guadalupe (2018) analyzed from an economic and thermodynamic point of view the integration of a Fresnel collector field and flat plate collectors field, in order to supply the saturated steam and the hot water demand, respectively of a poultry slaughterhouse located in Palotina in the state of Parana (Brazil).

As an important result, it was identified that the integration of the Fresnel concentrators promoted the highest levels of fuel economy. However, the high costs associated to the Fresnel collector turned this alternative unfeasible from an economic point of view. On the other hand, the alternative by the flat plates collectors for producing hot water was more economically attractive.

In this regard, in this work is proposed a cogeneration plant as an alternative for supplying the saturated steam, electrical and chilled water demands of a medium-size plant in the textile sector in Santa Catarina (Brazil). In the same way, it is analyzed the integration of a solar Fresnel Field into the cogeneration plant in order to produce saturated steam taking advantage of the solar resource. The proposed plants are analyzed from a technical and economic point of view.

1.1 OBJECTIVES

The main goal of this research is to analyze thermodynamically and economically a cogeneration plant and a solar-aided cogeneration plant proposed for supplying the demands of saturated steam, electricity and chilled water of a medium-size plant in the textile sector in Santa Catarina.

The specific objectives of this work are listed below:

1. To review previous works related to cogeneration and hybrid cogeneration power plants.
2. To analyze thermodynamically and economically the base case scenario, the proposed cogeneration plant and the proposed solar-aided cogeneration plant.
3. To perform a sensitive analysis to identify the influence of design and economic parameters on the technical and economical feasibility of the proposed plants.
4. To compare the results from an economic and technical point of view.

1.2 STRUCTURE OF DOCUMENT

The literature review of the cogeneration systems, the CSP technologies, hybrid power systems and of the Brazilian textile

sector are presented in Chapter 2 in order to provide the initial contextualization.

In Chapter 3, the studied scenarios are described (base case scenario, cogeneration plant scenario and solar-aided cogeneration plant). In the same way, it is presented the thermodynamic and economic performance indexes.

In Chapter 4 it is presented the cogeneration plant simulation model.

The Fresnel collector simulation models are present in Chapter 5.

The base case, cogeneration plant and the solar-aided cogeneration plant scenarios simulation results are presented in the the Chapter 6.

Finally, the conclusions are presented in the Chapter 7.

Chapter 2

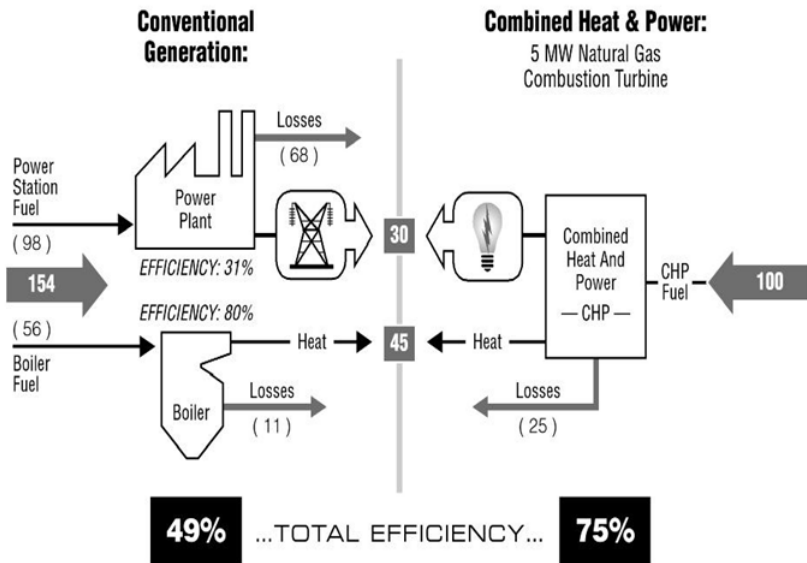
BACKGROUND

2.1 COMBINED HEAT AND POWER (CHP)

2.1.1 Definition and importance of the cogeneration

Cogeneration consists on the combined production of electricity and heat from the same fuel. The efficiency gain related to using CHP plants vary depending on power plant technology, fuel and the heat and power loads. The Figure 1 provides a helpful comparison between a CHP plant and the conventional concept in which heat and electricity are generated separately. As it can be seen, the CHP plant has a higher efficiency compared to the conventional systems to produce the same amount of useful energy.

Figure 1 – Comparison between CHP and conventional production



Source: Adapted from EIA (2018)

CHP plants consist on four basic elements: a prime mover (e.g. internal combustion engine, gas turbine), an electricity generator, a heat recovery system, and a control system. The prime mover, while driving the electricity generator, provides the usable heat to be recovered to feed the process heat demand. CHP units are generally classified according to the type of application, prime mover and fuel used (IEA, 2008).

The main technical advantage of cogeneration systems versus conventional systems consists on efficiency improvement of fuel usage in production of electricity and thermal energy.

Food processing, pulp, paper mills, chemical, metals and oil refining sectors have been traditional hosts of CHP facilities due to their intensive electricity and thermal energy usage. The economic benefits of any CHP system depend on design, equipment costs, CHP operating practices, plant efficiency, market aspects, among others.

In Brazil the resolution 021/2006 defined by Brazilian Electricity Regulatory Agency (ANEEL) shows the requirements for a plant to be classified as a qualified cogeneration unit and the incentives established by the government. As it is established by the resolution, it is possible to export the electricity surplus generated by qualified cogeneration plants. The requirements are listed below (ANEEL, 2006):

- To be legally registered in the Brazilian Electricity Regulatory Agency.
- To meet the minimum requirements for rational energy by calculating Equations 2.1 and 2.2.

$$\frac{E_t}{E_f} \geq 15 \% \quad (2.1)$$

$$\frac{E_t}{X \cdot E_f} + \frac{E_e}{E_f} \geq F_c \% \quad (2.2)$$

where E_f [kWh] is the total energy available from fuel or fuels, E_e [kWh] is the total electrical energy generated by cogeneration plant, E_t [kWh] is the thermal energy provided by the

cogeneration plant, F_c represents the cogeneration factor and X is the weighting factor.

The values of X and F_c indicated by ANEEL are presented at Table 1

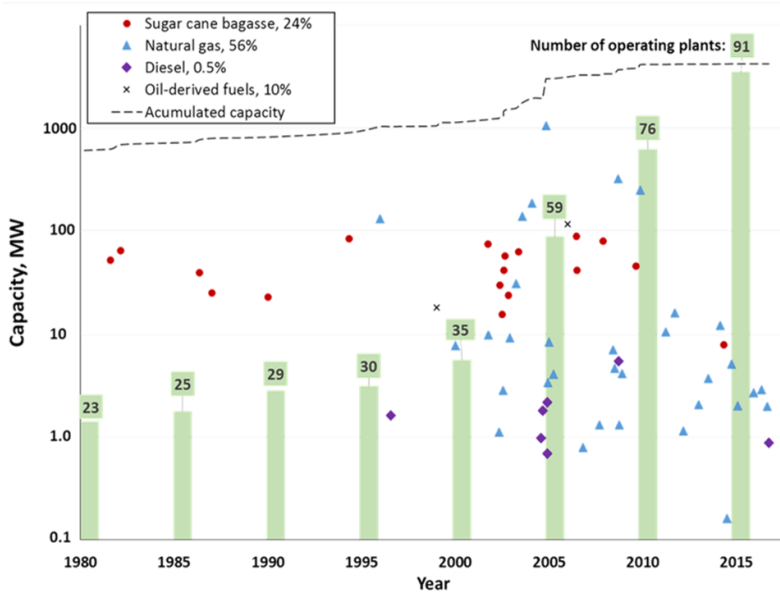
Table 1 – Values of X and F_c , Resolution 021/2006 ANEEL

| Power source/Installed electrical power | X | F_c |
|--|------|-------|
| Oil, natural gas and coal derivatives | | |
| Until 5 MW | 2.14 | 41 |
| Above of 5 MW and until 20 MW | 2.13 | 44 |
| Above of 20 MW | 2.00 | 50 |
| Other fuels | | |
| Until 5 MW | 2.5 | 32 |
| Above of 5 MW and until 20 MW | 2.14 | 37 |
| Above of 20 MW | 1.88 | 42 |
| Heat recovered from the process | | |
| Until 5 MW | 2.6 | 25 |
| Above of 5 MW and until 20 MW | 2.17 | 30 |
| Above of 20 MW | 1.86 | 35 |

Source: Adapted from ANEEL (2006)

In Figure 2, it is shown the cogeneration plants qualified in Brazil. As it is shown, natural gas is the main fuel used by qualified CHP plants representing a 56 %, followed by sugar cane bagasse representing a 24 %.

Figure 2 – Qualified cogeneration plants operating in Brazil



Source: (ANEEL, 2017)

2.1.2 Natural gas

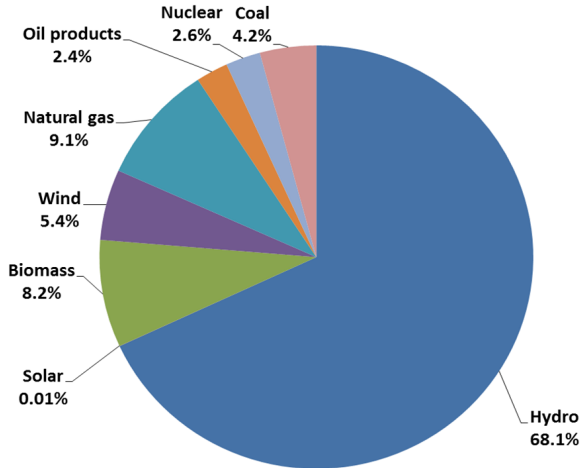
Natural gas is a fuel used in industries, commerce, residences, vehicles, thermal plants for power generation, among others. It is characterized by the mixture of light hydrocarbons such as methane, ethane and propane. Figures 3 and 4 shows the Brazilian energy and electricity supplies by source, respectively. Particularly, natural gas has a participation by 9 % in the electricity supply and by 12 % in the energy supply.

According to Santos (2017) the natural gas participation in the Brazilian energy supply has been growing. A key aspect that allows to increase the use of natural gas in Brazil is related to its competitive cost, in addition to its availability in some regions, specially in Santa Catarina.

According to Marbe *et al.* (2006) cogeneration plants based on the use of natural gas are expected to increase in the future due to its high efficiency and relatively low cost compared to coal or oil-fired CHP plants. Additionally, the CHP plants using natural gas, it was found that the CO₂ emissions are about 50 and 30 % lower

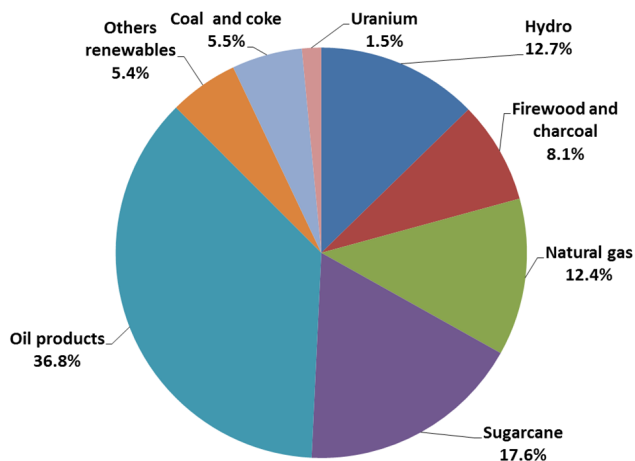
compared to coal or oil-fired CHP plants, respectively.

Figure 3 – Brazilian electricity supply by source



Source: Adapted from BEB (2017)

Figure 4 – Brazilian energy supply by source



Source: Adapted from BEB (2017)

2.1.3 CHP plant design

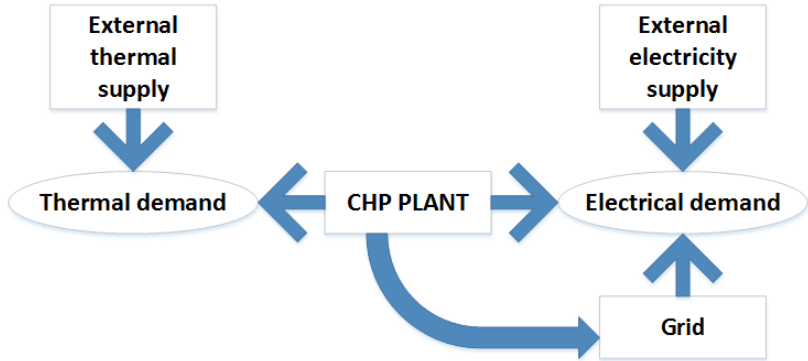
According to literature different CHP layouts have been studied. Fu *et al.* (2011) studied a natural gas CHP system based on the integration of an internal combustion engine, and an absorption heat pump (AHP). The system was analyzed for typical days in summer and winter. It was found the CHP system could increase the heat utilization efficiency by 10 % compared to conventional systems in winter. Kong *et al.* (2004) studied a CHP system driven by a natural gas engine integrated with a double effect absorption chiller and a heat exchanger for process heat recovery. It was found that the price of natural gas was a key factor that determined the feasibility of the system. Sun (2007) investigated the performance of an absorption chiller driven by the residual heat from distinct prime movers such as a Stirling engine, an internal combustion natural gas engine, and a micro-turbine. It was found that the economy related to primary energy demand of the combined system reached 40.9 % compared to conventional systems. Santo (2014) performed an annual analysis of a CHP system driven by engine to supply energy, steam, hot water and the refrigeration demands. The obtained results revealed a thermal efficiency between 58 - 77 % and an exergy efficiency between 35 - 41 % for the system.

According to Ashrae (2015) some key aspects must be defined, while designing CHP plants such as identification of target markets, determination of the thermal and electrical demands, fuel availability and characteristics, space availability, available of economic resources, among others.

In most cases, the CHP plant must interact with external suppliers to guarantee the thermal and electrical demands of the site. A typical interaction between a cogeneration plant and multiple suppliers is presented at the Figure 5. As it can be seen, the CHP plant is proposed to supply the electrical and thermal demands. Electrical surplus can be exported to the grid. In the same way, electrical deficit is imported to the grid. On the other hand, external thermal supplies such as electric chiller, steam generators, among others equipments can be used in order to attend the thermal demand. The most fundamental, and perhaps difficult, element to be considered during the design of a CHP application consists on mapping the site's thermal and electric loads. In fact, most CHP design failures occur because the systems were incorrectly sized to attend the site's thermal and electricity

loads taking into account that these demands vary throughout the day depending on aspects such as the local climate, work schedules, operation process, and unforeseen events (Balestieri, 2002).

Figure 5 – Basic scheme of interaction between cogeneration plant and multiple suppliers.



Source: Adapted from Balestieri (2002).

According to the above mentioned, the load profiles information might be considered to compare different CHP configurations scenarios during the design phase. The loads should be categorized into groups that are compatible with CHP output streams. Typical loads in CHP plants are shown at the table 2.

Table 2 – Typical CHP loads.

| Power | Heat | Cooling |
|------------|-----------------|------------------|
| Electric | Steam | Chilled Water |
| Mechanical | Hot Fluid | Refrigeration |
| | Hot Exhaust Air | Dehumidification |

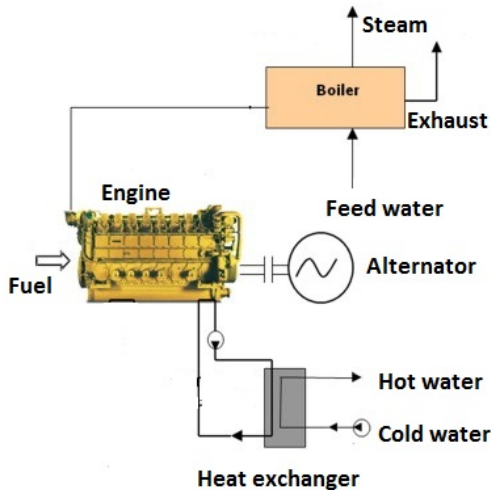
Source:(Ashrae, 2015)

The prime mover selection is an important step during the design phase. According to Ashrae (2015) some important aspects must be taken into account during the prime mover selection:

- Equipment sizes;
- Fuel availability;
- System availability;
- Maintenance Requirements;
- Start-up requirements;
- Electrical demand;
- Thermal demand;
- Type of industry.

Particularly, CHP systems equipped with internal combustion engines are most compatible with medium-sized industries or commercial applications that require an electrical demand between 100 kW and 5 MW. Engines can be operated with a wide range of fuels. However, natural gas is most commonly used in CHP plants. Figure 6 shows a scheme of an engine cogeneration plant.

Figure 6 – Scheme of an engine cogeneration plant



Source: Adapted from Çakir *et al.* (2012).

As it can be seen, the engine exhaust gas at high temperature, typically between 400 - 500 °C is used by a heat recovery steam generator that consist on equipment implemented to provide steam production by using the available heat. The residual heat dissipated by the engine's cooling system is used to produce hot water by a heat exchanger.

In the same way, solar energy can be utilized for cogeneration systems. For example, by using solar collectors solar energy can be converted in a central power plant to electrical energy which can be utilized to operate a vapor compression refrigerator to produce cooling. At the same time, the waste heat rejected by the heat engine can be used to drive an absorption chiller. From this perspective, these systems can play a dual role by saving energy and reducing the environmental pollution.

2.2 CONCENTRATED SOLAR POWER (CSP)

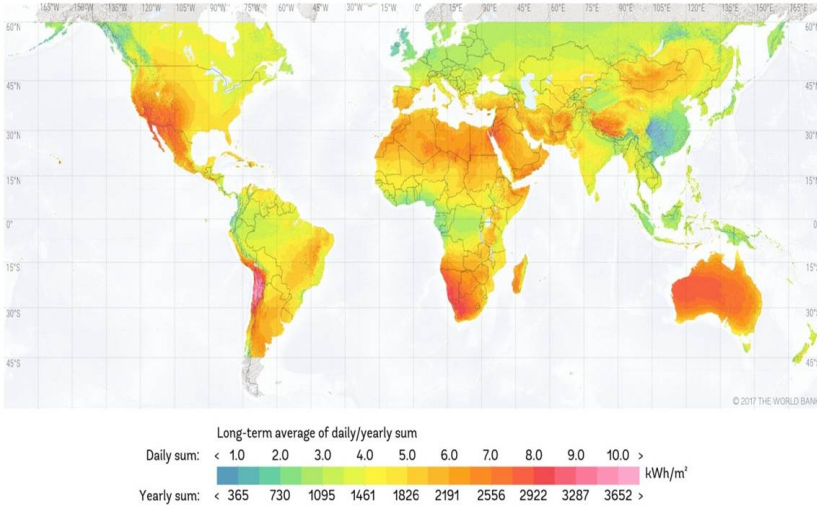
CSP technologies use different mirror configurations to concentrate the solar energy onto a receiver and convert it into heat. These systems can use thermal storage during cloudy periods or at night. In the same way, these systems can be integrated either with fossil fuels or biomass resulting in hybrid power plants.

CSP system is a relatively immature technology compared to Solar Photovoltaic (PV) technology and other electricity generating technologies (Gauché *et al.*, 2017). Furthermore, the CSP systems can play a fundamental role in the near future due to its capacity to reduce the CO₂ emissions. However, the high cost of CSP technologies is still non-competitive.

In this context, CSP technology is expected to reduce cost in the near future due to the increment of installed capacity. According to IRENA (2012), the global installed capacity could reach about 350 GW by 2030 (i.e., 3.8 % of the global electricity demand, with an average capacity factor by 39 %). Several emerging economies, such as South Africa, Chile and Morocco, have been identified as ideal for CSP applications due to its high DNI incidence levels (Gauché *et al.*, 2017).

In Figure 7, it is shown the DNI incidence levels around the world. Particularly, in Brazil, DNI can reach levels of 2200 kWh/m²-year in the city of Bom Jesus da Lapa at north-east in the state of Piauí (ATLAS, 2017).

Figure 7 – DNI around the world



Source: (SOLARGIS, 2018)

2.2.1 CSP technologies

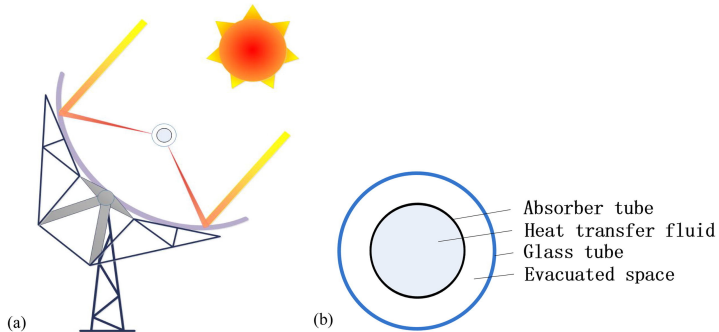
CSP technology includes four variants: Parabolic trough (PT), Linear Fresnel (LF), Solar Tower (ST) and Solar Dish (SD).

Parabolic trough solar collector consists on a reflector to concentrate sunrays in a receiver positioned at the focus line (see Figure 8). The receiver comprises an inner metal-absorber tube and an outer-glass envelope. The annular space between the inner and the outer tubes can be evacuated to reduce energy loss due to convection. In the outer surface of metal absorber a selective coating is applied to increase the solar radiation absorptivity and to reduce the surface emissivity at the infrared spectrum (Jin *et al.*, 2017).

Parabolic trough is the most mature CSP technology, accounting for more than 90 % of the current installed CSP capacity. Most plants in operation have capacities between 14 - 80 MW_e. The annual solar to electricity thermal efficiency ranges between 14 - 16 %. The maximum operation temperature is 390 °C due to the degradation of the synthetic oil. The use of molten salts turns possible to increase the temperature to 550 °C. Currently, the majority of the parabolic systems use synthetic oil

as the heat transfer fluid (IRENA, 2012).

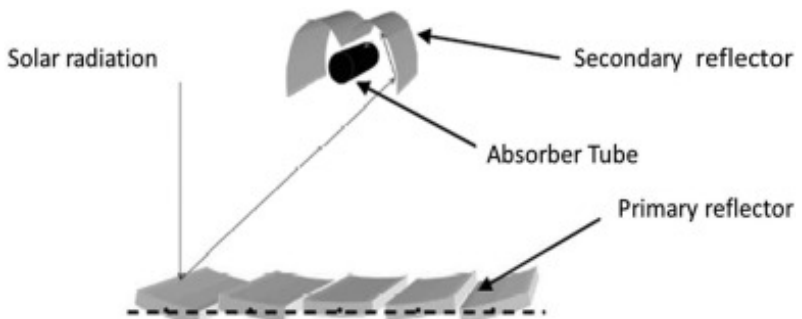
Figure 8 – Parabolic trough solar collector unit and cross section of collector tube



Source: (Jin *et al.*, 2017)

In Figure 9, it is shown the scheme of a Fresnel collector. Linear Fresnel plants are similar to parabolic trough plants but use a series of flat or slightly curved mirrors placed at different angles to concentrate the sunlight onto a fixed linear receiver, located some meters above the mirrors. A single axis tracking system orientate the parallel mirrors to concentrate the sunlight onto the fixed receiver during sunny hours. The receiver consists on a tube where flowing water is converted into saturated steam (Direct Steam Generation, DSG).

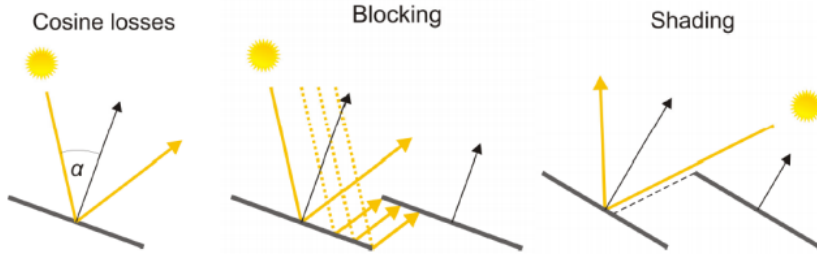
Figure 9 – Fresnel collector representation



Source: (Bendato *et al.*, 2016)

The linear Fresnel is not a mature technology in terms of global capacity installed (IRENA, 2012). The Linear Fresnel is a technology with an important potential to reduce the levelized cost of electricity (LCOE) in concentrating solar power. It is due to several facts such as mirrors are narrow and easy to manufacture, the supporting structures are light, the wind effects are not important compared to other technologies, there is no need for rotating joints, the land requirement is lower, among others aspects. Thereby, the installation costs for the same solar aperture area are between 20 - 30 % lower for LF than PT (Beltagy *et al.*, 2017). However, parabolic trough can reach higher efficiency compared to linear Fresnel. It is due to the Fresnel collector's optical efficiency is lower than parabolic trough due to the optical losses caused by cosine losses, blocking and shading. The Figure 10 shows the typical losses presented in the Fresnel collectors (Feldhoff, 2012).

Figure 10 – Cosine optical losses (left), blocking (center) and shading (right)



Source: (Feldhoff, 2012)

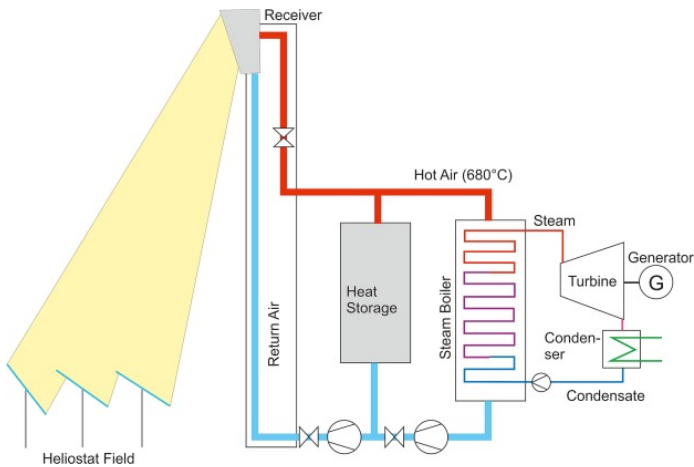
The fact that the receiver in a Fresnel collector is fixed and it is not connected to moving parts of the collector turns this technology indicated to implement the technology DSG (ENERMENA, 2014). DSG represents an important alternative to the existing Heat Transfer Fluid (HTF) (such as molten salt and oil). It uses water to feed the plant and convert it into steam to be used in an industrial process or in a steam turbine (Chiarappa, 2015).

In this context, DSG technology is an important option to reduce the costs related to the heat exchangers. However, the two-phase heat transfer fluid in DSG solar plants is a major challenge, and innovative Thermal Energy Storage (TES) concepts and new

integration solutions are required (Valenzuela, 2017).

Solar tower technology is based on a heliostat field which concentrates the direct normal irradiance onto a central receiver placed on the top of a tower. The solar field consists on thousands or even several tens of thousands of heliostats around the central tower that can be placed over 1 km far away from the receiver (Polo *et al.*, 2016). The Figure 11 shows a solar tower plant using air as a HTF.

Figure 11 – Solar Tower plant



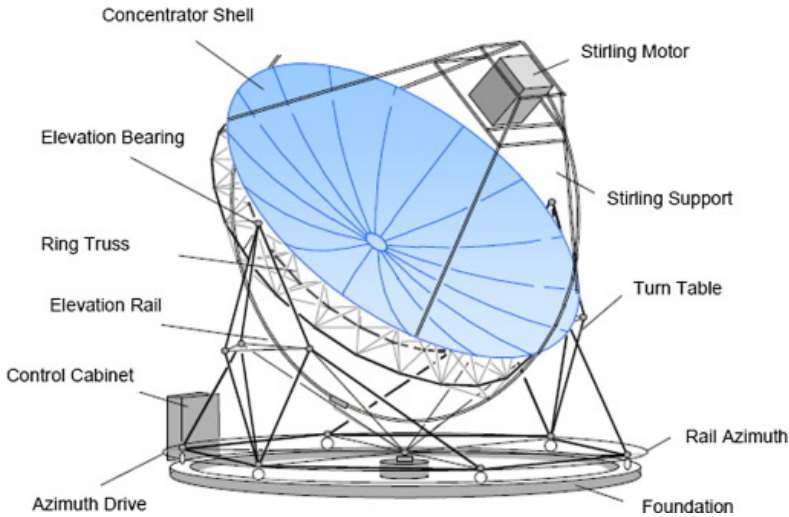
Source: (Polo *et al.*, 2016).

Solar tower plants can use water/steam (DSG), synthetic oil, molten salts and air as the primary heat transfer fluid. As already mentioned, DSG technology eliminates the need for the heat exchangers between the primary heat transfer fluid (e.g. molten salt or oil), and the steam cycle, but thermal storage capacity is limited. Depending on the primary heat transfer fluid and the receiver design, maximum operating temperatures may range from 250 - 550 °C (using water/steam) to 390 °C (using synthetic oil) and up to 565 °C (using molten salt). Temperatures above 800 °C can be obtained using air as HTF. Additionally, due to the higher temperatures, the annual thermal efficiency of tower systems plants tend to be higher compared to parabolic trough and linear Fresnel plants (IRENA, 2012).

Parabolic Dish system consists on a parabolic reflector in

the form of a dish with a supporting structure. A Stirling engine mounted in the focus of the parabolic dish receives solar radiation, and a generator generates electrical energy. Solar parabolic dishes are directed toward the sun throughout the day using a two-axis tracking control system (Hafez *et al.*, 2016). The typical temperature range of this concentrator is between 100 - 1500 °C. This technology is generally used in steam generators and other devices that require high temperatures (Prado *et al.*, 2016). The Figure 12 shows the scheme of a parabolic dish collector.

Figure 12 – Parabolic dish

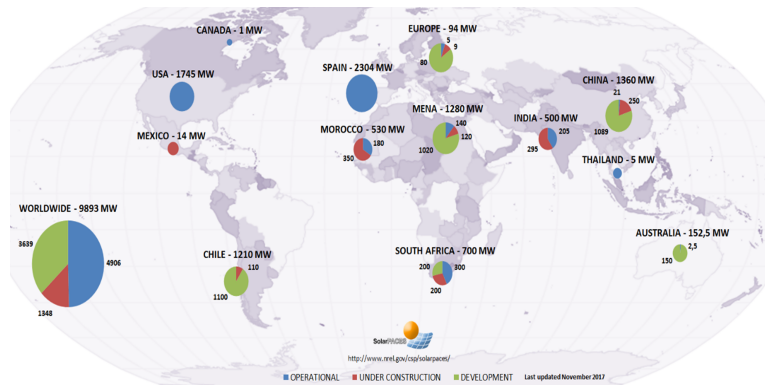


Source: (Hafez *et al.*, 2016).

2.2.2 CSP in the world

The distribution of CSP capacity around the world under the status of operational, under construction and under development is presented at Figure 13. Currently, the total installed capacity is 4.8 GW. Spain represents by 48 % of the total capacity, followed by USA that represents around 36 %.

Figure 13 – CSP projects around de world



Source: (SolarPACES, 2017)

The interest in CSP technologies has been growing over the past ten years. A number of new plants have been brought on line since 2006 as a result of declining investment costs and Levelized Cost of Electricity (LCOE), as well as new support policies. In the first years CSP technology was focused entirely on parabolic trough. However, the markets have been balancing between PT and the other CSP technologies (Ren21, 2016).

As already mentioned, CSP is a relatively immature technology compared to solar photovoltaic (PV) technology. The total worldwide installed CSP capacity exceeded 1000 MW in late 2011 (IRENA, 2012). By late 2013, it had more than doubled to around 3000 MW (NREL, 2013), and it reached almost 4800 MW at the end of 2015 (Ren21, 2016). On the other hand, PV systems have had a continued growth during the last years. Thus, the worldwide installed capacity exceeding 67 GW in 2011 (IRENA, 2012) and reaching about 227 GW at the end of 2015 (Ren21, 2016).

2.2.3 CSP cost

Generally, the electricity from CSP technology has higher costs than other renewable generation options. However, CSP could have a bright future due to its significant potential to reduce the current costs (Ren21, 2016). In Table 3, it is shown the Levelized Cost of Electricity (LCOE) of the existing plants in each region of the world.

Table 3 – Average LCOE of existing plants in the world

| Levelized Cost of Electricity | | |
|-------------------------------|----------------------|---------------------------------|
| Region | LCOE range [USD/kWh] | LCOE weighted average [USD/kWh] |
| Asia | 0.2 to 0.37 | 0.22 |
| Europe | 0.2 to 0.49 | 0.33 |
| Middle East | 0.19 to 0.28 | 0.24 |
| North America | 0.25 to 0.55 | 0.29 |
| India | 0.2 to 0.36 | 0.23 |

Source: (Ren21, 2016)

The solar field is the most expensive part of a CSP plant. Typically, it represents about 30 - 40 % of the total plant cost. In this regard, it is important to optimize collector design, performance and cost. The LCOE is an index used for evaluating different plant designs and technologies. It is widely used to evaluate the most cost-effective energy production technologies (Boubault *et al.*, 2016).

The LCOE can be reduced in two ways: 1) by lowering capital or the Operation and Maintenance (O&M) costs, and 2) by increasing annual performance. It gets clear, also, that LCOE is reduced when solar irradiance is higher. The capital equipment for CSP plant involves solar components (i.e., collector field, heat transfer piping, and TES system) and conventional thermodynamic power-cycle components (pumps, steam turbine, generator). Decreasing capital and operating cost can be achieved by technology advances and increased manufacturing volume and supply chain efficiency (NREL, 2016).

The operation and maintenance cost of CSP plants are low compared to fossil fuel power plants. The O&M includes costs of mirror washing, plant insurance, among others. These costs can be between 0.5 - 1 % of the initial capital cost. Technological improvements have reduced the requirement to replace mirrors and receivers. Automation can be reduced the cost of O&M by about 30 % (Blanco & Santigosa, 2016).

Finally, according to (NREL, 2016) substantial cost reduction for CSP plants can be expected by 2020. Thereby, the LCOE for

parabolic trough systems could decline between 38 - 50%. It is due to improvements in performance and capital cost reduction. The LCOE of solar tower projects could decline between 30 - 50 % by 2020.

2.2.4 Concentrated solar power hybridization

One of the major drawbacks of power generation in concentrated solar power plants is the discontinuous availability of the solar resource at the plant allocation. A useful strategy to overcome this problem is the hybridization of this technology with fossil fuels or biomass. Thereby, solar hybridization may be beneficial from a thermodynamic point of view, using solar power to produce saturated steam, the solar fraction up to about 17 - 20 % which leads a substantial saving of fossil fuel and a reduction of CO₂ emissions (Sánchez *et al.*, 2016).

Natural gas is frequently used as auxiliary fuel due to its low cost, clean combustion and rapid response, although the use of oil, mineral coal and biomass have also been reported. The minimum amount of auxiliary energy required to operate a commercial CSP installation varies depending on plant size and design, the intensity and daily hours of solar irradiance, ambient temperature, among others. (San Miguel & Corona, 2014). CSP hybridization can be performed by modifying an existing plant or designing an original one. Usually, there is more flexibility in designing and optimizing a new system. For design purposes, particular stationary conditions for solar irradiance and ambient temperature are adopted in order to calculate the solar area based on the particular requirements. (Pantaleo *et al.*, 2017).

Finally, CSP technology can be readily integrated into a convectional system, which has many potential benefits including increased dispatchability and reliability, improved efficiency, reduced CO₂ emissions and the opportunity for flexible operation by alternating between energy sources. Hybridized CSP plants present different types and levels of synergy, depending on the hybrid energy source, the location of the plant, the CSP technology used, and the plant configuration (Powell *et al.*, 2017).

A list of hybrid CSP projects around the world is presented at Table 4. As it can be observed, most cases are related to the integration of solar energy with fossil fuels. The Borges Termosolar can be mentioned as the only hybrid power plant with biomass.

Table 4 – Hybrid CSP projects around the world.

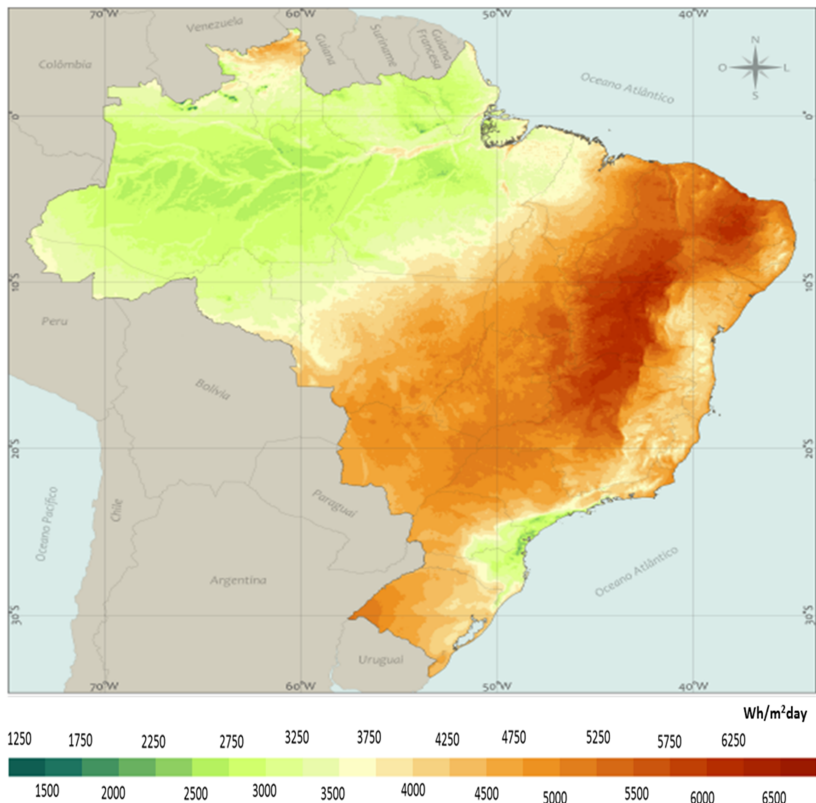
| CSP | Plant name | Fuel | MW | Location | Status |
|------------------|-----------------------------------|-------------|------|-----------|---------------------------|
| Linear Fresnel | ISCC Hassi R'mel | Natural gas | 20 | Algeria | Operational |
| Linear Fresnel | Kogan Creek | Natural gas | 44 | Australia | Under construction |
| Linear Fresnel | Liddell Power Solar boost | Coal | 9 | Australia | Currently non-operational |
| Parabolic trough | City of medicine hat ISSC project | Coal | 1 | Canada | Operational |
| Linear Fresnel | Mejillones | Coal | 5 | Chile | Planed |
| Parabolic trough | Agua Prieta II | Natural gas | 14 | Mexico | Under construction |
| Parabolic trough | Ain Beni Mathar | Natural gas | 20 | Morocco | Operational |
| Parabolic trough | Archimede | Natural gas | 4.72 | Italy | Operational |
| Parabolic trough | Borges Termosolar | Biomass | 22.5 | Spain | Operational |
| Tower | Solugas | Natural gas | 4.72 | Spain | Operational |
| Tower | Karaman | Natural gas | 50 | Turkey | Under construction |
| Parabolic trough | Colorado integrated solar project | Coal | 2 | USA | Currently non-operational |
| Parabolic trough | Marin integration | Natural gas | 75 | USA | Operational |
| Parabolic trough | Palmdale | Natural gas | 50 | USA | Planed |

Source: (SolarPACES, 2017)

2.3 THE BRAZILIAN SOLAR POTENTIAL

Brazil is privileged in terms of solar radiation. In Figure 14, it is shown the average daily DNI incidence in Brazil. As it can be seen, the highest rates are observed in the Northeast region, varying between 2,080 kWh/m²-year and 2,226 kWh/m²-year, what is similar to 2,100 kWh/m²-year level found in the South Spain. In the state of Santa Catarina DNI incidence levels are between 1,400 kWh/m²-year and 1,700 kWh/m²-year (ATLAS, 2017). In the same way, the availability of natural gas makes possible the use of the hybrid systems as an option for supporting the conventional energy sources.

Figure 14 – Average daily DNI in Brazil



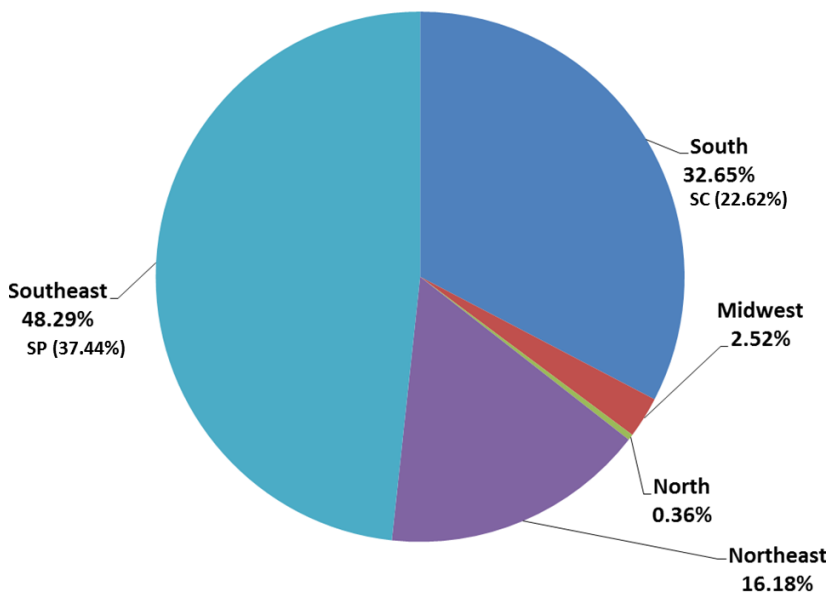
Source: (ATLAS, 2017)

2.4 THE BRAZILIAN TEXTILE SECTOR

In Figure 15, it is shown the region's participation in the Brazilian textile sector. As it can be seen, the main producing regions are southeast (48.29 %) and south (32.65 %). Particularly, Sao Paulo (36.4 %) and Santa Catarina (22.6 %) are the main productive states in the Brazilian textile sector. In the Northeast, the most representative states are Ceará (4.0 %), Bahia (3.6 %), Paraíba (2.6 %) and Rio Grande do Norte (2.1 %).

In Santa Catarina the textile industry represents about 17.74 % of the industrial sector in the state. The main industrial points are located in Blumenau, Joinville and Brusque.

Figure 15 – States participation in the Brazilian textile sector



Source: Adapted from IBGE (2017)

At Table 5, it is shown participation data of different sources in the energy supply in the Brazilian textile sector since the year 2010. Particularly, natural gas had have an average participation by 28 %. In the same way, the electricity participation have grown during the last years.

Table 5 – Energy sources participation in the Brazilian textile sector

| Sources | 2010 | 2011 | 2012 | 2013 | 2014 | 2015 | 2016 |
|-----------------|------|------|------|------|------|------|------|
| Natural gas [%] | 27.1 | 27.2 | 28.4 | 28.4 | 24.3 | 24.0 | 23.4 |
| Firewood [%] | 7.6 | 6.3 | 6.5 | 6.5 | 6.8 | 6.9 | 7.0 |
| Fuel oil [%] | 5.3 | 4.6 | 4.1 | 4.1 | 3.3 | 2.1 | 1.8 |
| Electricity [%] | 58.9 | 58.9 | 57.8 | 57.7 | 61.1 | 62.6 | 63.8 |
| Other [%] | 1.1 | 3.0 | 3.2 | 3.3 | 4.4 | 4.3 | 4.0 |
| Total [%] | 100 | 100 | 100 | 100 | 100 | 100 | 100 |

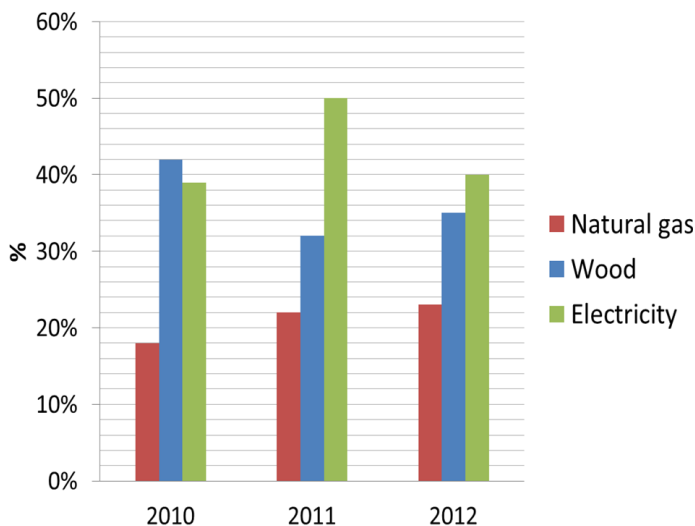
Source: Adapted from BEB (2017)

The energy efficiency is considered an important aspect in the textile sector. According to BEU (2009) there is a potential to improve energy efficiency at various stages of the textile chain in Brazil. In 2009, it was calculated a potential energy conservation for the Brazilian textile by 22 % of the total energy used in the sector. In this regard, optimization of existing equipment and the minimization of waste energy have a large potential in the Brazilian textile industry, especially in small and medium-sized plants. Therefore, it is important to carry out actions that allow to reduce the energetic losses in the textile sector. However, there are some barriers to the implementation of energy efficiency actions in the textile industry such as:

- **Information and professional training:** Some companies do not have information about energy efficiency and the financial and environmental benefits that it could provide.
- **Other priorities:** A lot of companies put at the second level possible actions of energy efficiency.
- **Economic problems:** Generally, the cost associated to energy efficiency are high.
- **Lack of incentives:** There are no clear incentives from the federal government to encourage companies to implement energy efficiency actions.

During the year 2012, the textile sector was responsible for a 5 % of the total energy consumption in the industrial sector Santa Catarina, electricity and biomass were the main energy sources with a participation by 41 % and 36 %, respectively. Natural gas was the third energy source by 23 % (BESC, 2013). The Figure 16 shows the participation of electricity, natural gas and biomass sources in the energy consumption in the textile sector in Santa Catarina. Particularly, the natural gas consumption has gradually increased.

Figure 16 – Energy sources participation in the textile industry in Santa Catarina

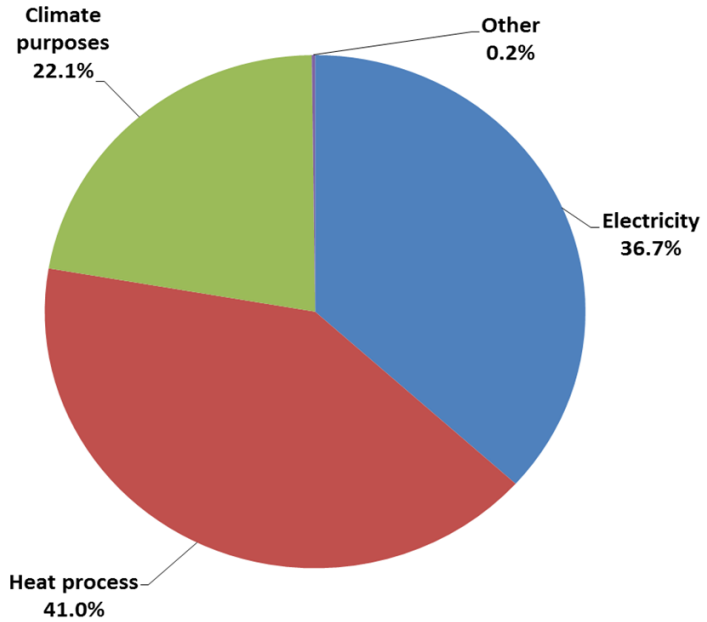


Source: Adapted from BESC (2013)

In Figure 17, it is shown the percentage distribution of the energy consumption in the Brazilian textile industry during the year 2009. As it is shown, the heat process (i.e., energy used in steam generators, water heating, among others) was the main energy consumption representing a 41 %. Electricity (i.e., energy used in textile machinery, energy used for lighting, among others), represented a 36.7 %. Climate purposes (i.e., energy used in refrigerators, freezers, refrigeration and air conditioning equipment, either compression cycle or absorption cycle), represented a 22.1 %. Other (i.e., energy used in computers,

telecommunications), represented a 0.2 %.

Figure 17 – Energy consumption in the Brazilian textile industry during the year 2009



Source: Adapted from Santana & Bajay (2010)

Chapter 3

PROPOSED SCENARIOS

3.1 INTRODUCTION

In this chapter are presented the proposed scenarios to be implemented for supplying the typical demands of saturated steam, electricity and chilled water of a medium-size plant in the sector textile in Santa Catarina.

In the section 3.2, it is presented the reference scenario in which the electrical demand is imported from the grid, the steam demand is produced by a natural gas steam generator and the chilled water demand is supplied by electric chillers.

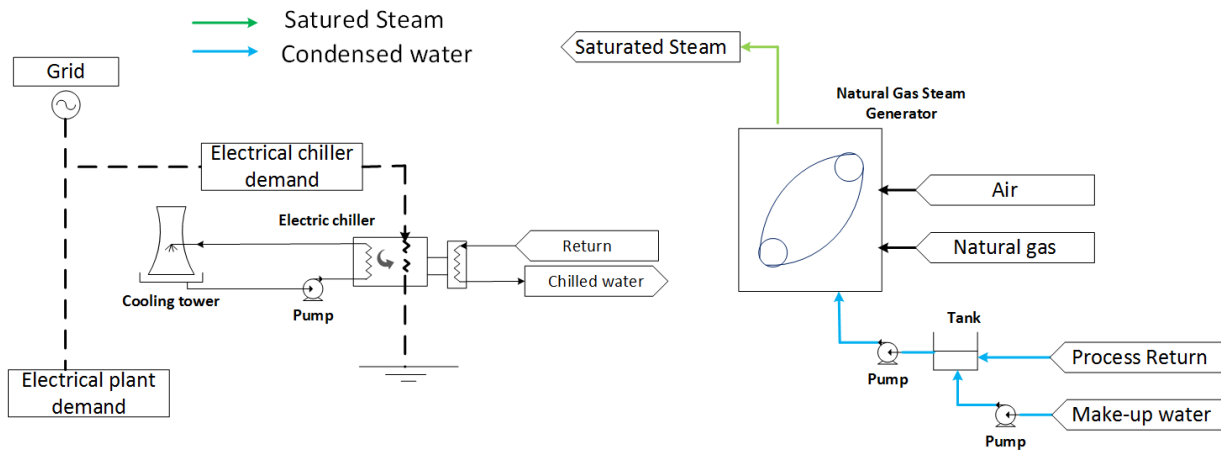
In the section 3.3, as an alternative scenario is proposed a cogeneration plant based on an internal combustion engine in order to supply the electrical and thermal demands. The exhaust gas is directed to a HRSG for producing saturated steam. Finally, taking advantage of the residual heat of the exhaust gas and the heat of the water's engine radiator is produced chilled water in an absorption chiller.

Finally, in the section 3.4, a solar-aided cogeneration plant is proposed. It consists on the integration of a solar Fresnel field into the cogeneration plant to produce directly saturated steam in order to reduce the fuel consumption and consequently the CO₂ emissions.

3.2 BASE CASE SCENARIO

The base case scenario represents the typical scheme used in the medium-size plants in the textile sector in Santa Catarina for supplying the thermal and electrical demands. In this context, the electrical plant demand (i.e., textile machines, lighting, offices, among others) and the electric chiller demand are imported from the grid. The electric chillers are used to produce chilled water for air conditioning purposes. Finally, the natural gas steam generator is used to attend the saturated steam demand. The plant layout for the base case scenario is shown at Figure 18.

Figure 18 – Base case scenario layout



3.3 COGENERATION PLANT SCENARIO

As mentioned earlier, the first alternative to supply the thermal and electrical demands of a medium-size plant in the textile sector is a cogeneration plant. In Figure 19, it is shown the layout of the proposed plant.

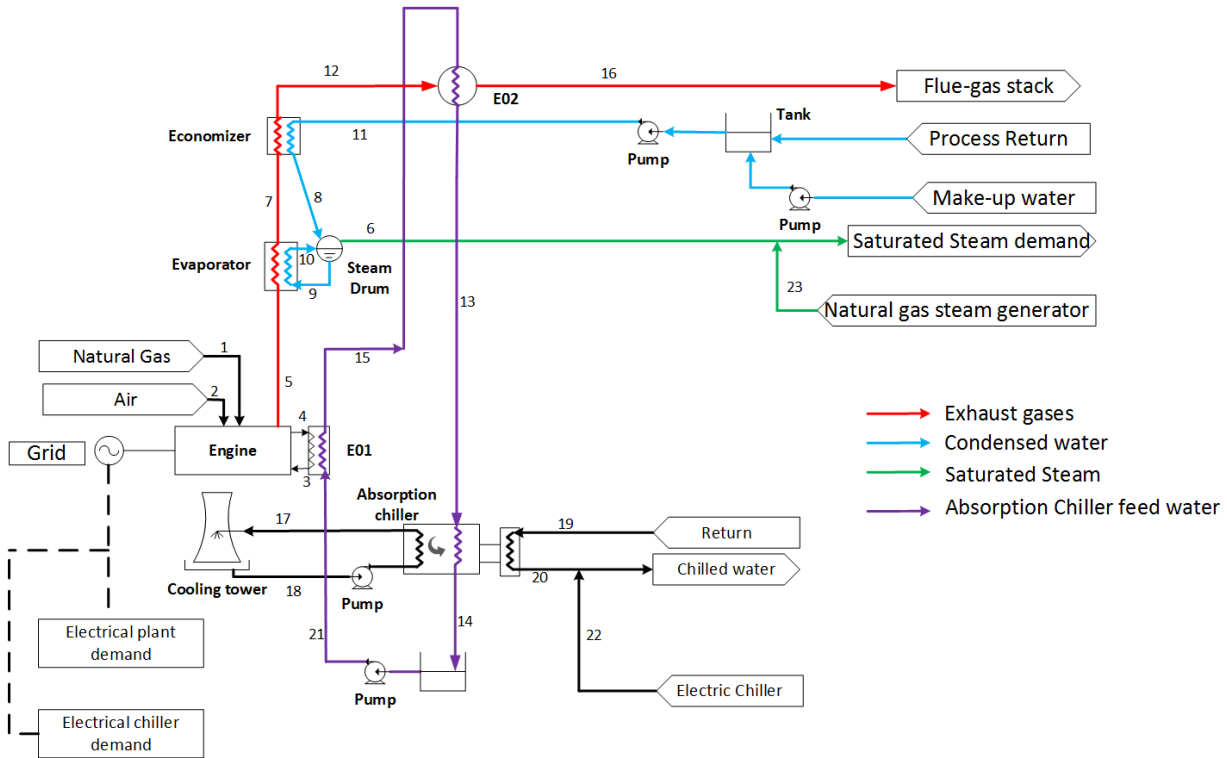
The proposed cogeneration plant uses a natural gas engine, an absorption chiller and a HRSG in order to attend the thermal and electrical demands. The technical features are imported from a database available by manufactures.

As it can be observed at Figure 19, natural gas (1) and combustion air stream (2) are fed into the engine for generating electricity to supply the electrical demand. The thermal energy associated to the exhaust gas (5) is used for producing saturated steam in the HRSG (6). Technical data related to typical steam pressure in the textile sector is considered. In the same way, pinch point and approach point temperatures are taken into account according to technical literature. Finally, the saturated steam demand is complemented by the existing natural gas steam generator (23).

On the other hand, the heat coming from the engine's water radiator is transferred to an internal hot water circuit through the heat exchanger (E01) taking into account that the temperature at the point (15) can not be higher than the temperature at point (4). Subsequently, it is heated up in the heat exchanger (E02) with the remnant thermal energy of the exhaust gas leaving the economizer (12) taking into account that the temperature at the flue-gas stack (16) cannot be lower than 120 °C due to the water vapor content of the waste gases could condense causing corrosion problems. The heated water (13) is used by the absorption chiller in order to produce chilled water (20). Finally, the chilled water demand is complemented by the existing electric chillers (22).

The proposed cogeneration plant modeling is shown at Chapter 4.

Figure 19 – Proposed cogeneration plant layout



3.4 SOLAR-AIDED COGENERATION PLANT SCENARIO

The second alternative to supply the thermal and electrical demands of a medium-size plant in the textile sector is a solar-aided cogeneration plant taking advantage of the availability of the solar resource. The solar-aided cogeneration plant layout is shown at Figure 20.

The proposed solar-aided cogeneration plant consists on the integration into the proposed cogeneration plant of a solar field based on linear Fresnel collector for producing saturated steam (DSG).

The water returning from the process is pumped to the steam drum. Subsequently, the water passes trough of the solar field absorbing latent heat during the sunny hours (25). The saturated steam produced by the solar field (24) is used to supply the steam demand. In the same way, the existing natural gas steam generator (23) and the HRSG (6) complement the steam demand.

The proposed solar system is analyzed during a typical meteorological year for the city of Florianopolis as an approximation of the solar resource in Santa Catarina. The models implemented to reproduce the solar field operation are presented at Chapter 5.

3.5 THERMODYNAMIC ANALYSIS

In this section are presented the thermodynamic indexes used to evaluate the thermal performance of the proposed scenarios.

The thermal efficiency of the cogeneration plant (η_{cog}) is defined as the ratio of the total amount of energy delivered by the steam generator and cogeneration plant, divided by the total energy available from natural gas. It is calculated based on Equation 3.1.

$$\eta_{cog} = \frac{W_{engine} + Q_L + Q_{HRSG} + Q_{boiler}}{E_{th,engine} + E_{th,boiler}} \quad (3.1)$$

where W_{engine} [kWh/year] is the annual electricity generated by the internal combustion engines, Q_L [kWh/year] is the annual refrigeration load delivered by the absorption chiller, Q_{HRSG} [kWh/year] is the annual heat delivered by the HRSG, Q_{boiler} [kWh/year] is the annual heat delivered by the steam generator, $E_{th,engine}$ [kWh/year] and $E_{th,boiler}$ [kWh/year] are the annual natural gas energy input to the engines and steam generator, respectively.

The thermal efficiency of the solar-aided cogeneration plant is defined as the rate of the total amount of energy delivered by the steam generator, solar field and cogeneration plant, divided by the total energy available from natural gas and solar resource. It is defined by Equation 3.2.

$$\eta_{hib} = \frac{W_{engine} + Q_L + Q_{HRSG} + Q_{boiler} + Q_{solar}}{E_{th,engine} + E_{th,boiler} + DNI \cdot A_{solar}} \quad (3.2)$$

where Q_{solar} [kWh/year] is the annual heat delivered by the solar field, DNI [kWh/m²-year] is the direct normal irradiation and A_{solar} [m²] is the solar field area.

The annual fuel economy is found according to Equation 3.3.

$$V_{eco,a} = \sum_{year} (\dot{V}_{cs,i} - \dot{V}_{hs,i}) \quad (3.3)$$

where $\dot{V}_{cs,i}$ [m³/h] is the hourly natural gas consumption by convective system and $\dot{V}_{hs,i}$ [m³/h] is the hourly natural gas consumption by the hybrid system.

An important parameter considered in hybrid system is the Solar Fraction (SF). According to Duffie & Beckman (1991) the solar fraction is defined as a ratio between the fuel economized due to the integration of the solar system and the total fuel consumption by the conventional system (without taking account the integration of the solar field). Generally, it is calculated monthly and annually according to Equations 3.4 and 3.5, respectively.

$$SF_m = \sum_{month} \frac{\dot{V}_{eco,i}}{\dot{V}_{cs,i}} \quad (3.4)$$

$$SF_a = \sum_{year} \frac{\dot{V}_{eco,i}}{\dot{V}_{cs,i}} \quad (3.5)$$

where \dot{V}_{eco} [m^3/h] is the hourly natural gas economized due to the integration of the solar field and \dot{V}_{cs} [m^3/h] is the hourly natural gas consumption by conventional system (cogeneration plant).

The solar field thermal efficiency is defined as the rate of the heat absorbed by the fluid, divided by the total energy coming from the solar resource. It can be calculated hourly and annually according to Equations 3.6 and 3.7, respectively.

$$\eta_{thermal,h} = \frac{Q''_{solar}}{G_{bn}} \quad (3.6)$$

$$\eta_{thermal,a} = \sum_{year} \frac{Q''_{solar,i}}{DNI} \quad (3.7)$$

where DNI [$\text{kWh}/\text{m}^2\text{-year}$] is the direct normal irradiation, Q''_{solar} [kW/m^2] is total heat absorbed by the water and G_{bn} [kW/m^2] is the hourly direct normal irradiance.

3.6 ECONOMIC ANALYSIS

In this work, the economic feasibility of the proposed plants is performed by calculating the net present value, the internal rate of return and the payback period of the investments.

3.6.1 Net present value

The net present value compares the amount invested today to the present value of the future cash receipts from the investment.

In other words, the amount invested is compared to the future cash inflow. Thus, the NPV is calculated according to Equation 3.8.

$$NPV = \left(\frac{CF_1}{(1+i)^1} + \frac{CF_2}{(1+i)^2} + \frac{CF_3}{(1+i)^3} + \dots + \frac{CF_m}{(1+i)^m} \right) - I_{ini} \quad (3.8)$$

where i [%] is the interest rate, CF_m [USD] is the net cash inflow at period m , I_{ini} [USD] is the initial investment.

3.6.2 Internal rate of return

The internal rate of return is the interest rate at which the net present value of the future cash inflow (both positive and negative) and the initial investment are equal to zero. Thus, the IRR is defined by Equation 3.9.

$$0 = \left(\frac{CF_1}{(1+i)^1} + \frac{CF_2}{(1+i)^2} + \frac{CF_3}{(1+i)^3} + \dots + \frac{CF_m}{(1+i)^m} \right) - I_{ini} \quad (3.9)$$

where i [%] is the interest rate, CF_m [USD] is the net cash inflow at period m and I_{ini} [USD] is the initial investment.

3.6.3 Payback period

The payback period is the time required to recover the cost of an investment. It has many advantages such as, it is very simple to calculate, it is helpful to analyze risk (i.e., allows to determine how long the investments will be at risk). However, it has some disadvantages such as, it does not take into account, the cash inflow that occur after the payback back. In the same way, it does not take into account the time value of money. In order to reduce this drawback, in this work, it is considered the time value of the money by calculating its present value according to Equation 3.10.

$$P_{value} = \frac{CF_m}{(1+i)^m} \quad (3.10)$$

where CF_m [USD] is the net future value cash inflow at period m , i [%] is the interest rate.

Chapter 4

COGENERATION PLANT MODELING

4.1 INTRODUCTION

The model to perform the operation behavior of the proposed cogeneration plant is based on the first law of thermodynamics. In this way, an energy balance is applied on every component of the cogeneration plant. The energy balances are performed at steady state condition, neglecting the heat losses to the environmental, the kinetic energy and potential energy. Furthermore, the cogeneration plant is simulated considering thermal parity. Thereby, the operation of the internal combustion natural gas engine is considered at nominal conditions.

4.2 NATURAL GAS ENGINE

In this work is proposed a natural gas engine in order to attend the electrical demand taking advantage of natural gas availability in Santa Catarina. Thus, the engine efficiency is calculated according to Equation 4.1.

$$\eta_{engine} = \frac{\dot{W}_{engine}}{LHV \cdot \dot{m}_{fuel,engine}} \quad (4.1)$$

where \dot{W}_{engine} [kW] is the power production, LHV [kJ/kg] is the fuel lower heating value and $\dot{m}_{fuel,engine}$ [kg/s] is the fuel consumption.

Therefore, the annual natural gas consumption is determined by Equation 4.2.

$$C_{fuel,engine} = F_a \cdot \sum_{year} \dot{m}_{fuel,engine,i} \quad (4.2)$$

where F_a is the availability of the plant. In this work is considered a $F_a=95\%$. It is a typical value considered in cogeneration plant using internal combustion engine.

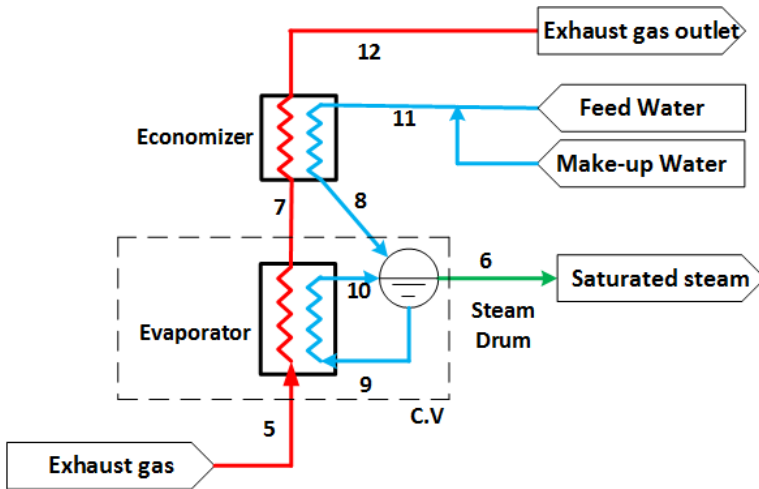
The LHV of natural gas was calculated according to the natural gas composition in Santa Catarina, as it is described in Appendix A.

4.3 HEAT RECOVERY STEAM GENERATOR

The heat recovery steam generator is proposed in order to use the residual heat associated to the exhaust gas for supplying the plant's saturated steam demand. A simplified sketch of the HRSG is shown at Figure 21. Thereby, the feed water is preheated in the economizer (11) before entering into the drum (8). Subsequently, the liquid flows through the evaporator absorbing latent heat from the exhaust gas (9). As a consequence, the steam enthalpy increases (11). Finally, the saturated steam leaves the HRSG to supply the process demand (6).

In this work the gas properties are calculated according to the air properties.

Figure 21 – Scheme of HRSG



Thus, the energy balance at the HRSG is represented by Equation 4.3.

$$\underbrace{\dot{m}_5 h_5 + \dot{m}_8 h_8}_{\text{Total inlet energy}} = \underbrace{\dot{m}_7 h_7 + \dot{m}_6 h_6}_{\text{Total outlet energy}} \quad (4.3)$$

Therefore, the saturated steam mass flow is calculated by

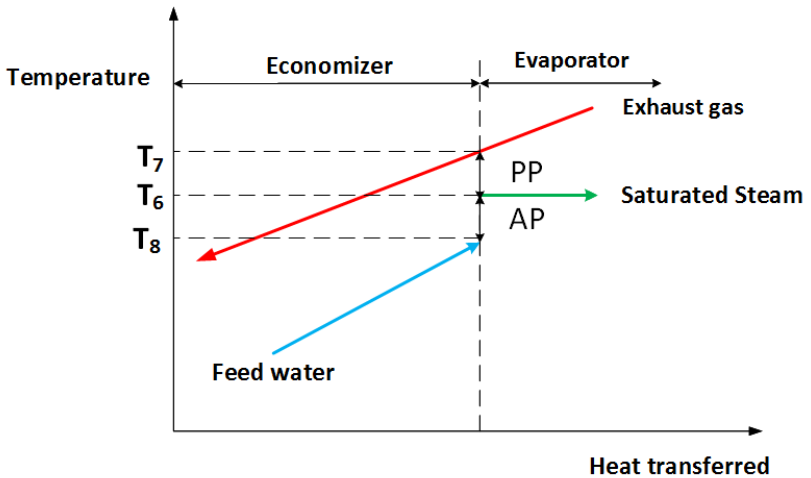
Equation 4.4.

$$\dot{m}_{HRSG} = \dot{m}_6 = \frac{\dot{m}_5 \cdot (h_5 - h_7)}{h_6 - h_8} \quad (4.4)$$

where $\dot{m}_5 = \dot{m}_7$ [kg/s] is the gas mass flow, $\dot{m}_8 = \dot{m}_6$ [kg/s] is the water mass flow, h_5 [kJ/kg] is the gas enthalpy at the engine outlet, h_8 [kJ/kg] (taking into account the approach point temperature) is the water enthalpy at the economizer outlet, h_7 [kJ/kg] (taking into account the pinch point temperature) is the gas enthalpy at the evaporator outlet and h_6 [kJ/kg] is the saturated steam enthalpy (at $P_{sat} = 800$ kPa).

In Figure 22, it is shown flue gas and water temperature profiles in the HRSG.

Figure 22 – Temperature profile at the HRSG.



As mentioned earlier, two parameters are critical at the design phase. These parameters are the approach point and the pinch point. The Pinch Point (PP) temperature is the difference between the temperature of the exhaust gas at the evaporator outlet (T_7) and the saturated steam temperature (T_6). The pinch point temperature difference is an important parameter in the HRSG's operation. It is typically between 8 and 20 K (Wu *et al.*, 2014). If the pinch point temperature is low, the heat exchanger cost would increase. However, the amount of heat recovered from

the exhaust gases to the water is higher. The Approach Point (AP) temperature is the difference between the feed water temperature at the economizer outlet (T_8) and the saturated steam temperature (T_6). This difference is necessary in order to avoid evaporation in the economizer tubes. The approach point temperature typically are between 10 to 20 K (Shah & London, 2014).

In this work, it is considered a water consumption due to the water losses during the textile process. Thereby, the HRSG annual make-up water consumption is determined by Equation 4.5.

$$C_{water,HRSG} = F_a \cdot (1 - F_c) \cdot \sum_{year} \dot{m}_{HRSG,i} \quad (4.5)$$

where \dot{m}_{HRSG} [kg/s] is the hourly saturated steam mass flow, F_a is availability of the plant and F_c is the condensate return rate. In this work is considered a $F_c=80\%$. It represents the typical value found in the textile industries in Santa Catarina.

4.4 ABSORPTION CHILLER

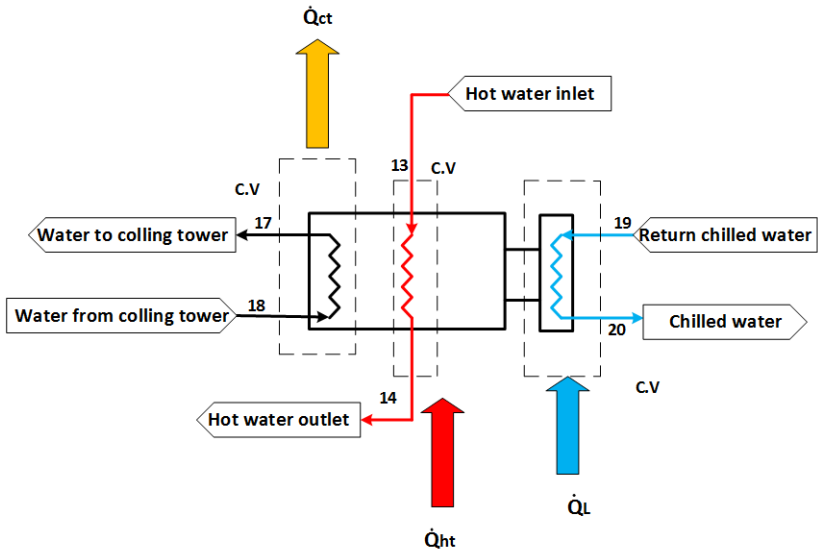
An important index used in regeneration systems is the Coefficient of Performance (COP). It is calculated by Equation 4.6. Particularly, the COP of the single effect chillers are between 0.4 and 0.8. Therefore, these systems consumes an amount of energy higher than its refrigeration production. These systems use thermal energy instead of electric energy. In this work, a single effect hot water absorption chiller is proposed in order to take advantage of the residual heat associated to the exhaust gas and the heat in the engine's water radiator for producing chilled water for air conditioning purposes.

$$COP = \frac{\dot{Q}_L}{\dot{Q}_{ht}} \quad (4.6)$$

where \dot{Q}_L [kW] is the cooling provided by the refrigeration system and \dot{Q}_{ht} [kW] is the heat delivered by the hot water.

In Figure 23, it is shown the energy balance at the absorption chiller.

Figure 23 – Energy balance at the absorption chiller



The system's cooling capacity \dot{Q}_L and the heat delivered by the hot fluid \dot{Q}_{ht} are calculated according to Equations 4.7 and 4.8, respectively. In this work the water properties at the absorption chiller are calculated considering the temperatures at each point delivered by the absorption chiller manufacturer (LG, 2017).

$$\dot{Q}_L = \dot{m}_{cw} \cdot (h_{19} - h_{20}) \quad (4.7)$$

$$\dot{Q}_{ht} = \dot{m}_{ht} \cdot (h_{13} - h_{14}) \quad (4.8)$$

where h_{19} [kJ/kg] (at $T=12$ °C and $P=120$ kPa) represents the enthalpy of the return chilled water, h_{20} [kJ/kg] (at $T=7$ °C $P=120$ kPa) represents the enthalpy of the chilled water, h_{13} [kJ/kg] (at $T=95$ °C and $P=120$ kPa) represents the enthalpy of the how water inlet, h_{14} [kJ/kg] (at $T=72$ °C and $P=120$ kPa) represents the enthalpy of the how water outlet, \dot{m}_{cw} [kg/s] is the chilled water mass flow and \dot{m}_{ht} [kg/s] is the hot water mass flow.

Therefore, the energy balance is determined by Equation 4.9.

$$\dot{Q}_{ct} = \dot{Q}_L + \dot{Q}_{ht} \quad (4.9)$$

where \dot{Q}_{ct} [kW] is the total heat dissipated by the cooling tower.

From this perspective, the cooling tower water mass flow can be calculated by Equation 4.10.

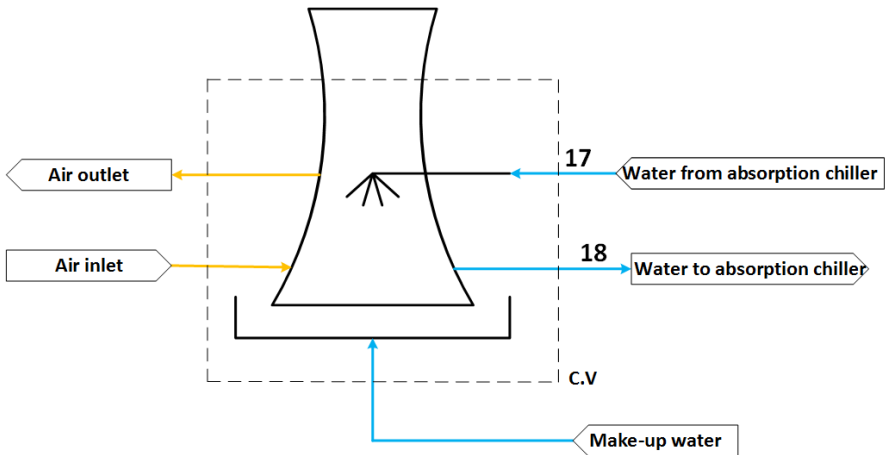
$$\dot{m}_{ct} = \frac{\dot{Q}_{ct}}{(h_{17} - h_{18})} \quad (4.10)$$

where h_{17} [kJ/kg] (at $T=34$ °C and $P=120$ kPa) represents the enthalpy of the water to the cooling tower and h_{18} [kJ/kg] (at $T=29$ °C and $P=120$ kPa) represents the enthalpy of the water from the cooling tower.

4.5 COOLING TOWER

The cooling tower is a heat exchanger in which air and water are brought into direct contact in order to reduce the water's temperature. Consequently, a small volume of water is evaporated. In this sense, the make-up water mass flow is adjusted in order to replace the evaporated water carried by the air. The basic scheme of the cooling tower is represent at Figure 24.

Figure 24 – Cooling tower scheme



The energy balance and the water mass balance at the colling

tower are determined by Equations 4.11 and 4.12, respectively.

$$\underbrace{\dot{m}_{17}h_{17} + \dot{m}_{air,in}h_{air,in} + \dot{m}_{mk}h_{mk}}_{\text{Total inlet energy}} = \underbrace{\dot{m}_{air,out}h_{air,out} + \dot{m}_{18}h_{18}}_{\text{Total outlet energy}} \quad (4.11)$$

$$\underbrace{\dot{m}_{air,in}\omega_{in} + \dot{m}_{mk}}_{\text{Total water mass inlet}} = \underbrace{\dot{m}_{air,out}\omega_{out}}_{\text{Total water mass outlet}} \quad (4.12)$$

where $\dot{m}_{air,in} = \dot{m}_{air,out}$ [kg/s] is the air mass flow, $\dot{m}_{17} = \dot{m}_{18}$ [kg/s] is the water mass flow, \dot{m}_{mk} is the make-up water mass flow, $h_{air,out}$ [kJ/kg] (at T=30 °C) is the air outlet enthalpy, $h_{air,in}$ [kJ/kg] (at T=25 °C) is the air inlet enthalpy, ω_{in} [kgH₂O/kg_{air}] (at T=25°C and $\phi_{air,in}=0.7$) is the inlet absolute humidity and ω_{out} [kgH₂O/kg_{air}] (at T=30°C and $\phi_{air,out}=1.0$) is the outlet absolute humidity .

Therefore, the air mass flow and the annual cooling tower make-up water consumption are calculated by Equations 4.13 and 4.14, respectively.

$$\dot{m}_{air} = \frac{\dot{m}_{17} \cdot (h_{17} - h_{18}) + \dot{m}_{mk}h_{mk}}{h_{air,out} - h_{air,in}} \quad (4.13)$$

$$C_{water,mk} = F_a \cdot \sum_{year} \dot{m}_{air,i} \cdot (\omega_{out} - \omega_{in}) \quad (4.14)$$

4.6 STEAM GENERATOR

In the proposed cogeneration plant is considered an existing natural gas steam generator in order to complement the saturated steam demand. The steam generator thermal efficiency is defined by Equation 4.15.

$$\eta_{boiler} = \frac{\dot{Q}_{steam}}{\dot{Q}_{total}} \quad (4.15)$$

where \dot{Q}_{steam} and \dot{Q}_{total} are defined by Equations 4.16 and 4.17, respectively.

$$\dot{Q}_{steam} = \dot{m}_{steam} \cdot (h_{23} - h_{11}) \quad (4.16)$$

$$\dot{Q}_{total} = LHV \cdot \dot{m}_{fuel,boiler} \quad (4.17)$$

where \dot{m}_{steam} [kg/s] is the saturated steam mass flow, h_{23} [kJ/kg] (at $P_{sat}=800$ kPa) is the saturated steam enthalpy, h_{11} [kJ/kg] (at $T=60$ °C) is the feed water enthalpy, LHV [kJ/kg] is the lower heating value and $\dot{m}_{fuel,boiler}$ [kg/s] is fuel consumption.

Therefore, the annual fuel consumption and the annual make-up water consumption by the steam generator are defined by Equations 4.18 and 4.19, respectively.

$$C_{fuel,boiler} = \sum_{year} \left(\frac{\dot{m}_{steam,i} \cdot (h_{23} - h_{11})}{LHV \cdot \eta_{boiler,i}} \right) \quad (4.18)$$

$$C_{water,boiler} = (1 - F_c) \cdot \sum_{year} m_{steam,i} \quad (4.19)$$

where $\dot{m}_{steam,i}$ [kg/s] is the saturated steam mass flow, $\eta_{boiler,i}$ is the boiler efficiency, and F_c is a condensate return rate.

In this work, it is used the boiler operation efficiency curve delivered by Showers (2002) in order to calculate the boiler's efficiency at part load. It is shown in the Appendix B.

Chapter 5

LINEAR FRESNEL SOLAR FIELD MODELING

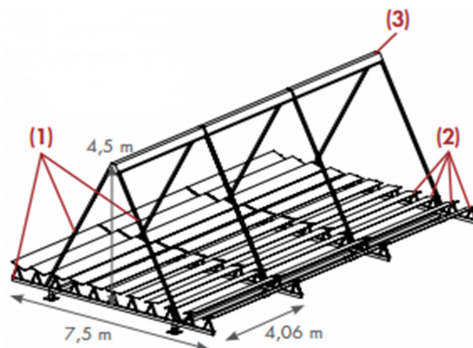
5.1 INTRODUCTION

The models implemented to identify the thermodynamic and the optical performance of the Fresnel solar field are calculated incorporating the variation of the solar irradiance by a Typical Meteorological Year (TMY) by hourly intervals. The model of solar collectors considered is based on the Fresnel technology provided by the German company Industrial Solar.

5.2 MAIN COMPONENTS

The solar linear Fresnel collector is a linear focusing solar system for generating process heat in the range of 100 kW_t to 10 MW_t at pressures up to 120 bar and temperatures up to $400 \text{ }^\circ\text{C}$ (Industrial Solar, 2017). The main components of the systems are shown at Figure 25.

Figure 25 – Scheme of Fresnel collector



Source: (Industrial Solar, 2017)

- (1) Supporting Structure (2) Primary Reflectors (3) Receiver, consisting on secondary reflectors and vacuum tubes.

According to Industrial Solar (2017) the basic module consists

on primary reflector units with a total mirror area of 22 m^2 and one receiver unit. In Table 6, it is shown the dimensional and technical characteristics of each module.

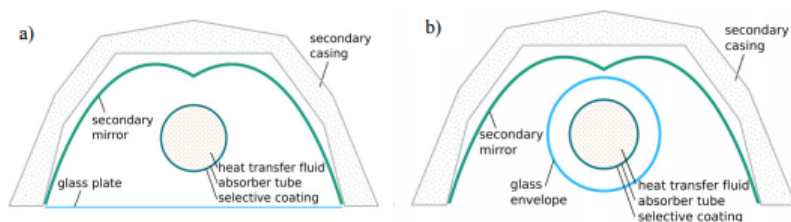
Table 6 – Characteristics of each module

| General data of basic module | |
|--|---------------------|
| Module width | 7.5 m |
| Module length | 4.06 m |
| Aperture surface of primary reflectors | 22 m^2 |
| Receiver height above primary reflector | 4.0 m |
| Height of primary reflector above ground level | 0.5 m |
| Specific weight (related to installation surface area) | 27 kg/m^2 |
| Maximum operational wind speed | 100 km/h |
| Life expectancy | +20 years |

Source: (Industrial Solar, 2017)

The linear Fresnel collector receiver consists on an absorber tube and a secondary concentrator (see Figure 26).

Figure 26 – Linear Fresnel collector receiver protected with a glass plate b) glass tube)



Source: (Heimsath *et al.*, 2014a)

In order to reduce heat losses, the absorber is usually either the bottom of the cavity is covered with a gas plate (shown at Fig.

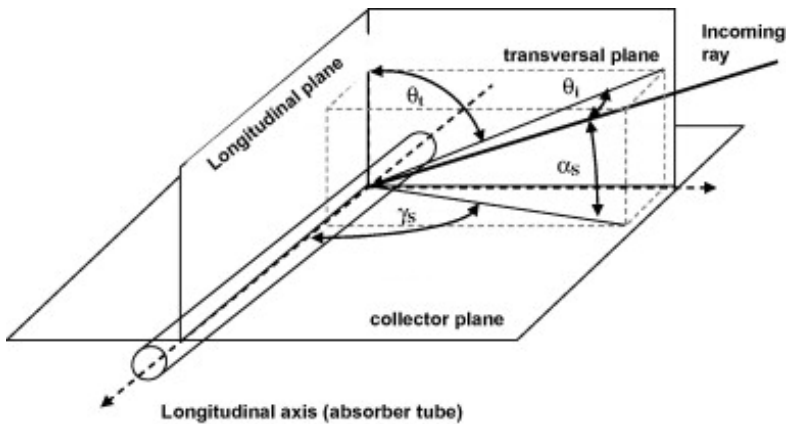
26.a) or protected with a gas envelope (shown at Fig. 26.b) A glass envelope with high transmissivity is used to form a vacuum region around the metal receiver, minimizing losses by convection.

5.3 OPTICAL AND THERMAL PERFORMANCE MODEL

5.3.1 Sun position and geometrical parameters

The sun position at the respective hour is required in order to calculate the annual energy output of the solar Fresnel power plants. These solar angles are required to calculate two other angles. In Figure 27, it is shown the longitudinal incidence angle θ_i and the transversal incidence angle θ_t . These angles describe the solar position in relation to a Fresnel module.

Figure 27 – Definition of angles in Fresnel collector



Source: (Morin *et al.*, 2012)

As it is known, these angles depend on the geographical localization of the collectors, its orientation, inclination and position of the sun during the day and throughout of the year. Therefore, the longitudinal incidence angle and the traversal angle are defined by Equations 5.1 and 5.2, respectively.

$$\theta_t = \arctan \left(\frac{|\sin(\gamma_s)|}{\tan(\alpha_s)} \right) \quad (5.1)$$

$$\theta_i = \arcsin(\cos(\gamma_s) \cdot \cos(\alpha_s)) \quad (5.2)$$

where γ_s [deg] is the solar azimuth angle. It represents the angular displacement from south of the projection of beam radiation on the horizontal plane and α_s [deg] is the solar altitude angle. It represents the angle between the vertical and the line to the sun. These angles are calculated according to Equations 5.3 and 5.4, respectively.

$$\gamma_s = \arccos \left(\frac{\sin(\alpha_s) \cdot \sin(\phi) - \sin(\delta)}{\cos(\alpha_s) \cdot \cos(\phi)} \right) \quad (5.3)$$

$$\alpha_s = 90 - \theta_z \quad (5.4)$$

where ϕ [deg] ($-90^\circ \leq \phi \leq 90^\circ$) is the latitude angle, θ_z [deg] is the zenith angle. It represents the angle between the vertical and the line to the sun. It is defined by Equation 5.5 and δ [deg] ($-23.45^\circ \leq \delta \leq 23.45^\circ$) is the declination angle. It defines how much the Sun rises above the plane of the equator. It is defined by Equation 5.6 proposed by Cooper (1969).

$$\theta_z = \arccos (\sin(\phi) \cdot \sin(\delta) + \cos(\phi) \cos(\delta) \cos(\omega_{solar})) \quad (5.5)$$

$$\delta = 23.45 \cdot \left(360 \frac{285 + n}{365} \right) \quad (5.6)$$

where n [day] ($1 \leq n \leq 365$; $n=1$: 1st January) is the day of the year and ω_{solar} [deg] is the solar time. It is defined by Equation 5.7.

$$\omega_{solar} = \omega + (L_{st} - L_{loc}) + 15 \cdot \frac{E}{60} \quad (5.7)$$

where ω [deg] is the angular displacement of the sun east or west of the local meridian due to the rotation of the Earth on its axis at 15° per hour (at noon $\omega = 0^\circ$), this angle is negative in the morning and positive in the afternoon. L_{st} [deg] is the standard meridian for the local time zone, L_{loc} [deg] is the local longitude of the location and E [min] is the correction of the time. It is calculated according to Equation 5.8 proposed by Spencer (1971).

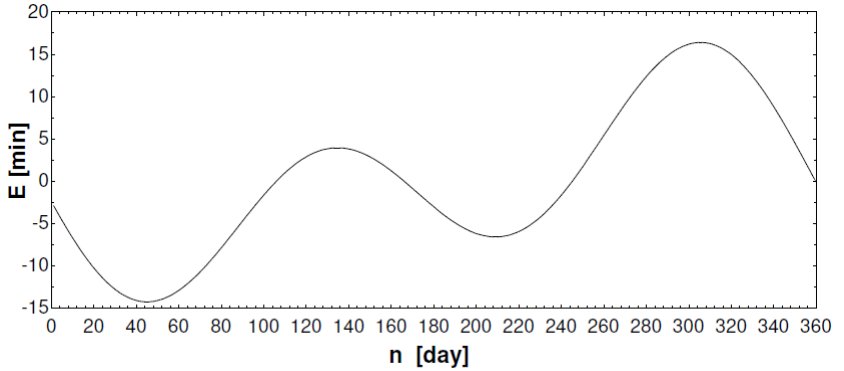
$$E = 229.2 \cdot (0.000075 + 0.001868 \cos(B) - 0.032077 \sin(B) - 0.014615 \cos(2B) - 0.04089 \sin(2B)) \quad (5.8)$$

where

$$B = (n - 1) \cdot \frac{360}{365} \quad (5.9)$$

The variation of E throughout of the year is shown at Figure 28.

Figure 28 – The equation of time E in minutes, as function of time of year



Source: Adapted from Duffie & Beckman (1991)

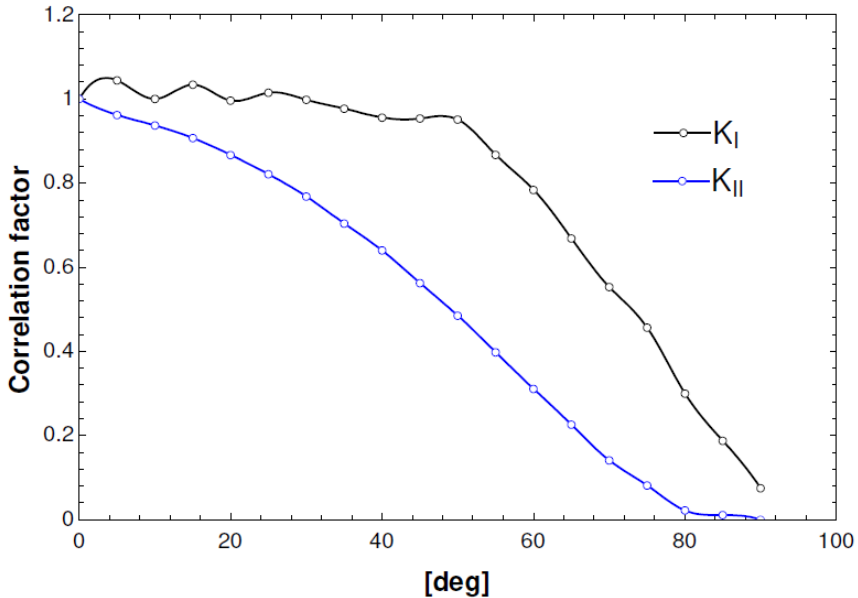
5.3.2 Optical efficiency

The optical efficiency is defined as the rate of optical energy reaching the absorber, divided by the energy coming from the solar resource. There are many factors that affect the optical efficiency of the collector, including incidence angle of light, shading and blocking between adjacent mirrors, the optical properties of different surfaces, among others. The hourly optical efficiency is calculated according to Equation 5.10 (Industrial Solar, 2017).

$$\eta_{opt,h} = 0.67 \cdot K_I \cdot K_{II} \quad (5.10)$$

where K_I is the transversal factor and K_{II} is longitudinal factor. These factors are function of θ_t and θ_i , respectively. In Figure 29, it is shown the factors K_I and K_{II} as a function of incidence angle and transversal angle.

Figure 29 – Correction factor



Source: Adapted from Industrial Solar (2017)

The annual optical efficiency is calculated according to the Equation 5.11.

$$\eta_{opt,a} = \sum_{year} \frac{G_{bn,i} \cdot \eta_{opt,i}}{DNI} \quad (5.11)$$

where DNI [kWh/m²-year] is the direct normal irradiation and $G_{bn,i}$ [kW/m²] is the hourly direct normal irradiance.

5.3.3 Heat losses

Heat losses from any solar water heating system take into account the three heat transfer mechanisms: radiation, convection and conduction. The conduction heat losses occur from sides and the back of the absorber tube. The convection heat losses take place from the absorber tube to the glazing cover and can be reduced by evacuating the space between the absorber tube and the glazing cover and by optimizing the gap between them. The radiation losses occur from the absorber tube due to the ambient temperature. In the literature there are several models to calculate the thermal losses

in the Fresnel collector; some of them were suggested by Häberle *et al.* (2002), Morin *et al.* (2012), Mills & Morrison (2000) Heimsath *et al.* (2014b). In this work is adopted the model for thermal losses for the Fresnel module LF-11 which is suggested by Industrial Solar (2017) according to Equation 5.12.

$$\dot{Q}_{losses,h}'' = \mu_1 \Delta T^2 \quad (5.12)$$

where μ_1 is a thermal losses coefficient:

$$\mu_1 = 0.00043 \frac{W}{m^2 K^2}$$

The temperature difference (ΔT) represents the difference between the average absorber temperature and the ambient temperature. It is calculated according to Equation 5.13.

$$\Delta T = \frac{T_{f,out} + T_{f,in}}{2} - T_{amb} \quad (5.13)$$

where $T_{f,in}$ [$^{\circ}C$] is the water inlet temperature in the solar field, $T_{f,out}$ [$^{\circ}C$] is the water outlet temperature in the solar field and T_{amb} [$^{\circ}C$] is the ambient temperature.

5.4 NET HEAT RATE AND SATURATED STEAM PRODUCED

For steady state operation regime, the hourly net heat rate delivered by solar field, $\dot{Q}_{solar,h}$ can be found discounting from absorbed heat $\dot{Q}_{abs,h}$ the terms related to heat losses. Thereby, it can be calculated by Equation 5.14.

$$\dot{Q}_{solar,h}'' = \underbrace{F_{cf} \cdot G_{bn} \cdot \eta_{opt,h}}_{\dot{Q}_{abs,h}} - \dot{Q}_{losses,h}'' \quad (5.14)$$

where G_{bn} [kW/m^2] is the hourly direct normal irradiance and F_{cf} is a cleanliness factor.

Once $\dot{Q}_{solar,h}''$ is found, the hourly saturated steam produced by the solar systems is calculated according to Equation 5.15.

$$\dot{m}_{solar,h} = \frac{\dot{Q}_{solar,h}'' \cdot A_{solar}}{h_s - h_{fw}} \quad (5.15)$$

where A_{solar} [m²] is the solar field area, h_s [kJ/kg] (at $P_{sat} = 800$ kPa) is the saturated steam enthalpy and h_{fw} [kJ/kg] (at 60 °C and $P=800$ kPa) is the feed water enthalpy.

5.5 SOLAR FIELD DESIGN

5.5.1 Desing point

The design point direct normal solar irradiance $G_{bn,ref}$ [W/m²] consists on a reference used to calculate the solar field area. It is an important step in a design phase once if a very high irradiance value is selected the frequency in which solar field will be operated at full load will be very low in the year. In the other side, if a low irradiance value is selected there will be many hours in a year in which solar field will be defocused. The procedure normally employed consist on not considering irradiance values smaller than certain lower boundary (e.g. 250 W/m²) and calculating the 95 % upper percentile to identify $G_{bn,ref}$. The solar field area is found by Equation 5.16.

$$A_{solar} = \frac{\dot{m}_{solar,DP} \cdot (h_s - h_{fw})}{Q''_{solar,DP}} \quad (5.16)$$

where $\dot{m}_{solar,DP}$ [kg/s] is the saturated steam flow at the design point and $Q''_{solar,DP}$ [kW/m²] is the neat heat rate delivered by the solar field at the design point.

5.5.2 Solar multiple

The determination of the optimum field size involves the calculation of the solar multiple. It represents the ratio at which the solar field is modified. Therefore, a value of $SM=1.2$ indicates that the solar area is increased a 20 % compared to design point ($SM=1.0$). Thus, if the solar multiple chosen was too big for a system without thermal storage, it would cause collected solar energy to be wasted alongside unnecessarily high investment cost. A small solar multiple will lead the system to operate at part load more frequently. It is calculated by Equation 5.17 (Izquierdo *et al.*, 2010).

$$SM = \frac{A_{solar}}{A_{pro}} \quad (5.17)$$

where A_{solar} [m²] is the solar area calculated at the design point and A_{pro} [m²] is the project solar area.

Chapter 6

SCENARIOS COMPARISON

6.1 INTRODUCTION

In this section are presented the results of thermodynamic and economic analyses of the scenarios presented in Chapter 3. In the same way, it is presented a sensitive analysis considering different electric tariff, DNI, natural gas cost, solar field area and Fresnel collector cost.

6.2 GENERAL ASSUMPTIONS

The electrical and thermal energy demands considered in this work are presented at Table 7. These demands are the typical demands of a medium-sized plant in the Santa Catarina's textile sector. In this work, it is considered a $COP_e=3.0$ (YORK, 2017) in order to calculate the chiller's electrical demand.

Table 7 – Thermal demands and electrical demands

| Parameter | Unit | Value |
|--------------------------|------|-------|
| Thermal demand | | |
| Saturated Steam | t/h | 12 |
| Chilled water | RT | 300 |
| Electrical demand | | |
| Plant | kW | 3,000 |

The plant site and TMY data used in simulations are presented at Table 8. Simulations are performed considering a TMY data of the city of Florianopolis - Santa Catarina considering 1-hour time steps. Simulations for scenarios comparison are performed by using EES.

Table 8 – Plant site and TMY data

| | |
|------------------------|--------------------------------|
| Plant site | Florianopolis - Santa Catarina |
| Coordinates | (27.5949° S, 48.5482° W) |
| TMY | SWERA (2017) |
| Time Resolution | 1 hour |

The adopted assumptions regarding economic analysis are presented at Table 9.

Table 9 – Assumptions adopted for economic analysis

| Parameter | Unit | Value |
|--|--------------------|--------------|
| Natural gas price ^a | R\$/m ³ | 1.5 |
| Make-up water ^b | R\$/m ³ | 10 |
| Green electricity tariff | | |
| Price at peak hours ^c | R\$/MWh | 1,445.25* |
| Price at off-peak hours ^c | R\$/MWh | 388.4* |
| Contracted demand ^c | R\$/kW | 15.81* |
| Blue electricity tariff | | |
| Price at peak hours ^c | R\$/MWh | 569.8* |
| Price at off-peak hours ^c | R\$/MWh | 388.4* |
| Contracted demand at peak hours ^c | R\$/kW | 36.1* |
| Contracted demand at off-peak hours ^c | R\$/kW | 15.81* |

Source: a Adopted value; b Estimated cost; c (CELESC, 2018)

* Considering a ICMS=25%

Particularly, for green electricity tariff, the price at peak hours and off-peak hours are 1,156.29 and 310.68 R\$/MWh

(without taxes), respectively. According to INTER (2017) the option for green or blue electricity tariff depends on many factors such as electrical consumption profile, consumption at peak hours, contracted demand, work schedules, among others. In this work, it is adopted green electricity tariff for the economic analysis. In the same way, it is evaluated (see section 6.4.3) the influence of blue electricity tariff on the economic feasibility of the proposed plants.

6.3 BASE CASE SCENARIO

6.3.1 Thermodynamic analysis

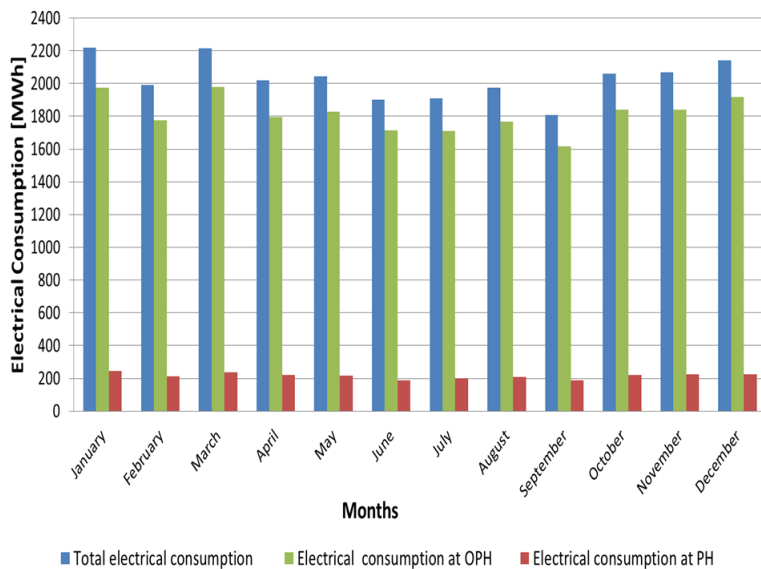
The base case scenario results at the design point are shown at Table 10. The heat dissipated by the cooling tower is calculated according to Equation 4.9, the electric chillers demand is calculated by the Equation 4.6 and the steam generator natural gas consumption is calculated by Equation 4.15.

Table 10 – Thermodynamic results at design point for the base case scenario

| Parameter | Unit | Value |
|---|-------------------|-------|
| Steam generator natural gas consumption | m ³ /h | 990.5 |
| Electric chillers refrigeration load | RT | 300 |
| Steam generator production | t/h | 12 |
| Electric chillers demand | kW | 412 |
| Electric plant demand | kW | 3,000 |
| Heat dissipated at the cooling tower | kW | 1,647 |
| Colling tower water consumption | m ³ /h | 1.98 |
| Plant water consumption | m ³ /h | 2.41 |

In Brazil the electrical consumption is charged depending on the consumption schedule: PH (Peak Hours) corresponds to the interval from 7:00 pm to 10:00 pm except on weekends, and the OPH (Off-Peak Hours) for the rest of the day. Thus, the electrical consumption profile is shown at Figure 30.

Figure 30 – Base case scenario monthly electrical consumption



The monthly electrical consumption is calculated by multiplying the electrical demand (3,000 kW) by the monthly hours at PH and OPH, respectively. In the same way, the monthly electrical chillers consumption is calculated by multiplying the electrical demand (412 kW) by the monthly hours in which the chillers are working. As it is known, the chillers do not work all the time, considering that the chillers are used for air conditioning purposes and taking into account that the ideal temperature where industrial activities are developed should be between 20 and 23 °C (NR17, 2017). From this perspective, it is considered as chiller working hours when the ambient temperature is higher than 21 °C.

As it can be seen, the highest electrical consumption occurs during the months of December and January (summer period). It is due to the high electrical consumption by the electric chillers for air conditioning purposes. Thereby, the average consumption at PH and OPH during this period is 228 MWh and 1,989 MWh, respectively. In the same way, during summer period the electrical chillers consumption at PH is 36 MWh. It represents by 16 % of the consumption at PH and the electrical chillers consumption at OPH is 234 MWh. It represents by 12 % of the consumption at OPH.

On the other hand, the lowest consumption occurs during the months of June and August (winter period). Thereby, the average consumption at PH and OPH during this period is 200 MWh and 1,729 MWh, respectively. In the same way, during winter period the electrical chillers consumption at PH is 2 MWh. It represents by 1 % of the consumption at PH and the electrical chillers consumption at OPH is 31 MWh. It represents by 2 % of the consumption at OPH.

Finally, the annual electrical consumption at PH and OPH is 2,592 MWh and 21,758 MWh, respectively. Particularly, the electrical chillers annual consumption at PH is 243 MWh. It represents a 9.38 % of the consumption at PH. and the electrical chillers annual consumption at OPH is 1,643 MWh. It represents a 7.55 % of the consumption at OPH.

The base case scenario annual performance is shown at Table 11. As it can be seen, the natural gas consumption for generating 90,102 t/year of saturated steam is 7,416,864 m³/year. It is calculated according to Equation 4.18. The colling tower make-up water consumption is calculated according to Equation 4.14. It represents a 0.71 % of the total mass flow at the cooling tower ($\dot{m}_{17}=78.63$ m³/h) and the plant make-up water consumption is calculated according to Equation 4.19.

Table 11 – Base case scenario annual performance

| Parameter | Unit | Value |
|---|----------------------|-----------|
| Natural gas consumption | m ³ /year | 7,416,864 |
| Electrical plant consumption at peak hours | MWh | 2,349 |
| Electrical plant consumption at off-peak hours | MWh | 20,115 |
| Electrical chillers consumption at peak hours | MWh | 243 |
| Electrical chillers consumption at off-peak hours | MWh | 1,643 |
| Make-up cooling tower water consumption | m ³ /year | 9,074 |
| Make-up plant water consumption | m ³ /year | 18,043 |
| Saturated steam production | t/year | 90,102 |

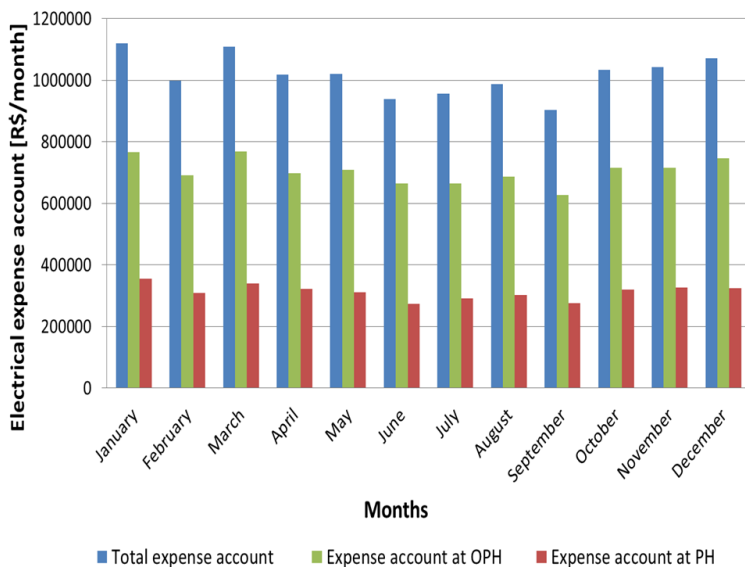
6.3.2 Economic analysis

The economic assumptions regarding natural gas and electricity prices are the same presented at Table 9. In the annual expense account for the base case scenario is considered a contingency factor of 5 % due to possible errors in some considerations.

As already mentioned, the electrical consumption is one of the most important expenses for the base case scenario. In Figure 31, it is shown the monthly electrical expense account considering green electricity tariff. As it is shown, during summer period the average electrical expense account at PH and OPH is 329,093 R\$/month and 733,881 R\$/month, respectively.

On the other hand, during winter period the average electrical expense account at PH and OPH is 288,938 R\$/month and 671,578 R\$/month, respectively. In this context, the expense account increase by 15 % and by 9 % at PH and OPH, respectively during summer period. Finally, the annual electrical expense account at OPH is 8,449,741 R\$/year and the electrical expense account at PH is 3,746,203 R\$/year. Thereby, the annual electrical expense account is 12,195,945 R\$/year.

Figure 31 – Base case scenario monthly electrical expense account



The base case scenario annual expense account is shown at Table 12. As it is shown, the annual expense account is 24,772,031 R\$/year. In the same way, the electrical consumption is the main expense account representing a 49.23 % of the total expense account. Besides, the natural gas expense account represents a 44.91 %.

Table 12 – Base case scenario annual expense account

| Parameter | Unit | Value |
|------------------------------------|----------|------------|
| Natural gas expense account | R\$/year | 11,125,296 |
| Water expense account | R\$/year | 271,170 |
| Electrical plant expense account | R\$/year | 11,206,553 |
| Electrical chiller expense account | R\$/year | 989,392 |
| Subtotal expense account | R\$/year | 23,592,411 |
| Contingency Factor | % | 5 |
| Total expense account | R\$/year | 24,772,031 |

6.4 COGENERATION PLANT SCENARIO

6.4.1 Thermodynamic analysis

The assumptions adopted for cogeneration plant scenario simulation are presented at Table 13. Equipment performance data are based on manufacturer's data-sheet information. In this work, it is considered as prime mover an Engine Caterpillar 2000 kW due to its performance data is available in the literature (Caterpillar, 2017). In the same way, the commercial hot water fired absorption chiller LG series WCMH model 030 with a nominal capacity of 110 RT (LG, 2017) is considered to supply the cold water demand. Additionally, it is considered a factor of 0.2 kW/RT for calculating the electrical pumps demand used in electric and absorption chillers. As already mentioned, the cogeneration plant is simulated considering thermal parity. Thereby, the operation of the natural gas engine is considered at nominal conditions.

Table 13 – Assumptions adopted for cogeneration plant simulation

| Parameter | Unit | Value |
|---|-------|-------|
| Engine electrical power production ^a | kW | 2,000 |
| Engine electrical efficiency ^a | % | 41 |
| Exhaust gases outlet temperature ^a | °C | 414 |
| Availability of the plant ^c | % | 95 |
| Exhaust gases mass flow ^a | kg/s | 3.018 |
| Radiator water inlet temperature ^a | °C | 80 |
| Radiator water outlet temperature ^a | °C | 93 |
| Radiator water mass flow ^a | kg/s | 19.72 |
| HRSG Pinch Point ^c | °C | 15 |
| HRSG Approach Point ^c | °C | 15 |
| Absorption chiller COP ^b | - | 0.8 |
| Chiller pumps electrical consumption ^c | kW/RT | 0.2 |
| Hot water inlet temperature ^b | °C | 95 |
| Hot water outlet temperature ^b | °C | 72 |
| Gas temperature at flue-gas stack ^c | °C | 120 |

Source: a (Caterpillar, 2017); b (LG, 2017); c Adopted value

The thermodynamic results for the cogeneration plant scenario simulation at design point are shown at Table 14. As it can be seen, the absorption chiller refrigeration load is 94 RT (see Equation 4.7). In order to attend the chilled water demand, the electric chillers are required to produce 206 RT, leading an electrical demand of 283.1 kW. The HRSG saturated steam production is 2.46 t/h (see Equation 4.4). In the same way, in order to attend the steam demand, the steam generator produces 9.54 t/h of saturated steam, leading a natural gas consumption of

713.1 m³/h (see Equation 4.15). As already mentioned, the plant demand is 3,000 kW. Therefore, for attending the electrical demand are considered two engines to produce 4,000 kW. Finally, the total heat dissipated at the colling tower is 1,873 kW, it represents an increase of 13.73% compared to base case scenario (1,647 kW). It is due to the low COP of the absorption chiller. Finally, the thermodynamic results at each point in the cogeneration plant (see Figure 19) are shown in the Appendix C.

Table 14 – Thermodynamic results at design point

| Parameter | Unit | Value |
|---|-------------------|-------|
| Absorption chiller refrigeration load | RT | 94 |
| Electric chillers refrigeration load | RT | 206 |
| Electrical plant demand | kW | 3,000 |
| Electric chiller demand* | kW | 283.1 |
| Absorption chiller electrical demand* | kW | 26 |
| Steam generator production | t/h | 9.54 |
| HRSG steam production | t/h | 2.46 |
| Engines electrical power production | kW | 4,000 |
| Electrical surplus | kW | 690.9 |
| Engines natural gas consumption | m ³ /h | 956.5 |
| Steam generator natural gas consumption | m ³ /h | 713.1 |
| Heat dissipated at cooling tower | kW | 1,873 |
| Colling tower water consumption | m ³ /h | 2.27 |
| Plant water consumption | m ³ /h | 2.41 |
| Cogeneration plant efficiency | % | 73.13 |

*Including electrical pumps demand

In Table 15, it is shown the operation parameters of the cogeneration plant. In this regard, the results show that the proposed cogeneration plant can be considered as a qualified cogeneration unit according to ANEEL (2006).

Table 15 – Qualified cogeneration pant

| Parameter | Unit | Value |
|-----------------------------------|-------------|--------------|
| Electrical energy produced, E_e | kWh | 28,454,400 |
| Thermal energy produced, E_t | kWh | 14,565,807 |
| Total energy from the fuel, E_f | kWh | 69,415,079 |
| Parameter 1 (See Equation 2.1) | % | 20.98 |
| Parameter 2* (See Equation 2.2) | % | 50.79 |

* Considering $X=2.14$ $F_c=41$ (natural gas and until 5 MW)

In Table 16, it is shown the annual performance of the cogeneration plant scenario.

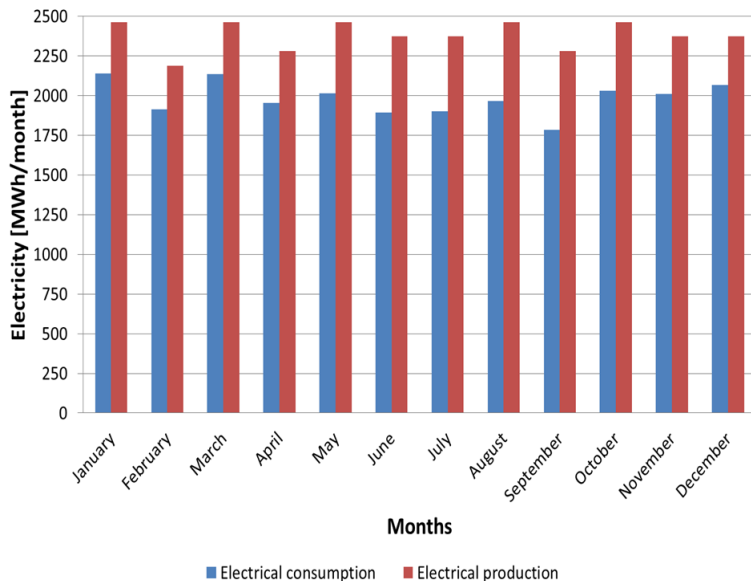
Table 16 – Cogeneration plant scenario annual performance

| Parameter | Unit | Value |
|--|-------------|--------------|
| Steam generator natural gas consumption | m^3 /year | 5,339,693 |
| Engines natural gas consumption | m^3 /year | 7,162,272 |
| Electrical consumption at peak hours | MWh | 188 |
| Electrical consumption at off-peak hours | MWh | 1,307 |
| Cooling tower make-up water consumption | m^3 /year | 10,433 |
| Plant make-up water consumption | m^3 /year | 18,043 |
| Boiler saturated steam production | t/year | 67,551 |
| HRSG saturated steam production | t/year | 22,543 |

As it can be seen, the natural gas consumption by the engines is $7,162,272 \text{ m}^3/\text{year}$. As already mentioned, in this work is considered an availability of the cogeneration plant ($F_a=95 \%$) (see Table 13). Hence, during this period (375 h) is imported 3,412 kW from the grid (to attend the electrical and chilled water demand). For that reason, the electrical consumption at PH and OPH is 188 MWh and 1,307 MWh, respectively. In order to attend the steam demand, the HRSG produces 22,543 t/year of saturated steam representing a 25 % of the total steam demand. In this respect, it is complemented by the steam generator producing 67,551 t/year of saturated steam leading an annual natural gas consumption of $5,339,693 \text{ m}^3/\text{year}$.

As already mentioned, there is an electrical surplus. Thus, the total electrical production and the total electrical consumption during a year are shown at Figure 32.

Figure 32 – Monthly electrical production and electrical consumption



As it can be seen, the electrical production is greater than the electrical consumption throughout the year. During summer period the average electrical production is 2,341 MWh/month and the average consumption is 2,040 MWh/month resulting in an average electrical surplus of 301 MWh/month. On the other hand,

during winter period the average electrical production is 2,402 MWh/month and the average consumption is 1,920 MWh/month resulting in an average electrical surplus of 482 MWh/month. Therefore, the electrical surplus increases by 60 % during winter period.

6.4.2 Economic analysis

The adopted assumptions regarding economic assumptions are presented at Table 17.

Table 17 – Assumptions adopted for economic analysis

| Parameter | Unit | Value |
|--|---------------------|-----------------------|
| Natural gas engines (4000 kW) ^a | USD/kW | 1,000 |
| Economizer ^b | USD/kW _t | 27 |
| Evaporator ^b | USD/kW _t | 47 |
| Absorption chiller ^c | USD/kW _t | 1,000 |
| Heat exchanger water-gas ^c | USD/m ² | 280 |
| Heat exchanger water-water ^c | USD/kW _t | 10 |
| Colling tower ^c | USD/kW _t | 100 |
| Electrical auxiliaries ^d | USD | 3% of equipment cost |
| Instrumentation and control ^d | USD | 3% of equipment cost |
| Mechanical auxiliaries ^d | USD | 5% of equipment cost |
| Civil works ^d | USD | 5% of equipment cost |
| Engineering services ^d | USD | 5% of equipment cost |
| Installation ^d | USD | 20% of equipment cost |
| Contingency ^d | USD | 10% of equipment cost |

Source: a (SOLUTIONS, 2017); b (Manzolini *et al.*, 2011);
c (SUMMERHEAT, 2009) d Adopted value

Thereby, the total cogeneration plant cost is shown at Table 18. As it is shown, the total cogeneration plant cost is \$R 22,563,440.

Table 18 – Cogeneration plant cost

| Parameter | Unit | Value |
|-------------------------------|-------------|--------------|
| Natural gas engines (4000 kW) | USD | 4,000,000 |
| Economizer | USD | 7,447 |
| Evaporator | USD | 67,774 |
| Absorption chiller | USD | 387,000 |
| Heat exchanger water-gas | USD | 20,065 |
| Heat exchanger water-water | USD | 2,864 |
| Colling tower | USD | 187,300 |
| Subtotal | USD | 4,669,586 |
| Electrical auxiliaries | USD | 140,088 |
| Instrumentation and control | USD | 140,088 |
| Mechanical auxiliaries | USD | 233,479 |
| Civil works | USD | 233,479 |
| Engineering services | USD | 233,479 |
| Installation | USD | 933,918 |
| Contingency | USD | 466,958 |
| Total | USD | 7,051,075 |
| Real/US | R\$/USD | 3.2 |
| Total | R\$ | 22,563,440 |

The total plant cost is based on quotations performed with manufacturers and on literature data. Furthermore, in this work

are considered investment factors based on the Total Equipment Cost (TEC). Thereby, the costs associated to electrical and the mechanical auxiliaries factor are considered a 3 % of the TEC. In the same way, the costs related to instrumentation and control, civil works and engineering services are considered a 5 % of the TEC. Finally, the costs associated to installation of the plant are considered a 20 % of the TEC. These considerations are result of an extensive discussion with expert in cogeneration systems during a project developed in cooperation with PETROBRAS. Besides, it is considered a contingency factor of 10 % in order to take into account other factors as errors in some considerations, in equipments cost, among others.

The cogeneration plant scenario annual expense is shown at Table 19. In the same way, the economic analysis regarding natural gas price and electricity tariff are the same presented at Table 9.

Table 19 – Cogeneration plant scenario annual expense account

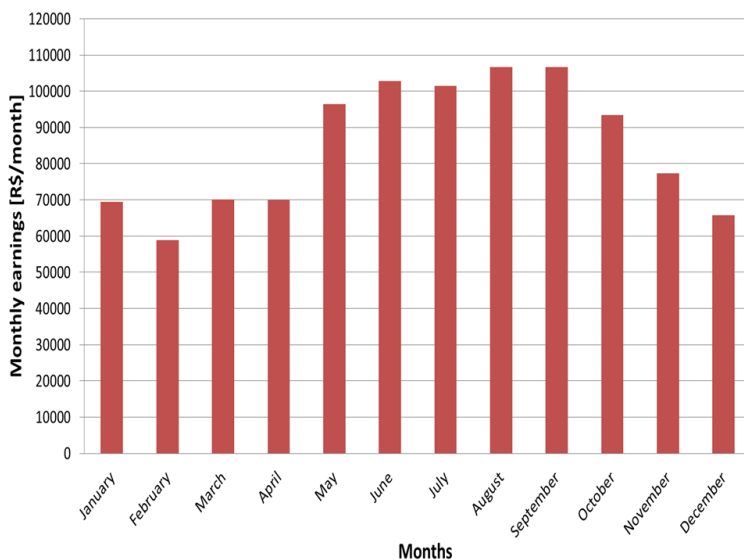
| Parameter | Unit | Value |
|--|-------------|--------------|
| Natural gas expense account | R\$/year | 18,752,947 |
| Water expense account | R\$/year | 281,087 |
| Electrical plant account | R\$/year | 779,280 |
| Engines maintenance expense | R\$/year | 57,600 |
| HRSG maintenance expense | R\$/year | 24,070 |
| Absorption chiller maintenance expense | R\$/year | 38,400 |
| Colling tower maintenance expense | R\$/year | 59,936 |
| Heat exchangers maintenance expense | R/year | 6,420 |
| Subtotal expense account | R\$/year | 19,999,740 |
| Contingency Factor | % | 5 |
| Total expense account | R\$/year | 20,999,727 |

The costs associated to equipment maintenance are

calculated based on literature data. Thereby, the engine maintenance is considered 1,500 USD/month (SOLUTIONS, 2017). The annual costs associated to HRGS and the colling tower maintenance are considered 1 % and 0.5 % of each equipment cost, respectively. Likewise, the absorption chiller maintenance is considered 1,000 USD/month (SUMMERHEAT, 2009). As it can be seen, it is considered a contingency factor (5 %) due to possible errors in some considerations. Particularly, the natural gas account increases by 69 % compared to base case scenario. However, the electrical expense account decreases by 94 % compared to the base case scenario. Finally, the annual expense account for cogeneration plant is 20,999,727 R\$/year. It represents an annual economy of 3,772,303 R\$/year compared to base case scenario (see Table 12).

As already mentioned, in this work is considered the electrical surplus exportation to the grid taking into account that it is considered the engine operation at nominal conditions (thermal parity). According to CCEE (2017) the average electricity sale tariff during the year 2017 in the southern region of Brazil was 230 R\$/MWh. In this regard, the monthly earnings due to the electricity sale are shown at Figure 33.

Figure 33 – Monthly earnings due to the electricity sale



As it can be seen, the highest earnings occur during winter period (June to August). In this period the average earnings are 104,947 R\$/month and the lowest earnings occur during summer period (December to February). In this period the average earnings are 64,739 R\$/month. In this context, during summer period the earnings are reduced by 38 %. Finally, the annual earnings are 1,019,054 R\$/year. Therefore, the annual economy due to the integration of the cogeneration plant compared to base case scenario considering the electricity sale increases to 4,791,357 R\$/year.

The economic parameters for cogeneration plant scenario are shown at Table 20. In this work, the economic parameters are calculated based on a life time of plant of 20 years and based on an interest rate of 10 %. As it is shown, the payback period is 81.2 months (~ 6.77 years), the interest rate of return is 20.56 % and the net present value is R\$ 17,638,156.

Table 20 – Economic parameters for cogeneration plant scenario

| Parameter | Unit | Value |
|-------------------------|--------|------------|
| Life time of plant | Years | 20 |
| Interest rate | % | 10 |
| Payback period | Months | 81.2 |
| Interest rate of return | % | 20.56 |
| Net present value | R\$ | 17,638,156 |

6.4.3 Sensitive analysis

As mentioned earlier, natural gas and electricity costs have an important role in the economic feasibility of cogeneration plant scenario. In this regard, it is performed a sensitive analysis considering the electricity tariff choice (green tariff), the blue electricity tariff and natural gas cost shown at Table 9.

In Figures 34, 35 and 36, it is shown the economic parameters as a function of natural gas cost for green and blue electricity tariffs.

Figure 34 – Payback period as a function of natural gas cost for green and blue electricity tariffs

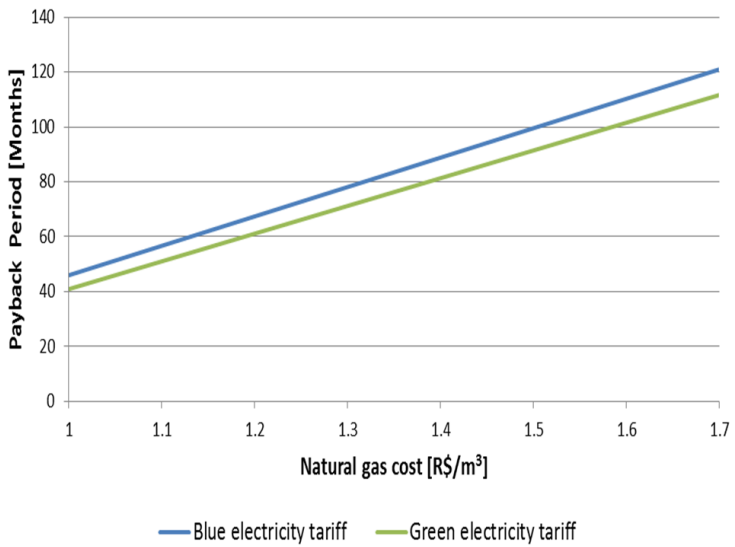


Figure 35 – NPV as a function of natural gas cost for green and blue electricity tariffs

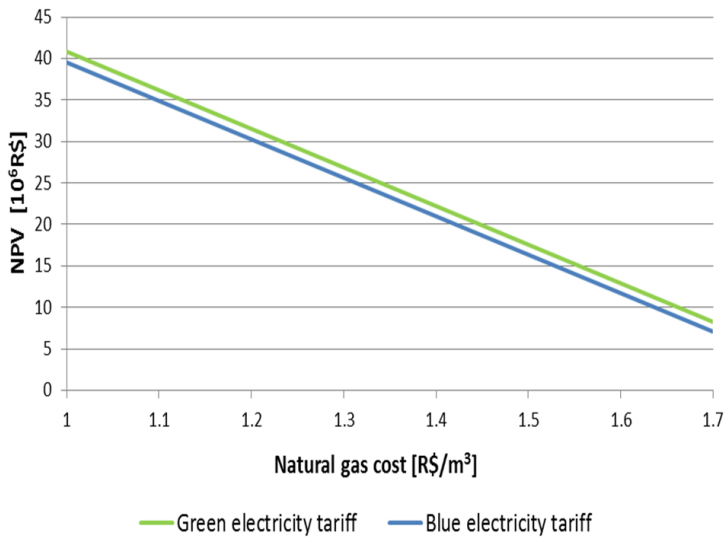
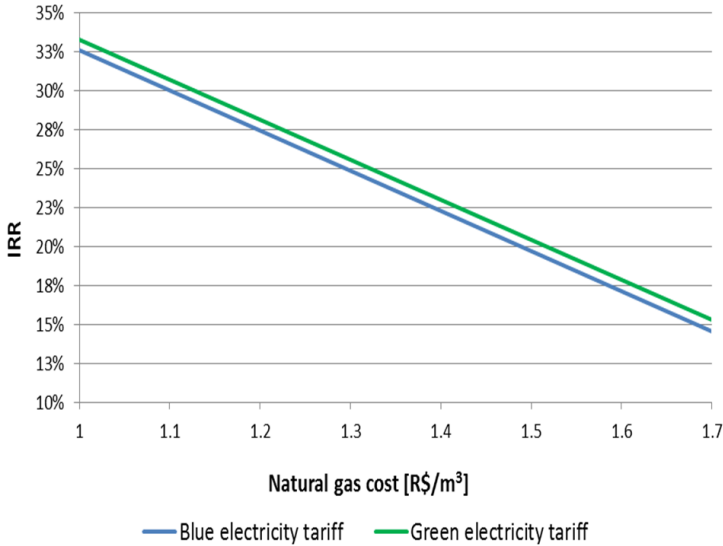


Figure 36 – IRR as a function of natural gas cost for green and blue electricity tariffs



As it can be seen, the NPV and the IRR decrease by 12 % and by 8 %, respectively when the natural gas cost increases 0.1 R\$/m³. On the other hand, the payback period increases about 19 % when the natural gas increases 0.1 R\$/m³. From this perspective, it is identified that the natural gas cost has a significant influence on the economic feasibility of the cogeneration plant scenario. In the same way, the results show that the option for green or blue electricity tariff has a little influence on the economic feasibility.

6.5 SOLAR-AIDED COGENERATION PLANT SCENARIO

6.5.1 Thermodynamic analysis

The adopted assumptions related to the Fresnel solar field at the design point are presented at Table 21. The solar Fresnel collector LF-11 produced by the German company Industrial Solar is considered for this simulation once technical performance data are available in the literature and quotations were provided by the manufacturer. Furthermore, these Fresnel collectors are typically used to produce saturated steam by direct steam generation. In the same way, the design point irradiance (see Section 5.5.1),

ambient temperature, water inlet temperature, water outlet temperature, thermal losses factors (see Equation 5.12) are necessary in order to determine the solar field size (see Equation 5.16). The cleanliness factor depend on the cleaning strategy implemented in the solar field. Normally, the solar field might be cleaned once or twice a week depending on the the ambient and soil conditions.

Table 21 – Adopted parameters for solar field simulation

| Parameter | Unit | Value |
|--|--------------------|---------|
| Solar Fresnel Collector type ^a | - | LF-11 |
| Design point irradiance ^c | W/m ² | 957.7 |
| Ambient temperature ^c | °C | 28 |
| Water inlet temperature ^c | °C | 25 |
| Water outlet temperature ^b | °C | 170.4 |
| Thermal losses factor μ_1 ^a | W/m ² K | 0.00043 |
| Cleanliness factor ^c | % | 95 |

Source: a (Industrial Solar, 2017); b Saturation temperature at 800 kPa; c Adopted value.

The results related to the solar field performance at the design point are present at Table 22. As it can be seen, the saturated steam production adopted at the design point is 4 t/h. In this way, the total production by HRSG (2.46 t/h) and by the solar field is 6.46 t/h representing a 53.83 % of the total demand (12 t/h). Therefore, the steam generator load is reduced up to a value of 46.17 %. Thereby, the steam generator works above 30 % (established minimum load). Likewise, the solar field area (See equation 5.16) to produce 4 t/h of the saturated steam at the design point is 4,700 m² (Solar Multiple (SM) equal one, SM=1.00). Moreover, due to the implementation of the solar field the steam generator natural gas consumption is reduced from 713.1 m³/h (see Table 14) to 425.6 m³/h at the design point. In this sense, the fuel economy at the design point is 287.5 m³/h.

Table 22 – Results at the design point

| Parameter | Unit | Value |
|----------------------------|-------------------|-------|
| Solar Field Area | m ² | 4,700 |
| Steam generator production | t/h | 5.54 |
| Optical efficiency, | % | 63.47 |
| Thermal efficiency | % | 62.42 |
| Saturated steam production | t/h | 4 |
| Fuel economy | m ³ /h | 287.5 |

As it is known, the solar field output depends on irradiance incidence at the plant's site. In this regard, Figures 37 and 38 show the solar field steam production and the steam generator production during summer solstice and winter solstice respectively.

Figure 37 – Solar field performance during the summer solstice

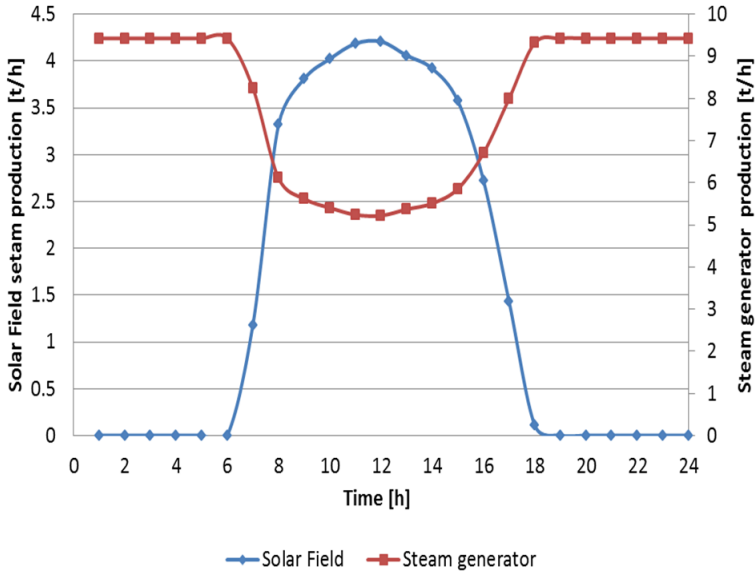
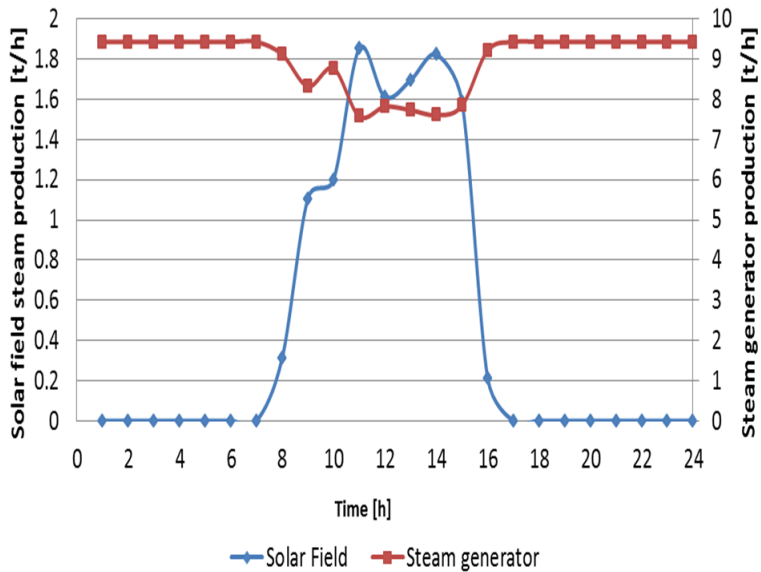


Figure 38 – Solar field performance during the winter solstice

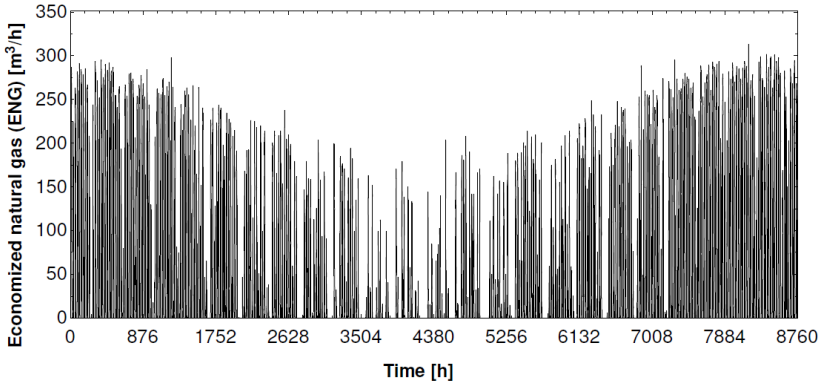


As it is shown, during summer solstice the maximum steam production is 4.2 t/h while the steam production by the steam generator is 5.22 t/h. On the other hand, during winter solstice the maximum steam production by the solar field is reduced to 1.85 t/h, while the steam production by the natural gas steam generator increases to 7.57 t/h in order to attend the plant's steam demand. From this perspective, during the winter period the natural gas consumption is higher due to the lower DNI incidence.

According to the above mentioned, the fuel economy is an advantage of the solar field. In this regard, the economized natural gas mass flow rate profile along the year is presented at Figure 39. As it can be seen, the fuel economy varies during the year. Thus, the highest values of fuel economy occur during summer period and the lowest values of fuel economy occur during winter period. This behavior is associated to the variation of solar field's optical efficiency.

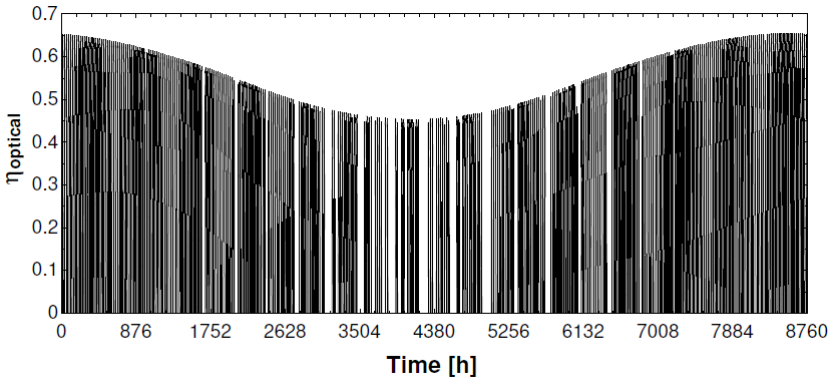
Finally, the annual fuel economy due to the integration of the solar field into cogeneration plant is 377,714 m³/year.

Figure 39 – Economized natural gas during a year



As mentioned earlier, the optical efficiency (see Equation 5.10) represents the influence of the cosine, blocking and shading on the optical performance of the solar field. In Figure 40, it is shown the optical efficiency throughout the year. As it is shown, the maximum optical efficiencies occur during summer period reaching average values close to 63.54 % and the minimum optical efficiencies occur during winter period reaching average values close to 47.05 %. In this respect, the optical efficiency decreases by 26 % during winter period.

Figure 40 – Optical efficiency during a year



Finally, the annual performance by the solar field is shown

at Table 23. As it might be seen, the annual saturated steam production is 5,302 t/year. The solar-aided cogeneration plant efficiency is 73.51 % (See Equation 3.2). It is slightly smaller than cogeneration plant efficiency (~ 74.84 %) Finally, the solar fraction is 5.89 % (see Equation 3.4). It represents the fuel economy due to the integration of the solar field.

Table 23 – Solar field annual performance

| Parameter | Unit | Value |
|---|--------|-------|
| Annual thermal efficiency | % | 48.86 |
| Annual optical efficiency | % | 50.72 |
| Solar-aided cogeneration plant efficiency | % | 71.70 |
| Saturated steam production | t/year | 5,302 |
| Solar fraction | % | 5.89 |

6.5.2 Economic analysis

The adopted assumptions used for economic analysis of the solar-aided cogeneration plant are presented at Table 24.

Table 24 – Adopted assumptions for economic analysis

| Parameter | Unit | Value |
|------------------------------|----------------------|-------------------------|
| Solar field ^{a*} | €/MW _t ** | 550,000 |
| O&M ^c | % | 1 % of solar field cost |
| Land investment ^b | €/m ² | 3 |
| Life time plant ^b | years | 20 |
| Interest rate ^b | % | 10 |

Source: a Quoted cost ,b Adopted value,
c (Blanco & Santigosa, 2016), *Including EPC costs.
** Heat delivered by the solar field at the design point

The quoted cost for the solar field is 550,000 €/MW_t. It includes the cost associated to installation of the solar field. In the same way, the economic parameters are calculated based on a life time of plant of 20 years and an interest rate of 10 %. The land cost is calculated based on the assumption of 3 €/m². The O&M is the annual operation and maintenance cost. It can be reduced in many different ways, in particular, through the adoption of new operating and control strategies (Blanco & Santigosa, 2016).

In Table 25, it is shown the solar-aided cogeneration plant cost.

Table 25 – Solar assisted cogeneration plant cost

| Parameter | Unit | Value |
|------------------------------------|---------|------------|
| Subtotal Cogeneration plant | USD | 7,051,075 |
| Solar field | USD | 1,431,360 |
| EPC costs* | USD | 357,840 |
| Subtotal hybrid power plant | USD | 8,840,275 |
| Contingency | USD | 178,950 |
| Total | USD | 9,019,225 |
| Real/US | R\$/USD | 3.2 |
| Total | R\$ | 28,861,520 |

*Engineering, Procurement, and Construction costs

As mentioned earlier, the total cogeneration plant cost is R\$ 22,563,440 (~ USD 7,051,075). In this sense, the solar-aided cogeneration plant cost is calculated by adding the solar field cost to the cogeneration plant cost. In this respect, the total cost of the solar field is USD 1,789,200 (including EPC costs). According to Morin *et al.* (2012) the costs due to installation, procurement construction, engineering services and site improvements represent a 20 % of the solar field cost. Thus, the costs associated with EPC of the solar field are USD 357,840. In the same way, it is considered a contingency factor of 10 % in order to take into account other factors as errors in some considerations, some errors

in the equipments costs, among other. Finally, the total solar-aided cogeneration plant cost is R\$ 28,861,520.

The total annual expense account for solar-aided cogeneration plant is shown at Table 26.

Table 26 – Solar assisted cogeneration plant annual expense account

| Parameter | Unit | Value |
|--|----------|------------|
| Natural gas expense account | R\$/year | 18,266,027 |
| Water expense account | R\$/year | 281,087 |
| Electricity plant account | R\$/year | 779,280 |
| Engine maintenance expense | R\$/year | 57,600 |
| HRSG maintenance expense | R\$/year | 24,070 |
| Absorption chiller maintenance expense | R\$/year | 38,400 |
| Colling tower maintenance expense | R\$/year | 59,936 |
| Heat exchangers maintenance expense | R\$/year | 6,420 |
| Solar field maintenance expense | R\$/year | 57,263 |
| Subtotal expense account | R\$/year | 19,570,083 |
| Contingency Factor | % | 5 |
| Total expense account | R\$/year | 20,548,587 |

The assumptions adopted for the solar-aided cogeneration plant equipment maintenance costs are the same values considered in the cogeneration plant scenario (see Table 19). In the same way, the natural gas cost and electricity tariff are the same presented at Table 9. Likewise, it is considered a contingency factor (5 %) due to possible errors in some considerations. As it might be seen, the total expense account for solar-aided cogeneration plant is 20,548,587 R\$/year. It represents an annual economy of R\$ 576,289 R\$/year (see table 19) compared to cogeneration plant scenario. It is due the fuel economy provided by the solar field. On

the other hand, it represents an economy of 4,223,444 R\$/year compared to base case scenario (see Table 12). As already mentioned, the annual earnings due to the electricity sale are 1,019,054 R\$/year. Therefore, the annual economy compared to base case scenario increases to 5,242,498 R\$/year.

The economic results for solar-aided cogeneration plant are shown at Table 27. As it is shown, the payback period is 102 months (~ 8.5 years) representing an increase by 26 % compared to cogeneration plant for which the payback back is 81.2 months (~ 6.8 years). Moreover, the internal rate of return is 17.31 % representing a decrease by 16 % compared to cogeneration plant (IRR=20.56 %). In the same way, the net present value decreases from a value of R\$ 17,638,156 (cogeneration plant) to a value of R\$ 15,488,699 (solar-aided cogeneration plant) representing a decrease by 12 %.

Although the solar field promotes a fuel economy, the results show that the integration of the solar field into cogeneration plant decreases its feasibility from an economic point of view.

Table 27 – Economic parameters for solar-aided cogeneration plant

| Parameter | Unit | Value |
|-------------------------|--------|------------|
| Life time of plant | Years | 20 |
| Interest rate | % | 10 |
| Payback period | Months | 102 |
| Interest rate of return | % | 17.31 |
| Net present value | R\$ | 15,488,699 |

6.5.3 Sensitive analysis

As already mentioned, the natural gas has a significant influence on the economic feasibility of the cogeneration plant scenario. In this context, in Figures 41, 42 and 43, it is shown the economic parameters as function of natural gas for the conventional and the solar-aided proposed cogeneration plants considering green electricity tariff.

Figure 41 – IRR as a function of natural gas cost for the conventional and the solar-aided proposed cogeneration plants

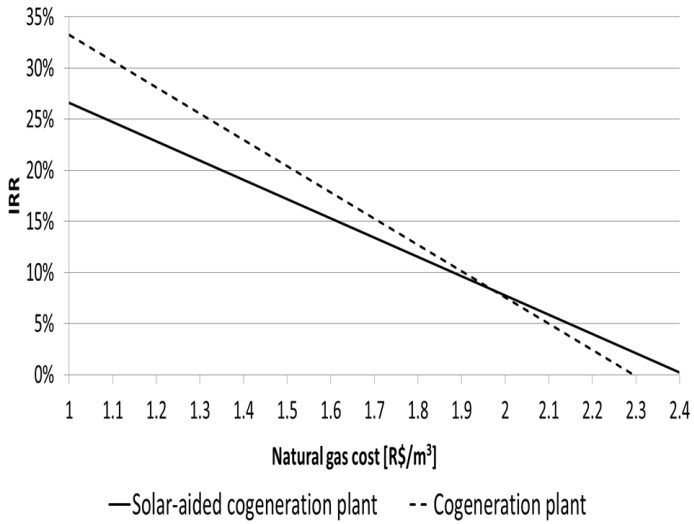


Figure 42 – NPV as a function of natural gas cost for the conventional and the solar-aided proposed cogeneration plants

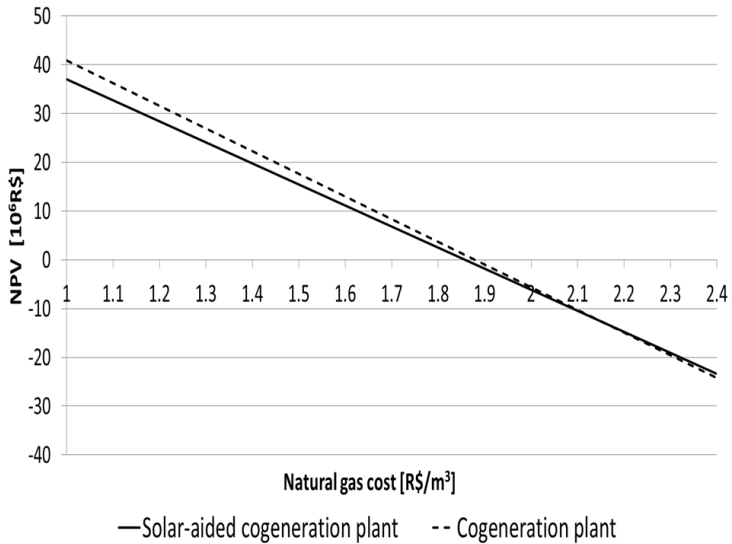


Figure 43 – Payback period as a function of natural gas cost for the conventional and the solar-aided proposed cogeneration plants

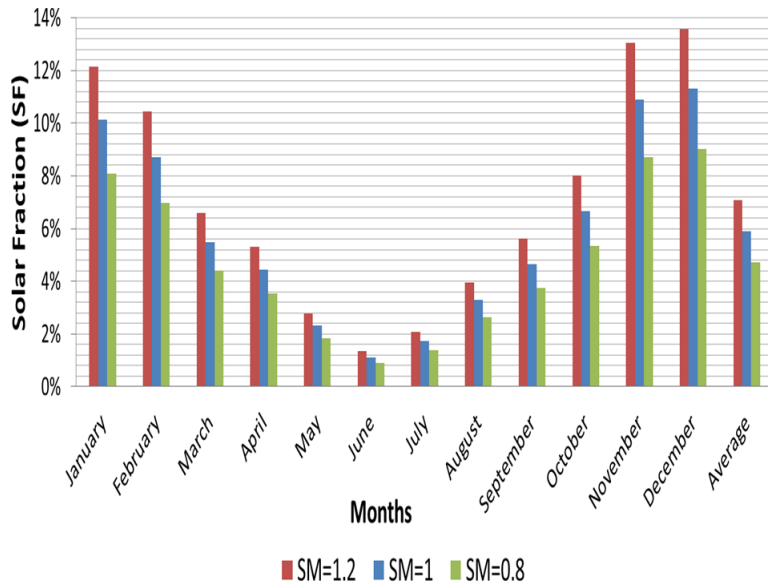


As it can be seen, the increase in the natural gas cost tends to favor the solar-aided cogeneration plant once the fuel consumption is reduced. Thereby, it was found that the solar-aided cogeneration plant has a higher economic feasibility than cogeneration plant when the natural gas cost is higher than 2.1 R\$/m³. However, this increase in the natural gas cost is not enough to make the solar-aided cogeneration plant feasible in economic terms. This behavior is due to the high investment associated to the Fresnel collector coupled with a low prices natural gas scenario. In this context, it is important to research the development of new technologies that allow reducing the current cost.

Another important parameter that influence on the technical and the economical feasibility of the solar-aided cogeneration plant is the solar field area. As already mentioned, the solar multiple represents the ratio at which the solar field area is modified compared to design point area (SM=1.0) calculated during design phase (see equation 5.16). Thus, the SM=1.2 means that the aperture area is increased by 20 % in comparison with design point. In Figure 44, it is shown the solar fraction (see

equation 5.16) for different SM values. As mentioned earlier, the solar fraction represents the fuel economy due to the integration of the solar field.

Figure 44 – Solar fraction throughout the year for different SM values

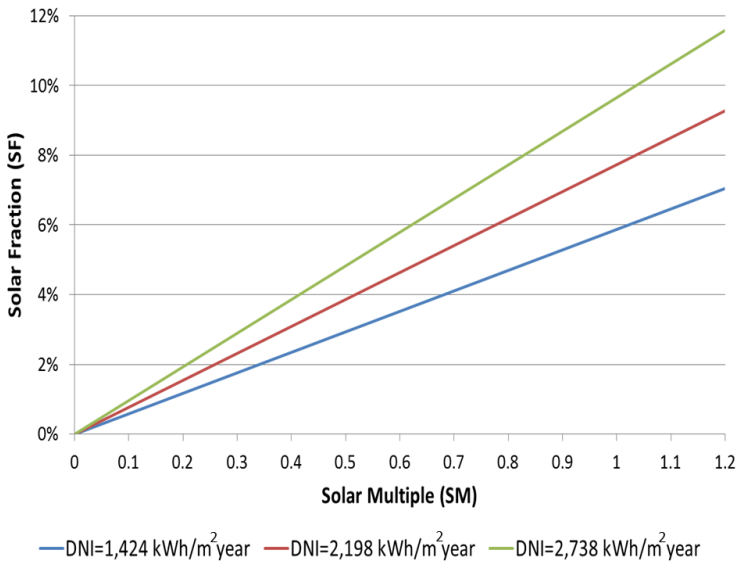


As it can be seen, the highest values of solar fraction occur during the summer period. In this period, the average solar fraction can reach values by 8.03 % (SM=0.8), by 10.01 % (SM=1.0) and by 12.05 % (SM=1.2). On the other hand, the lowest values of solar fraction occur during the winter period. In this period, the average solar fraction can reach values by 1.64 % (SM=0.8), by 2.04 % (SM=1.0) and by 2.47 % (SM=1.2). Therefore, the solar fraction decreases by 80 % during winter period. Finally, the annual average solar fraction is 4.72 % (SM=0.8), 5.89 % (SM=1) and 7.08 % (SM=1.2). Additionally, the results show that when the SM=1.4, the steam generator load decrease up to the value of 31.49 % at the design point. As mentioned earlier, the establish minimum load value is 30 %.

As it is known, the analysis of the solar-aided cogeneration plant is focused on the city Florianopolis as an approximation of the solar data in Santa Catarina. According to the TMY data used in the simulations, the DNI incidence in the city of Florianopolis is

1,424 kWh/m²-year. Therefore, in order to evaluate the influence of the DNI incidence on the thermodynamic performance and on the economic feasibility of the solar-aided cogeneration plant two DNI incidence levels are analyzed. According to INMET (2017) one of the cities with the highest DNI incidence in Brazil is the city of Bom Jesus da Lapa, located at the north east in the state of Piauí. The DNI incidence in this city can reach 2,198 kWh/m²-year. Another DNI incidence analyzed is 2,738 kWh/m²-year, this value is reaching in the city of Port Hedland (Australia). Although, this city is not located in Brazil, its high DNI incidence allows to compare to the Brazilian scenario. In Figure 45, it is shown the solar fraction as a function of SM for different DNI incidence levels.

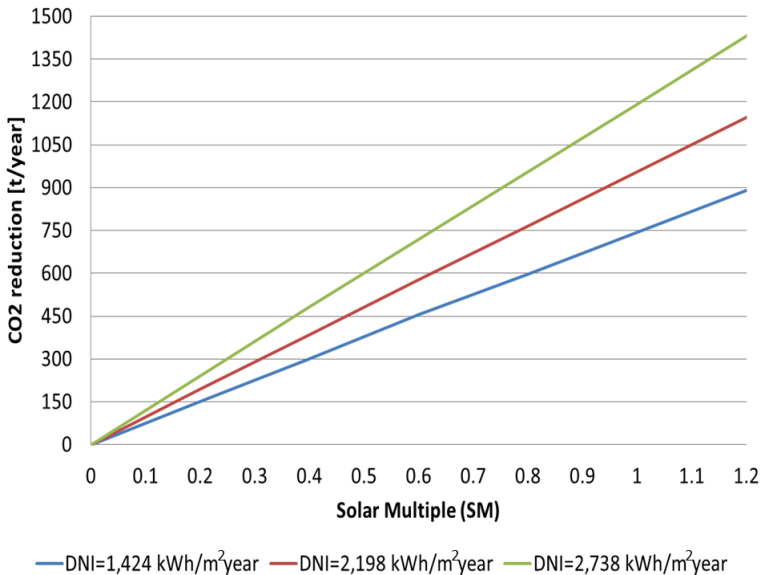
Figure 45 – Solar fraction as a function of SM for different DNI incidence levels



As it is shown, the solar fraction at the design point (SM=1.0) is 5.89 % considering a DNI=1,424 kWh/m²-year. In the same way, the solar fraction at the design point (SM=1.0) is 7.72 % considering a DNI=2,198 kWh/m²-year representing an increase by 31 % compared to Florianópolis. Finally, the solar fraction is 9.66 % considering a DNI=2,738 kWh/m²-year representing an increase by 64 % compared to Florianópolis.

As mentioned earlier, the solar-aided cogeneration plant is not a feasible option from an economic point of view. However, it is identified an important characteristic of the solar field from an environmental point of view. It is due to its potential to reduce greenhouse gas emissions. In this regard, in Figure 46, it is shown the annual reduction of CO₂ emissions as a function of SM for different DNI incidence levels.

Figure 46 – Reduction of CO₂ emissions as a function of SM for different DNI incidence levels



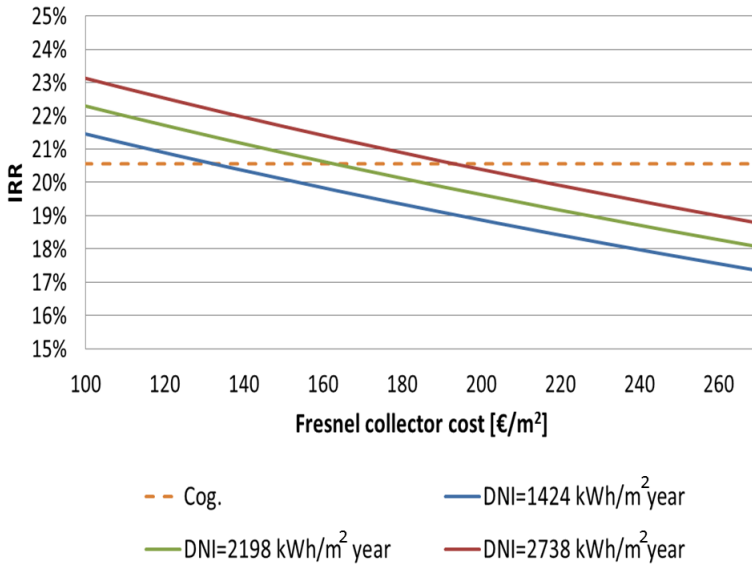
As it can be seen, the annual CO₂ reduction at the design point (SM=1.0) is 743.9 t/year considering a DNI=1,424 kWh/m²-year. In the same way, the annual CO₂ reduction considering a DNI=2,198 kWh/m²-year increases up 955.9 t/year representing an increase by 29 %. Finally, considering a DNI=2,738 kWh/m²-year the annual CO₂ reduction increases up 1,193 t/year representing an increase by 60 %.

As mentioned above, the solar-aided cogeneration plant has an important advantage from an environmental point of view. Therefore, it is important that local governments encourage the use of solar energy applications by policymakers that allow to drive down solar costs. As result of these policy efforts, a

significant amount of incentives should be directed to the solar energy (Matisoff & Johnson, 2017). According to Sarzynski *et al.* (2012) many states in USA have adopted financial incentives to encourage market deployment of solar energy. The results show that states offering cash incentives such as discounts and grants experienced more extensive and rapid deployment of photovoltaic systems than states without cash incentives. In Brazil the CSP is still not regulated. However, the solar photovoltaic has received stimulus, such as discounts on the use of transmission systems, the use of distribution systems, the solar photovoltaic is also ICMS tax free in Brazil. (Marques *et al.*, 2015).

As already mentioned, the Fresnel collector cost plays an important role in the economic feasibility of the solar-aided cogeneration plant. In Figure 47, it is shown the IRR as a function of Fresnel collector cost for different DNI incidence levels considering a natural gas cost of 1.5 R\$/m³.

Figure 47 – IRR as a function of Fresnel collector cost for different DNI incidence levels considering a natural gas cost of 1.5 R\$/m³



As it might be seen, the solar field cogeneration plant has a greater economic feasibility than cogeneration plant for Fresnel collectors costs less than 133 €/m² considering a DNI=1,424

kWh/m²-year. According to quotations performed under this work, the current Fresnel collector cost in Brazil is by 265 €/m². Therefore, according to the assumptions and results obtained in this work, it is expected a reduction by 50 % in order to turn the Fresnel system economically feasible to displace natural gas consumption. In the same way, it is expected a reduction by 39 % (~ 163 €/m²) considering a DNI=2,198 kWh/m²-year. Finally, it is expected a reduction by 27 % (~ 193 €/m²) considering a DNI=2,738 kWh/m²-year.

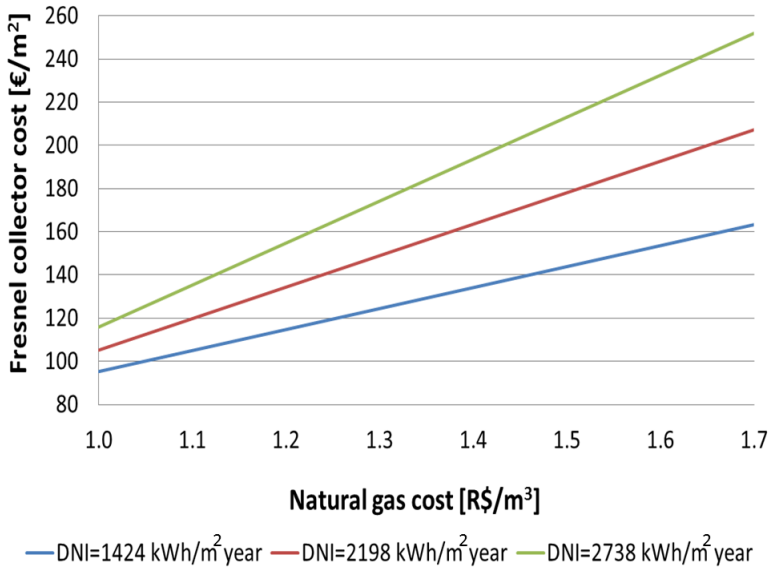
According to the Gabbrielli *et al.* (2014), Fresnel solar collectors can be competitive with natural gas even in the actual low gas price scenario and without any government subsidy with specific cost under 150 €/m² and DNI larger than 1900 kWh/m²-year. This level of cost can be achieved with simple and robust design and economy of scale that only a mature market can assure.

As already stated above, the Fresnel collector cost for which the solar-aided cogeneration plant has a greater economic feasibility than cogeneration plant depends on the natural gas cost. Thus, at Figure 48 are presented the Fresnel collector's cost at which the solar-aided cogeneration plant has greater economic feasibility than the cogeneration plant as a function of natural gas cost for different DNI incidence levels.

From a market point of view, it is expected that the hybrid systems have an important role, opening promising perspectives for this systems in market areas such as Brazil (over 2000 kWh/m²-year), USA (over 2,100 kWh/m²-year), Spain (over 2,150 kWh/m²-year), among others. From this perspective, the hybrid system appear as an important promising option for industrial applications once it shows a great potential to reduce manufacturing costs (IRENA, 2016). Several studies, such as (Sharma *et al.*, 2018a) and (ESMAP, 2012) have reported that the cost of CSP technology can be reduced in the near future. According to Sharma *et al.* (2018b) the aspects which can contribute to a CSP cost reduction include, technological advancements in the components (i.e., concentrators, receiver tubes, heat transfer fluid, among other).

Currently, in Santa Catarina the natural gas cost for cogeneration purposes is between 1 and 1.5 R\$/m³. Therefore, the Fresnel collector cost should be between 100 - 140 €/m² in that region where DNI is around 1,500 kWh/m²-year.

Figure 48 – Fresnel collector cost as a function of natural gas cost for different DNI incidence levels



Chapter 7

CONCLUDING REMARKS

In this work, it was analyzed two different scenarios proposed for supplying the demands of saturated steam, electricity and chilled water of a medium-sized plant in the Santa Catarina's textile sector. The first scenario consisted on a cogeneration plant using an internal combustion engine, a HRSG and an absorption chiller in order to attend the electrical, the saturated steam and the chilled water demands, respectively. The second scenario consisted on the integration of a solar field based on the Fresnel collector technology into the cogeneration plant (first scenario) for producing saturated steam by DSG. The solar system was analyzed during a TMY for the city of Florianopolis, as an approximation of the solar data in Santa Catarina. These scenarios were compared to the typical scenario of a medium-size plant in the textile sector in which the electrical demand is imported from the grid, the saturated steam is produced by a natural gas steam generator and the chilled water (used for air conditioning purposes) is attended by an electric chiller. Furthermore, a sensitive analysis was performed with parameters that influence on the economic and technical feasibility of the proposed plants. Thereby, different natural gas costs, electricity tariffs, Fresnel collector costs, solar field sizes and DNI incidence levels were evaluated.

The economic results showed a significant influence of the natural gas cost on the economic feasibility of the proposed plants. Moreover, the results showed an unfavorable feasibility for the solar-aided cogeneration plant in economic terms compared to cogeneration plant. It is due to the high investment cost, low DNI incidence in Florianopolis (1,423 kWh/m²-year) and a low natural gas cost cost scenario for cogeneration purposes. On the other hand, it was found that the increase in the natural gas cost favors the use of the solar-aided cogeneration plant once the fuel consumption is reduced. However, the increase in the natural gas cost is not enough to make the solar-aided cogeneration plant feasible in economic terms considering the current solar field cost. Finally, the results show that the option for green or blue electricity tariff has a little influence on the economic feasibility of

the proposed plants.

In this context, other DNI incidence levels were considered for cities with higher DNI than Florianopolis. Thus, the chosen cities were the city of Port Headland in Australia (2,738 kWh/m²-year) and the city of Bom Jesus da Lapa in Brazil (2,198 kWh/m²-year). The results showed a higher economic feasibility than Florianopolis. However, the cogeneration plant continues to have the highest economic feasibility. In this regard, the Fresnel collector cost should be reduced in order to be competitive with the current low natural gas cost scenario. Particularly, in Santa Catarina for which the solar incidence level is around 1,500 kWh/m²-year, the Fresnel collector cost should be between 100 - 140 €/m². It represents a decrease by 55 % of the current Fresnel collector cost in Brazil (265 €/m²). On the other hand, it was identified a great potential of the solar-aided cogeneration plant from an environmental point of view due to its potential to reduce the CO₂ emissions. In this regard, it is important that the local governments encourage the use of solar energy by policymakers to drive down the current costs.

Finally, despite the limitations of the proposed solar-aided cogeneration plant from an economic point of view. An important aspect was identified, solar energy can be integrated into natural gas power plants. In the same way, it is expected that the hybrid systems have an important role in the near future, once CSP technology costs are expected to decrease, due to its substantially contribution to the global energy transition to a low carbon future.

Some of the activities recommended to give continuity to this work are listed as follows:

1. To analyze the hybridization for other types of industries with higher DNI incidence levels and other types of fuels (biomass or coal).
2. To analyze the hybridization considering the option of thermal storage.
3. To analyze the hybridization considering other types of CSP technologies such as solar dish, parabolic trough and solar tower.
4. To analyze the hybridization considering other layout plant such as natural gas turbine, steam absorption chiller (single and double effect).

5. To analyze the hybridization of a Rankine cycle for different applications such as generate saturated steam to the process, to heat the steam generator feed water or to generate superheated steam to feed the steam turbine for producing electricity.
6. To analyze the hybridization considering an analysis of second law of thermodynamics.

BIBLIOGRAPHY

ABUSOGLU, A.; KANOGLU, M. Exergetic and thermoeconomic analyses of diesel engine powered cogeneration. *Applied Thermal Engineering*, v. 29, n. 2, p. 234–241, 2009. ISSN 1359-4311.

Available at: <<http://www.sciencedirect.com/science/article/pii/S1359431108001038>>.

ÇAKIR, U.; ÇOMAKLI, K.; YÜKSEL, F. The role of cogeneration systems in sustainability of energy. *Energy Conversion and Management*, v. 63, p. 196 – 202, 2012. ISSN 0196-8904. 10th International Conference on Sustainable Energy Technologies (SET 2011). Available at: <<http://www.sciencedirect.com/science/article/pii/S0196890412001264>>.

ANEEL. *Resolução normativa 235*. 2006.

ANEEL. *BIG - Banco de Informações de Geração*. 2017. Available at: <<http://www2.aneel.gov.br/aplicacoes/capacidadebrasil/CoGeracao.cfm>>.

ASHRAE. *Combined Heat and Power*. [S.l.]: ASHRAE, 2015. ISBN 978-1-936504-87-9.

ATLAS. *Atlas Brasileiro de energia solar*. 2017. Available at: <http://ftp.cptec.inpe.br/labren/publ/livros/Atlas_Brasileiro_Energia_Solar_2a_Edicao.pdf>.

BALESTIERI, J. A. P. *Cogeração: Geração combinada de eletricidade e calor*. Editora da UFSC, 2002. Available at: <<http://scholar.google.com/scholar?cluster=12062325933594676571{&}hl=en{&}oi=scholarr>>.

BEB. *BRAZILIAN ENERGY BALANCE*. 2017. 1-284 p.

BELTAGY, H.; SEMMAR, D.; LEHAUT, C.; SAID, N. Theoretical and experimental performance analysis of a Fresnel type solar concentrator. *Renewable Energy*, v. 101, p. 782–793, 2017. ISSN 0960-1481. Available at: <<http://www.sciencedirect.com/science/article/pii/S096014811630828X>>.

BENDATO, I.; CASSETTARI, L.; MOSCA, M.; MOSCA, R. Stochastic techno-economic assessment based on Monte Carlo simulation and the Response Surface Methodology: The case of an innovative linear Fresnel CSP (Concentrated Solar Power) system. *Energy*, v. 101, p. 309–324, 2016. ISSN 0360-5442. Available at: <<http://www.sciencedirect.com/science/article/pii/S0360544216300913>>.

BESC. *Balanço energético de Santa Catarina*. 2013. 1-78 p.

BEU. *Ministério de Minas e Energia. Balanço de energia útil*. 2009.

BLANCO, M.; SANTIGOSA, L. R. *Advances in Concentrating Solar Thermal Research and Technology*. [s.n.], 2016. ISBN 9780081005163. Available at: <<https://books.google.co.uk/books?id=OJLsjwEACAAJ>>.

BOUBAULT, A.; HO, C. K.; HALL, A.; LAMBERT, T. N.; AMBROSINI, A. Levelized cost of energy (LCOE) metric to characterize solar absorber coatings for the CSP industry. *Renew. Energy*, v. 85, p. 472–483, 2016. ISSN 0960-1481. Available at: <<http://www.sciencedirect.com/science/article/pii/S0960148115300823>>.

BURIN, E.; VOGEL, T.; MULTHAUPT, S.; THELEN, A.; OELJEKLAUS, G.; GÖRNER, K.; BAZZO, E. Thermodynamic and economic evaluation of a solar aided sugarcane bagasse cogeneration power plant. v. 117, 06 2016.

CATERPILLAR. *Power systems Oil and Gas*. 2017. Available at: <https://www.cat.com/en_US/products/new/power-systems/oil-and-gas.html>.

CCEE. *Câmara de Comercialização de Energia Elétrica*. 2017. Available at: <https://www.ccee.org.br/portal/faces/pages_publico/inicio?_adf.ctrl-state=7ga7pbuwg_4&_afLoop=83699777127011>.

CELESC. *Tarifas CELESC*. 2018. Available at: <<http://www.celesc.com.br/portal/index.php/duvidas-mais-frequentes/1140-tarifa>>.

CHIARAPPA, T. Performance of Direct Steam Generator Solar Receiver: Laboratory vs Real Plant. In: *Energy Procedia*. Elsevier,

2015. v. 69, p. 328–339. ISBN 3907589548. ISSN 18766102.

Available at: <<https://www.sciencedirect.com/science/article/pii/S1876610215003434>>.

COOPER, P. I. The absorption of radiation in solar stills. *Solar Energy*, v. 12, n. 3, p. 333–346, Jan. 1969. ISSN 0038-092X.

Available at: <<http://www.sciencedirect.com/science/article/pii/0038092X69900474>>.

DUFFIE, J. A.; BECKMAN, W. A. *Solar Engineering of Thermal Processes*. [S.l.]: Wiley, 1991. ISBN 978-0-471-51056-7.

EIA. *EIA- Energy Information Administration*. 2018. Available at: <<https://www.e3nv.com/cogeneration>>.

ERDINC, O.; UZUNOGLU, M. Optimum design of hybrid renewable energy systems: Overview of different approaches.

Renewable and Sustainable Energy Reviews, v. 16, n. 3, p. 1412–1425, 2012. ISSN 1364-0321. Available at: <<http://www.sciencedirect.com/science/article/pii/S1364032111005478>>.

ESMAP. *The Energy Sector Management Assistance Program (ESMAP)*, World Bank, Washington D.C., 2012. Available at: <<https://www.esmap.org/publications>>.

FELDHOFF, J. F. *Linear Fresnel Collectors - Technology Overview*. 2012. 1-59 p.

FU, L.; ZHAO, X.; ZHANG, S.; LI, Y.; JIANG, Y.; LI, H.; SUN, Z. Performance study of an innovative natural gas CHP system. *Energy Conversion and Management*, v. 52, n. 1, p. 321–328, 2011. ISSN 0196-8904. Available at: <<http://www.sciencedirect.com/science/article/pii/S0196890410002955>>.

GABRIELLI, R.; CASTRATARO, P.; Del Medico, F.; Di Palo, M.; LENZO, B. Levelized Cost of Heat for Linear Fresnel Concentrated Solar Systems. *Energy Procedia*, v. 49, p. 1340–1349, 2014. ISSN 1876-6102. Available at: <<http://www.sciencedirect.com/science/article/pii/S1876610214005979>>.

GALANTE, R. *Análise termodinâmica de uma planta termoeétrica a biomassa assistida por energia solar*. 2015. Available at: <<http://tede.ufsc.br/teses/PEMC1590-D.pdf>>.

GAUCHÉ, P.; RUDMAN, J.; MABASO, M.; LANDMAN, W. A.; BACKSTRÖM, T. W. von; BRENT, A. C. System value and progress of CSP. *Sol. Energy*, 2017. ISSN 0038-092X. Available at: <<http://www.sciencedirect.com/science/article/pii/S0038092X17302529>>.

GUADALUPE, T. *Energia termossolar como alternativa na geração de vapor e água quente no setor agroindustrial*. 2018.

HAFEZ, A. Z.; SOLIMAN, A.; EL-METWALLY, K. A.; ISMAIL, I. M. Solar parabolic dish Stirling engine system design, simulation, and thermal analysis. *Energy Convers. Manag.*, v. 126, p. 60–75, 2016. ISSN 0196-8904. Available at: <<http://www.sciencedirect.com/science/article/pii/S0196890416306458>>.

HäBERLE, A.; ZÄHLER, C.; LERCHENMÜLLER, H.; MERTINS, M.; WITTEWER, C.; TRIEB, F.; DERSCH, J. The solarmundo line focussing fresnel collector. optical and thermal performance and cost calculations. 01 2002.

HEIMSATH, A.; CUEVAS, F.; HOFER, A.; NITZ, P.; PLATZER, W. J. Linear Fresnel Collector Receiver: Heat Loss and Temperatures. *Energy Procedia*, v. 49, n. Supplement C, p. 386–397, Jan. 2014. ISSN 1876-6102. Available at: <<http://www.sciencedirect.com/science/article/pii/S1876610214004962>>.

HEIMSATH, A.; CUEVAS, F.; ZIRKEL-HOFER, A.; NITZ, P.; PLATZER, W. Linear fresnel collector receiver: Heat loss and temperatures. v. 49, p. 386–397, 12 2014.

IBGE. *Instituto Brasileiro de Geografia y Estadística*. 2017. Available at: <<https://www.ibge.gov.br/>>.

IEA. *Combined Heat and Power: Evaluating the benefits of greater global investment*. 2008.

Industrial Solar. *Solar Fresnel Collector Characteristics*. 2017. Available at: <<http://www.industrial-solar.de/content/en/maerkte/fresnel-collector/>>.

INMET. *Instituto Nacional de Meteorologia*. 2017. Available at: <<http://www.inmet.gov.br/portal/{},urldate={2017-11-02}>>.

INTER. *Gestão e Representação de Consumidores no Mercado Livre de Energia*. 2017. Available at: <<http://www.interenergia.com.br/>>.

- IRENA. *Renewable Power Generation Costs in 2012*. 2012. 1-88 p.
- IRENA. *The power to change: Solar and wind cost reduction potential to 2025*. 2016. 1-105 p.
- IRENA. *RENA Report 2017 CSP's cost Reductions*. 2017.
- IZQUIERDO, S.; MONTAÑÉS, C.; DOPAZO, C.; FUEYO, N. Analysis of CSP plants for the definition of energy policies: The influence on electricity cost of solar multiples, capacity factors and energy storage. *Energy Policy*, v. 38, n. 10, p. 6215–6221, 2010. ISSN 0301-4215. Available at: <<http://www.sciencedirect.com/science/article/pii/S0301421510004726>>.
- JIN, J.; LING, Y.; HAO, Y. Similarity analysis of parabolic-trough solar collectors. *Appl. Energy*, may 2017. ISSN 0306-2619. Available at: <<http://www.sciencedirect.com/science/article/pii/S0306261917304609>>.
- KONG, X. Q.; WANG, R. Z.; HUANG, X. H. Energy efficiency and economic feasibility of CCHP driven by stirling engine. *Energy Convers. Manag.*, v. 45, n. 9, p. 1433–1442, 2004. ISSN 0196-8904. Available at: <<http://www.sciencedirect.com/science/article/pii/S0196890403002528>>.
- LG. *Absorption chiller*. 2017. Available at: <<http://www.lg.com/global/business/air-solution/chiller/direct-fired-absorption-chiller>>.
- MANZOLINI, G.; GIOSTRI, A.; SACCILOTTO, C.; SILVA, P.; MACCHI, E. Development of an innovative code for the design of thermodynamic solar power plants part A: Code description and test case. *Renewable Energy*, Pergamon, v. 36, n. 7, p. 1993–2003, jul 2011. ISSN 09601481. Available at: <<https://www.sciencedirect.com/science/article/pii/S0960148111000061>>.
- MARBE Âsa; HARVEY, S.; BERNTSSON, T. Technical, environmental and economic analysis of co-firing of gasified biofuel in a natural gas combined cycle (ngcc) combined heat and power (chp) plant. *Energy*, v. 31, n. 10, p. 1614 – 1631, 2006. ISSN 0360-5442. ECOS 2003. Available at: <<http://www.sciencedirect.com/science/article/pii/S0360544205001386>>.
- MARQUES, R.; SILVA, D.; Para Discussão, T. ENERGIA SOLAR NO BRASIL: dos incentivos aos desafios. 2015. Available at:

<<http://www2.senado.leg.br/bdsf/bitstream/handle/id/507212/TD166-RutellyMSilva.pdf?sequence=1>>.

MATISOFF, D. C.; JOHNSON, E. P. The comparative effectiveness of residential solar incentives. *Energy Policy*, v. 108, p. 44–54, Sep. 2017. ISSN 0301-4215. Available at: <<http://www.sciencedirect.com/science/article/pii/S0301421517303166>>.

MILLS, D. R.; MORRISON, G. L. Compact linear fresnel reflector solar thermal powerplants. *Solar Energy*, v. 68, n. 3, p. 263 – 283, 2000. ISSN 0038-092X. Available at: <<http://www.sciencedirect.com/science/article/pii/S0038092X99000687>>.

MORIN, G.; DERSCH, J.; PLATZER, W.; ECK, M.; HÄBERLE, A. Comparison of Linear Fresnel and Parabolic Trough Collector power plants. *Sol. Energy*, v. 86, n. 1, p. 1–12, 2012. ISSN 0038-092X. Available at: <<http://www.sciencedirect.com/science/article/pii/S0038092X11002325>>.

NR17. *Norma regulamentadora 17 do Ministério do Trabalho*. 2017.

NREL. *Concentrating Solar Power Projects*. 2013. Available at: <<https://www.nrel.gov/csp/solarpaces/>>.

NREL. *Concentrating Solar Power Projects*. 2016. Available at: <<https://www.nrel.gov/csp/solarpaces/>>.

PANTALEO, A. M.; CAMPOREALE, S. M.; MILIOZZI, A.; RUSSO, V.; SHAH, N.; MARKIDES, C. N. Novel hybrid csp-biomass chp for flexible generation: Thermo-economic analysis and profitability assessment. *Applied Energy*, v. 204, p. 994 – 1006, 2017. ISSN 0306-2619. Available at: <<http://www.sciencedirect.com/science/article/pii/S0306261917305287>>.

POLO, J.; BALLESTRÍN, J.; CARRA, E. Sensitivity study for modelling atmospheric attenuation of solar radiation with radiative transfer models and the impact in solar tower plant production. *Solar Energy*, v. 134, p. 219–227, 2016. ISSN 0038-092X. Available at: <<http://www.sciencedirect.com/science/article/pii/S0038092X16300974>>.

POWELL, K. M.; RASHID, K.; ELLINGWOOD, K.; TUTTLE, J.; IVERSON, B. D. Hybrid concentrated solar thermal power systems: A review. *Renewable and Sustainable Energy Reviews*, v. 80, p. 215 – 237, 2017. ISSN 1364-0321. Available at: <<http://www.sciencedirect.com/science/article/pii/S1364032117306998>>.

- PRADO, G. O.; VIEIRA, L. G. M.; DAMASCENO, J. J. R. Solar dish concentrator for desalting water. *Solar Energy*, v. 136, n. Supplement C, p. 659–667, Oct. 2016. ISSN 0038-092X. Available at: <<http://www.sciencedirect.com/science/article/pii/S0038092X16302973>>.
- REN21. *Renewables 2016 Global Status Report*. Paris. 2016.
- SAMPAIO, P. G. V.; GONZÁLEZ, M. O. A. Photovoltaic solar energy: Conceptual framework. *Renewable and Sustainable Energy Reviews*, v. 74, p. 590–601, Jul. 2017. ISSN 1364-0321. Available at: <<http://www.sciencedirect.com/science/article/pii/S1364032117303076>>.
- San Miguel, G.; CORONA, B. Hybridizing concentrated solar power (CSP) with biogas and biomethane as an alternative to natural gas: Analysis of environmental performance using LCA. *Renew. Energy*, v. 66, p. 580–587, 2014. ISSN 0960-1481. Available at: <<http://www.sciencedirect.com/science/article/pii/S0960148113007003>>.
- SÁNCHEZ, F.; SÁNCHEZ, J.; MIGUEL, G. S. Biomass Resources to Hybridize CSP with Biomethane: Potential of Horticultural Residues and Drought tolerant Crops. *Procedia Comput. Sci.*, v. 83, p. 1102–1109, 2016. ISSN 1877-0509. Available at: <<http://www.sciencedirect.com/science/article/pii/S1877050916302630>>.
- SANTANA, P. h. D. M.; BAJAY, S. *Oportunidades de eficiência energética para indústria: setor têxtil*. [S.l.: s.n.], 2010. ISBN 978-85-7957-013-1.
- SANTO, D. B. d. E. An energy and exergy analysis of a high-efficiency engine trigeneration system for a hospital: A case study methodology based on annual energy demand profiles. *Energy Build.*, v. 76, p. 185–198, 2014. ISSN 0378-7788. Available at: <<http://www.sciencedirect.com/science/article/pii/S037877881400125X>>.
- SANTOS, A. B. dos. *Natural Gas Consumption Overview In Brazil*. 2017. Available at: <<http://www.questjournals.org/jrme/papers/vol3-issue3/D332428.pdf>>.
- SARZYNSKI, A.; LARRIEU, J.; SHRIMALI, G. The impact of state financial incentives on market deployment of solar technology. *Energy Policy*, Elsevier, v. 46, p. 550–557, jul 2012. ISSN 03014215.

Available at: <[#">https://www.sciencedirect.com/science/article/pii/S0301421512003321](https://www.sciencedirect.com/science/article/pii/S0301421512003321){#}!>

SHAH, R. K.; LONDON, A. L. *Laminar Flow Forced Convection in Ducts: A Source Book for Compact Heat Exchanger Analytical Data*. [S.l.]: Academic Press, 2014. ISBN 978-1-4831-9130-0.

SHARMA, C.; SHARMA, A. K.; MULLICK, S. C.; KANDPAL, T. C. Cost reduction potential of parabolic trough based concentrating solar power plants in India. *Energy for Sustainable Development*, v. 42, p. 121–128, Feb. 2018. ISSN 0973-0826.
Available at: <<http://www.sciencedirect.com/science/article/pii/S0973082616308729>>.

SHARMA, C.; SHARMA, A. K.; MULLICK, S. C.; KANDPAL, T. C. Cost reduction potential of parabolic trough based concentrating solar power plants in india. *Energy for Sustainable Development*, v. 42, p. 121 – 128, 2018. ISSN 0973-0826.
Available at: <<http://www.sciencedirect.com/science/article/pii/S0973082616308729>>.

SHOWERS, G. *Boiler operation efficiency*. 2002.

SOLARGIS. *Solar resource maps*. 2018. Available at: <<https://solargis.com/maps-and-gis-data/download/world>>.

SOLARPACES. *CSP Projects Around the World*. 2017.
Available at: <<http://www.solarpaces.org/csp-technologies/csp-projects-around-the-world/>>.

SOLUTIONS, M. *How Much Does it Cost to Buy a Natural Gas Generator?* 2017. Available at: <<http://www.247mesa.com/how-much-does-it-cost-to-buy-a-natural-gas-generator-3/>>.

SPENCER, J. Fourier series representation of the position of the sun. *Search*, v. 2, n. 5, p. 172, May 1971. Available at: <<http://www.mail-archive.com/sundial@uni-koeln.de/msg01050.html>>.

SUMMERHEAT. *Meeting cooling demands in SUMMER by applying HEAT from cogeneration*. 2009. Available at: <https://ec.europa.eu/energy/intelligent/projects/sites/iee-projects/files/projects/documents/summerheat_publishable_final_report_en.pdf>.

SUN, Z.-G. A combined heat and cold system driven by a gas industrial engine. *Energy Conversion and Management*, v. 48, n. 2, p. 366–369, 2007. ISSN 0196-8904. Available at: <<http://www.sciencedirect.com/science/article/pii/S0196890406002305>>.

SWERA. *Solar and Wind Energy Resource Assessment*. 2017. Available at: <[https://openei.org/wiki/Solar_and_Wind_Energy_Resource_Assessment_\(SWERA\)](https://openei.org/wiki/Solar_and_Wind_Energy_Resource_Assessment_(SWERA))>.

VALENZUELA, L. Thermal energy storage concepts for direct steam generation (DSG) solar plants. In: BLANCO, M. J.; SANTIGOSA, L. R. (Ed.). *Adv. Concentrating Solar Thermal Research Technology*. Woodhead Publishing, 2017, (Woodhead Publishing Series in Energy). p. 269–289. ISBN 978-0-08-100516-3. Available at: <<http://www.sciencedirect.com/science/article/pii/B9780081005163000125>>.

WU, S.-Y.; ZHOU, S.-M.; XIAO, L.; LI, Y.-R.; LIU, C.; XU, J.-L. Determining the optimal pinch point temperature difference of evaporator for waste heat recovery. *Journal of the Energy Institute*, v. 87, n. 2, p. 140–151, may 2014. ISSN 1743-9671. Available at: <<http://www.sciencedirect.com/science/article/pii/S1743967114000208>>.

YORK. *Industrial and Commercial HVAC Chillers for Sustainable Solutions*. 2017.

APPENDIX A - LHV CALCULATION

The heat combustion (ΔH_c) is numerically equal to the enthalpy of reaction (ΔH_R), but with opposite sign. The higher heating value, HHV, is the heat combustion calculated assuming that all of the water in the products has condensed to liquid. The lower heating value, LHV, corresponds to the case where none of the water is assumed to condense.

Equation A.1 allows to calculate either the higher or lower heating value:

$$\Delta H_c = -\Delta H_R = H_{reac} - H_{prod} \quad (\text{A.1})$$

where H_{reac} [kJ/kg] is the enthalpy of reactants and H_{prod} [kJ/kg] is the enthalpy of products depends on whether the H_2O in the products (determining higher heating value) or gaseous (determining lower heating value).

The values of H_{reac} and H_{prod} are calculated according to Equations A.2 and A.3 respectively.

$$H_{reac} = \sum_{reac} N_i \bar{h}_i \quad (\text{A.2})$$

$$H_{prod} = \sum_{prod} N_i \bar{h}_i \quad (\text{A.3})$$

where N_i represents the number of moles of the chemical specie i and h_i represents the enthalpy of the chemical specie i .

At Tables 28 and 29 it is shown the calculate of H_{reac} and H_{prod} respectively.

Table 28 – Enthalpy of reactants at 298 K

| Chemical species | N_i [kmol] | \bar{h}_i [kJ/kmol] | $N_i \bar{h}_i$ [kJ] |
|-------------------------------|--------------|--------------------------|----------------------|
| CH ₄ | 0.8924 | -74,831 | -66,779.18 |
| C ₂ H ₆ | 0.0786 | -84,667 | -6,654.83 |
| CO ₂ | 0.0125 | -393,546 | -4,919.33 |
| C ₃ H ₈ | 0.0024 | -103,847 | -249.23 |
| O ₂ | 0.0141 | 0 | 0 |
| | | H_{react} | -78,602.57 |

Table 29 – Enthalpy of products at 298 K

| Chemical species | N_i [kmol] | \bar{h}_i [kJ/kmol] | $N_i \bar{h}_i$ [kJ] |
|------------------|--------------|-------------------------|----------------------|
| CO ₂ | 1.0693 | -393,546 | -420,818.74 |
| H ₂ O | 2.0302 | -241,847 | -490,997.78 |
| N ₂ | 7,773 | 0 | 0 |
| | | H_{prod} | -911,816.52 |

Then, it is possible to calculate the LHV as:

$$\Delta \bar{h}_c = \frac{\Delta H_c}{N_{GN}} = \frac{833,213.95}{1 \text{ kmol}} = 833,213.95 \text{ kJ/kmol}_{GN}$$

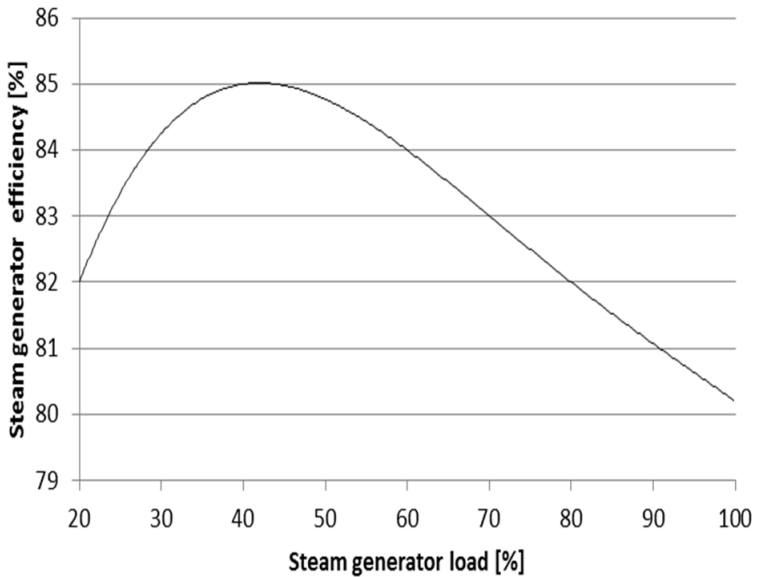
or

$$\Delta h_c = \frac{\Delta \bar{h}_c}{MW_{GN}} = \frac{833,213.95 \text{ kJ/kmol}_{GN}}{17.74 \text{ kg/kmol}} = \mathbf{46,968.09 \text{ kJ/kg}_{GN}}$$

APPENDIX B - STEAM GENERATOR OPERATION EFFICIENCY

The steam generator operation efficiency as a function of steam generator load is shown at Figure 49.

Figure 49 – Steam Generator operation efficiency as a function of load



Source: Adapted from Showers (2002)

APPENDIX C - COGENERATION PLANT SIMULATION

The water thermodynamic properties at each point in the cogeneration plant are presented at Table 30. (See Figure 19)

Table 30 – Water thermodynamic properties

| Point | Water thermodynamic properties | | | |
|-------|--------------------------------|--------------------|-------------|------------|
| | h_i [kJ/kg] | \dot{m}_i [kg/s] | P_i [kPa] | T_i [°C] |
| 3 | 335 | 19.72 | 150 | 80 |
| 4 | 389.6 | 19.72 | 150 | 93 |
| 6 | 2769 | 0.6826 | 800 | 170.4 |
| 8 | 655.9 | 0.6826 | 800 | 155.4 |
| 9 | 251.8 | 0.6826 | 800 | 60 |
| 10 | 2365 | 0.6826 | 800 | 170.4 |
| 11 | 251.8 | 0.6826 | 800 | 60 |
| 13 | 398 | 4.268 | 150 | 95 |
| 14 | 301.5 | 4.268 | 150 | 72 |
| 15 | 368.6 | 4.268 | 150 | 88 |
| 17 | 142.5 | 35.46 | 150 | 34 |
| 18 | 121.6 | 35.46 | 150 | 29 |
| 19 | 50.51 | 15.74 | 150 | 12 |
| 20 | 29.56 | 15.74 | 150 | 7 |

The exhaust gas thermodynamic properties at each point in

the cogeneration plant are presented at Table 31.

Table 31 – Exhaust gas thermodynamic properties

| Point | Exhaust gas thermodynamic properties | | | |
|-------|--------------------------------------|--------------------|-------------|------------|
| | h_i [kJ/kg] | \dot{m}_i [kg/s] | P_i [kPa] | T_i [°C] |
| 5 | 699.8 | 3,018 | 150 | 414 |
| 7 | 460.8 | 3,018 | 150 | 185.4 |
| 12 | 415.1 | 3.018 | 150 | 140.5 |
| 16 | 394.3 | 3.018 | 150 | 120 |